

Diss. ETH No. 22917

# Large-scale simulations of load-adaptive bone remodeling in human vertebrae from native osteoporotic to augmented bone

A thesis submitted to attain the degree of  
DOCTOR OF SCIENCES of ETH ZURICH  
(Dr. sc. ETH Zurich)

presented by

**Sandro Domenico Badilatti**

M.Sc. Biomedical Engineering, ETH Zurich

born on the 14<sup>th</sup> of March, 1983

citizen of Zuoz (Graubünden) and Poschiavo (Graubünden)

accepted on the recommendation of

Prof. Dr. Ralph Müller, examiner

Prof. Dr. Stephen John Ferguson, co-examiner

2015



*dedicated to my family*





# Table of Contents

<b>Acknowledgements</b>	<b>iii</b>
<b>Summary</b>	<b>v</b>
<b>Zusammenfassung</b>	<b>ix</b>
<b>Riassunt</b>	<b>xiii</b>
<b>1 Introduction</b>	<b>1</b>
1.1 Thesis motivation . . . . .	1
1.2 Thesis aims . . . . .	4
1.3 Thesis outline . . . . .	5
<b>2 Background</b>	<b>13</b>
2.1 Computational modelling of bone augmentation in the spine . . . . .	15
<b>3 Development of large-scale simulations of load-adaptive bone remodeling in whole human vertebrae</b>	<b>41</b>
3.1 Simulations of healthy bone adaptation in whole human vertebrae . .	43
<b>4 Applications of large-scale simulations of load-adaptive bone remodeling</b>	<b>71</b>
4.1 Simulations of osteoporotic bone loss in native whole human vertebrae	73
4.2 Simulations of microstructural bone adaptation in augmented whole human vertebrae . . . . .	103
<b>5 Synthesis</b>	<b>121</b>
5.1 Large-scale simulations of load-adaptive bone remodeling . . . . .	122
5.2 Simulations of osteoporotic bone loss in native vertebrae . . . . .	124
5.3 Simulations of microstructural bone adaptation in augmented vertebrae	125
5.4 Limitations and future research . . . . .	125
5.5 Conclusion . . . . .	128
<b>Curriculum Vitae</b>	<b>133</b>



# Acknowledgements

The work presented in this thesis was carried out at the Institute for Biomechanics at ETH Zurich and would not have been possible without the help of numerous people. I would like to express my profound gratitude to them.

I would like to thank Prof. Dr. Ralph Müller for giving me the opportunity to work in the exciting field of computational biomechanics. His inspiring solution-oriented thinking and his passion for research were a great help and motivator throughout my years at the institute. I deeply appreciated his support and guidance as well as the academic freedom with my research.

Furthermore, I would like to thank Prof. Dr. Stephen Ferguson for always being available to discuss my work and for his excellent inputs and constructive criticisms which considerably improved the quality of the presented work.

I would like to thank all the members and alumni of the Institute for Biomechanics. Special thank goes to Dr. Gisela Kuhn, Dr. Duncan Webster and Dr. Friederike Schulte who supported me a lot in the initial part of the thesis, to Alexander Zwahlen who was a great companion throughout the whole thesis and to Dr. Patrik Christen and Duncan Betts who were invaluable in the final stages of the project. In addition, I would like to mention Dr. David Christen, Dr. Ben Helgason, Dr. Silvio Lorenzetti, Dr. Laura Nebuloni, Dr. Davide Ruffoni, Dr. Kathryn Stok, Dr. Antonia Torcasio, Dr. Esther Wehrle, Dr. René Widmer, Ilaria Chiapparini, Elliott Goff, Dominika Ignasiak, Alina Levchuk, Zihui Li and Yabin Wu who have helped me completing this work.

Thank you to Lukas Sommerhalder, Nathalie Cuerq and John Traxler who have written a thesis under my supervision, as well as to Dr. Hans Gerber and Dr. Thomas Kohler who were great tutors and coworkers for the work on the VMS cluster. I would also like to greatly acknowledge the secretariat for their continuous support regarding administrative issues and Catherine Palmer in particular for the proofreading of several chapters of this thesis. A big thank you goes also to my sister Valeria Badilatti who helped with the translation of the summary to our mother tongue.

Finally, I would like to express my deepest appreciation to my family and friends

## *Acknowledgements*

---

for their uninterrupted support and backing over the last few years.

Zurich, in July 2015

# Summary

In daily life, bones are usually being experienced as something static. In reality, bone is a very dynamic tissue where cells constantly change its shape in a process known as bone remodeling. Bone forming and bone resorbing cells adapt the microstructure so it is optimized to withstand the loads the bone has to carry. When the equilibrium between formation and resorption is perturbed, it can lead to excessive bone loss, such as in the case of osteoporosis. The disease affects mostly the elderly, thus becoming an increasingly important concern in our ageing societies. The weakened bone gets more susceptible to fractures, which are painful, require protracted treatment and are linked with high costs for healthcare systems.

While new approaches to treat the fractures are constantly being developed, ideally, these fractures would be prevented right from the beginning. A key for such successful prevention would be to accurately define the individuals at risk. Today, fracture risk assessment is performed by dual-energy X-ray absorptiometry, where the mineral density of the bone is evaluated. More accurate prediction can be achieved by including information of the microstructure, as used when calculating bone tissue loading running micro-finite element ( $\mu$ FE) analysis on scans from high-resolution peripheral quantitative computer tomography. However, all these techniques are limited by the fact that they merely look at the risk of fracture at the day of the measurements and thus have limited predictive power for the future stability of the bones.

Computational simulations of bone remodeling can predict the changes of the microstructure, but were limited to small biopsies so far. For an accurate fracture risk assessment, large extents of the organ must be considered however. The primary aim of this thesis was to develop a framework for the simulation of bone remodeling with mechanical feedback on high-resolution whole human bones and to investigate its potential to evaluate disease and treatment in the long-term.

To begin, a framework for large-scale simulations of load-adaptive bone remodeling in whole human vertebrae was developed. It includes the calculation of subject-specific boundary conditions as determined with a bone loading estimation algorithm providing physiological loading conditions. Mechanical signals were calculated by

means of  $\mu$ FE analysis with model sizes of up to 365 million elements. On two vertebrae, healthy bone remodeling for the duration of ten years was realistically simulated, as confirmed by bone morphometry. The algorithm was extensively evaluated in a series of simulations on subvolumes and single trabeculae, where accurate functioning of mechanical bone adaption was shown in a well-controlled environment, also demonstrating the necessity of adding complex boundary conditions. In addition, the influence of the sample resolution on the calculation of the mechanical signal was investigated, revealing that a resolution of  $43.5\ \mu\text{m}$  was sufficient in our case.

In a first application, the potential of the bone remodeling framework was demonstrated by simulating osteoporotic bone loss in a group of seven high-resolution human vertebrae datasets. Five parameter sets were studied and the morphometric parameters of the simulated bones compared to experimental studies. Remodeling models that decrease the cell sensitivity led to the best match compared to the experiments. Detailed analysis of the biomechanical competence was performed including stiffness and fracture load calculations revealing realistic outcomes for the simulated 30 years of bone loss. On average, the samples lost 31% of the bone volume. In general, morphometric indices matched experimental findings well, although reduction of trabecular number (-5.8%) and increase in trabecular spacing (+7.8%) was conservative. While stiffness was mostly conserved (-7.9%), fracture loads were 13% lower for error loadings compared to normal loading at the age of 50, and were further reduced to 17% at the age of 80.

In a second application, the bone remodeling framework was used to investigate the long-term effects of preventive cement augmentation on the remodeling in osteoporotic bone. We studied the effects of the augmentation volume and time-point of the intervention. Larger augmentation volumes increased stress-shielding and led to additional bone loss (-11%). The beneficial increase in overall mechanical stiffness, however, dominated over the increase in bone loss (+50% for large augmentation volumes). The time point of the augmentation had no effect on the mechanical stability. Bone tissue was maintained in particular around the augmentation cement, where a reduction of only 12% was observed compared to a reduction of 23% in the nonaugmented case (small augmentation volumes). With these results, insight into the long-term effects of cement augmentation was possible for the first time, suggesting that the intervention is less detrimental in respect to stress shielding than previously assumed.

Bone remodeling simulations of small volumes have been available for years. In this thesis, simulations of large-scale load-adaptive bone remodeling on whole human

bones demonstrating realistic bone loss and evaluating preventive vertebroplasty were achieved. Although a simplified biological model was used, the simulations have the potential to improve future fracture risk prediction and can be useful to investigate novel treatments in bones and their impact in the long-term.





# Zusammenfassung

Im Alltag werden Knochen meist als statisch wahrgenommen, obwohl es sich in Wirklichkeit um ein dynamisches, sich kontinuierlich veränderndes Gewebe handelt. Dieser Prozess der Veränderung wird als Knochenumbau bezeichnet. Knochenbildende und absorbierende Zellen passen die Mikrostruktur der jeweiligen lokalen Belastung an, sodass der Knochen der alltäglichen Traglast standhalten kann. Wird dieses Gleichgewicht zwischen Auf- und Abbau gestört, kann dies zu exzessivem Knochenschwund führen, wie zum Beispiel bei Osteoporose. Da diese Krankheit hauptsächlich die ältere Bevölkerung betrifft, wird sie in unserer alternenden Gesellschaft von zunehmender Dringlichkeit. Die geschwächten Knochen der Betroffenen werden anfällig auf Brüche, welche nicht nur schmerzhaft und mit langwieriger Behandlung verbunden sind, sondern auch entsprechend grosse Kosten für das Gesundheitswesen verursachen.

Neue Ansätze zur Behandlung von Knochenbrüchen werden fortlaufend entwickelt. Besser wäre es jedoch, würden diese Brüche von Anfang an verhindert. Der Schlüssel zur besseren Prävention liegt in einer genaueren Bestimmung derjenigen Personen, welche gefährdet sind. Zurzeit wird das Frakturrisiko anhand der mit Doppelröntgenabsorptiometrie ermittelten Knochendichte abgeleitet. Eine genauere Bestimmung ist mittels neuer Bildgebungsverfahren (hochaufgelöste periphere Computertomographie) und der Finite-Elemente-Methode möglich, weil in diesem Fall die Mikrostruktur mitberücksichtigt wird. Allerdings sind sämtliche dieser Verfahren dadurch eingeschränkt, dass sie das Frakturrisiko am Tag der Untersuchung bestimmen und dadurch begrenzt aussagekräftig für eine Prognose des Zukunftszustands sind.

Computersimulationen des Knochenumbaus können die Veränderungen der Mikrostruktur bestimmen, waren bisher allerdings nur auf Datensätze kleinerer Biopsien möglich. Damit eine sorgfältige Frakturbestimmung möglich ist, müssen Knochen weitgehend vollständig betrachtet werden. Das Hauptziel der vorliegenden Doktorarbeit war die Entwicklung eines Verfahrens für die Simulation von Knochenumbau mit mechanischer Rückkopplung auf Datensätzen mit hochaufgelösten Knochen sowie eine Veranschaulichung der Einsatzmöglichkeiten

bei der Erforschung von Osteoporose und neuer Behandlungsansätze.

Als erstes wurde ein Verfahren für die Simulation von Knochenumbau entwickelt, welches die Berechnung auf Datensätzen mit grossem Umfang ermöglicht. Dieses beinhaltet die Berechnung von Patientspezifischen Randbedingungen für die Simulation von Knochenumbau unter physiologischer Belastung. Die lokale mechanische Belastung wurde mittels mikro-Finite-Elemente-Analyse ermittelt mit Modellen bestehend aus bis zu 365 Millionen Elementen. Auf zwei Wirbelkörper wurde gesunder Knochenumbau über eine Dauer von zehn Jahren realistisch simuliert, wie der Vergleich von morphometrischen Parameter gezeigt hat. Das angewandte Verfahren wurde in einer Reihe von Versuchen ausführlich beurteilt, von der Wirkungsweise auf einzelne Trabekel bis auf die Notwendigkeit von komplexen Randbedingungen. Zusätzlich wurde der Einfluss der Auflösung der Datensätze auf die Berechnung der lokalen mechanischen Belastung ermittelt, wobei gezeigt wurde, dass in unserem Fall eine Auflösung von  $43.5\ \mu\text{m}$  hinreichend ist.

In einer ersten Anwendung wurde das Potenzial des entwickelten Verfahrens in der Simulation von osteoporotischem Knochenschwund auf sieben ganzer menschlichen Wirbelkörper gezeigt. Fünf Parametersätze für die Simulation von Osteoporose wurden entwickelt und dasjenige mit der höchsten Übereinstimmung im Vergleich zu experimenteller Messungen erörtert. Es hat sich herausgestellt, dass insbesondere eine Reduktion der Zellsensibilität zu realistischen Resultaten führt. Die Wirkung des Knochenschwunds auf die mechanische Belastbarkeit wurde durch die Steifigkeit sowie der Bruchfestigkeit ermittelt und zeigte realistische Veränderungen über die Dauer von 30 Jahren Osteoporose. Im Durchschnitt ist ein Knochenverlust von 31% simuliert worden. Die morphometrischen Grössen wurden im Vergleich zu Experimenten gut nachgebildet, allerdings sind die Reduktion der Trabekulärzahl (-5.8%) und die Zunahme des Trabekelabstandes (+7.8%) etwas konservativ ausgefallen. Die Steifigkeit ist grösstenteils erhalten worden (-7.9%), die Bruchlast gegenüber ungewöhnlichen Belastungen hat jedoch von 13% unter der Bruchlast bei normaler Belastung innerhalb von 30 Jahren auf 17% abgenommen.

In einer zweiten Anwendung wurde das Verfahren verwendet, um die Langzeitwirkung von präventiver Augmentation mit Knochenzement auf die Mikrostruktur in osteoporotischem Knochen zu erforschen. Es wurde insbesondere die Auswirkung der Wahl des Zeitpunktes der Intervention und des Augmentationsvolumens untersucht. Grössere Volumina führten zu erhöhter Abschirmung der Belastung und somit zu erhöhtem Knochenschwund (-11%). Die mechanische Belastbarkeit wurde langfristig jedoch dennoch erhöht, trotz grösseren Knochenrückgangs (+50% im Fall der grossen Augmentationsvolumina). Der Zeitpunkt der

Intervention hatte keinen Einfluss auf die Belastbarkeit. Das Gewebe wurde insbesondere in der Nähe des Zements gut erhalten, wo die Abnahme nur 12% betragen hat, gegenüber 23% beim Nichtaugmentierten Knochen. Diese Resultate ermöglichen einen ersten Einblick in die Langzeitfolgen der Intervention und lassen daraus schliessen, dass der Eingriff weniger schädlich für die Mikrostruktur ist, als ursprünglich angenommen werden konnte..

Seit vielen Jahren schon wird Knochenumbau simuliert, bisher jedoch bloss auf kleinen Strukturen. Die vorliegende Doktorarbeit hat gezeigt, dass Simulationen auf grossen Datensätzen möglich sind indem Knochenumbau mit mechanischer Rückkopplung realistisch auf hochaufgelösten Bildern menschlicher Wirbelkörper berechnet wurde. Das Potenzial solcher Simulationen wurde am Beispiel von Knochen-schwund und präventiver Augmentation veranschaulicht. Auch wenn die Biologie im vorliegenden Verfahren stark vereinfacht wird, haben solche Simulationen die Möglichkeit die Bestimmung des Frakturrisikos zu verbessern und bessere Einblicke in neue Behandlungsmöglichkeiten zu geben.



# Riassunt

I'l minchadi resentinsa l'ossa scu üna chosa statica. In vardet as tratta que però dad ün materiel dinamic chi's transfuorma cuntinuedamaing tenor ün process chi vain numno remodelraziun da l'ossa. Cellas chi fuorman e cellas chi resorbeschan ossa adattan la microstructura chi tres que vain optimeda per ch'ella riva da sustgnair las chargias quotidiana. Scha l'equiliber traunter crescer e resorber vain disturbo, po que avair per conseguenza üna perdita da l'ossa, scu per exaimpel i'l cas da l'osteoporosa. Quista malatia pertuocha surtuot glieud pü veglia. Causa als müdamaints demografics dvaint'la dimena viepü relevanta per nossa societad. L'ossa indeblida es suottaposta a fracturas chi nu sun be dulurusas, ma chi dumandan üna lungia reconvalescenza e chi chaschunan grands cuosts a la sanited publica.

A vegnan successivmaing preschantedas novas idejas pel trattamaint da fracturas. L'ideel füss però dad impedir quistas da prüm innò. Decisiv per üna megltra prevenziun füss surtuot üna classificaziun detagliada da las persunas chi sun periclitadas. Hozindi vain il ris-ch dedüt da la spessüra da l'öss chi vain imsüreda cun üna metoda speciela da radiografias numneda DEXA. üna megltra classificaziun es uossa pussibla grazcha a mezs pü moderns, scu per exaimpel la tomografia computeriseda periferica ad ota resoluziun in cumbinaziun culla metoda dad elemaints finits. In quist cas as resguarda nempe eir la microstructura. Quistas metodos haun però tuottüna üna restricziun cumünaivla, nempe ch'ellas determineschan il ris-ch da fracturas il di da l'examinaziun e paun dunque prevzair il ris-ch i'l futur be in müd limitu.

Simulaziuns da la remodelraziun da l'ossa sun capablas da descriver ils müdamaints da la microstructura. Fin uossa d'eiran quistas però be pussiblas cun agüd d'ün set da datas da pitschnas biopsias. Per pussibilter üna determinaziun dal ris-ch da fracturas es que però important da resguarder l'öss in sia totalited. Il böt principel da quista dissertaziun d'eira da svilupper üna metoda per simuler la remodelraziun da l'ossa tres reacziun mecanica cun sets da datas dad öss cun ota resoluziun ed al listess mumaint dad illustrer pussibiliteds d'adöver illa perscrutaziun da l'osteoporosa e da novs trattamaints.

In üna prüma part es gnida sviluppada üna metoda per simuler la remodelraziun

da l'ossa cun sets da datas a larg volumen. Quista cuntegna la calculaziun da cundiziuns periferas individuelas per la simulaziun da remodelraziun suot cundiziuns fisiologicas. La chargia mecanica locala es gnida eruida cun micro-elemaints finits in models chi consistan da fin passa 365 milliuns elemaints. Per la düreda da 10 ans es gnida simuleda realisticamaing la remodelraziun da l'ossa in duos spondils inters. La metoda es gnida valüteda i'l cuors da divers experimaints. Mincha pass es gnieu analiso, da l'effet sün singuls trabecula fin a la necessited da cundiziuns periferas complexas. Impü es gnieu controllo l'effet da la resoluziun dals sets da datas sül calcul da la chargia mecanica locala. Ad es gnieu demusso cha la resoluziun da 43.5 micrometers taundscha per quist gener da simulaziuns.

In üna prüm'applicaziun es gnieu preschanto il potenziel da quista disposiziun da remodelraziun da l'ossa in üna simulaziun da perdita da l'öss causa l'osteoporosa in üna gruppa da sets da datas ad ota resoluziun cuntgnind set spondils. In tuot sun gnieu examinatos tschinch sets da parameters. La megltra congruenza cun experimaints es gnida raggiunta cun redüer la sensitivited da las cellas. La cumpetenza biomecanica es gnida eruida in detagl. Quist process cumpiglia calculaziuns da la dürezza da l'öss e la forza da fracturas e demuossa cha las simulaziuns rapreschaintan realisticamaing decadenzas da la structura chi correspuondan ad üna perioda dad osteoporosa da passa trenta ans. In media haun ils spondils pers 30.7% da la massa. Indices morfometrics sun gnieu represchaintos bain, eir scha la reducziun da la cifra da *trabeculus* (-5.8%) ed il spazzi traوتر *trabeculi* es gnieu (+7.8%) sun gnieu suottestimos. La dürezza es per granda part gnida conservada (-7.9%), ma la charga da fracturas es gnida redotta ulteriuramaing düraunt l'osteoporosa.

In üna seguond'applicaziun s'ho druvo las simulaziuns da remodelraziun da l'ossa per analiser ils effects dad augmentaziun preventiva cun cement a lungia düreda, l'uschè numneda vertebroplastia preventiva, sül l'ossa osteoporotica. In quist connex sun gnieu examinatos l'effet dal volumen d'augmentaziun scu eir l'effet dal temp da l'intervenziun. Ils grands volumens haun gieu per consequenza üna perdita da l'ossa supplementera (-11%). A medem temp es però eir gnida ingrandida la stabilitad mecanica da l'öss augmento (+50% in cas da largs volumens). In quist regard es gnieu constatato cha'l temp da l'intervenziun nun ho üngiün effet sün la stabilitad da l'öss. L'ossa s'ho impustüt mantgnida intuorn il materiel d'augmentaziun, inua cha la massa es gnida redotta per 12% in conquel cun 23% tar l'öss sainza cement. Grazcha a quists resultats es, per la prüm vouta, sto pussibel da prevzair effects da vertebroplastia preventiva a lungia düreda e da musser sü cha l'intervenziun es main dannavla scu supponieu fin in uossa.

Daspö ans staun simulaziuns da remodelraziun da l'ossa a nossa disposiziun. Fin

uossa però unicamaing per pitschens sets da datas. Illa seguainta dissertaziun sun quistas simulaziuns gnidas amegldredas uschè cha eir grands sets da datas haun pudieu gnir simulos. Perdita da l'ossa es gnida simuleda realisticamaing e per la prüma vouta es sto pussibel da preschanter effets da lungia düreda vi da l'öss zieva ün'augmentaziun cun cement. Cun agüd d'ün model bainschi simplificho, es gnieu cumpruvo cha quistas simulaziuns chi pussibilteschan da prevzair il ris-ch da fracturas ed eir da cuntinuer culla perscrutaziun scientifica in regard al trattamaint da ruottadüras haun ün grand potenziel.





# Chapter 1

## Introduction

### 1.1 Thesis motivation

#### 1.1.1 Osteoporosis and vertebral fractures

Osteoporosis is a widespread disease affecting mostly the elderly population. It is characterized by excessive bone loss resulting in fractures because of the reduction in bone strength [1]. Osteoporotic bone fractures lead to significant morbidity; severe fractures in the hip and spine are also associated with increased mortality [2]. While it is in the first place painful for the concerned, because of the frequent occurrence of these fractures and because of the often extensive treatments needed, osteoporosis is also a major socioeconomic burden. Changes in demography are likely going to tighten this issue, as advancements in modern medicine allow many members of our society to reach old age. While there are about 810 million people aged 60 years or older today, by 2050 this number is expected to surpass two billion [3]. Recent estimates show that osteoporotic fractures cost European healthcare systems €36 billion every year, and with the rising population of the elderly, these costs are expected to more than double in 2050 [4].

An important part of this financial burden is due to vertebral fractures. Estimations of clinically diagnosed vertebral fractures show that the lifetime risk of a vertebral fracture at the age of 50 years can be more than 15% for women [5]. Worldwide, more than 1.4 million vertebral fractures are estimated to happen every year - that is; a fracture occurs every 23 seconds [6]. The yearly costs for osteoporotic vertebral fractures sum up to a total of €719 million in Europe only [4]. Research in novel treatment options for spine fractures might therefore not only help reducing pain and impairments for patients, but also support controlling rising costs in general healthcare.

Vertebral compression fractures are mostly found in weak osteoporotic bone, be-

cause of the deterioration of the trabecular microstructure in the course of the disease [7,8]. Compression fractures are often wedge-shaped, with the anterior part of the vertebral body compressed. The fractures are painful because of the vicinity to the vertebral chord and the subsequent bad posture leads to additional pain. Patients typically need bed rest and are treated with medication [9,10]. Not only is there need for better treatment of patients suffering such fractures, where particular hope lays in bone augmentation procedures - but preventing fractures right from the start must be the primary goal.

### **1.1.2 Cement augmentation for treatment and prevention of vertebral compression fractures**

Advances in biomedical engineering give hope for a more widespread use of new intervention approaches that will help to reduce the period of bed rest, pain and the need for pharmacologic treatment of vertebral fractures or even ideally prevent them. Particularly promising are bone augmentation procedures where bone cement, commonly poly-methyl-methacrylate (PMMA), is injected percutaneous into the fractured vertebral body. These interventions, referred to as vertebroplasty, are minimally invasive and not only stabilize the spine, but lead to pain relief [11–15]. However, recent studies question the beneficial effect of the intervention [16,17]. Reported complications are cement leakage [14] and fractures of the adjacent vertebrae as a result of increased stresses [18,19]. As a possibility to avoid such fractures of the adjacent vertebrae, preventive vertebroplasty has been suggested [20]. If the fracture risk in the spine can be better estimated for concerned patients, preventive vertebroplasty could possibly also be used for patients with no previous fracture record [19]. In order to be able to advice a patient for preventive vertebroplasty, however, more knowledge about the long-term effects of augmentation on the bone microstructure is needed.

### **1.1.3 Bone strength assessment and fracture risk prediction**

Today, fracture risk is commonly determined by dual-energy X-ray absorptiometry [21], but this technique is not able to capture the bone microstructure and thus the microstructural changes occurring during osteoporotic bone loss, although such deteriorations of the microstructure greatly affect bone strength and thus fracture risk. Assessment of bone microstructure is however possible with micro-computed tomography ( $\mu$ CT) of biopsies or of small animals providing resolutions from 1-10  $\mu$ m *in vitro* or *in vivo* respectively. In patients, high-resolution peripheral quantitative

computed tomography (HR-pQCT) allows to image the three-dimensional trabecular microstructure with high fidelity providing resolutions of up to  $50\text{ }\mu\text{m}$  *in vivo* [22]. Feeding this image data into micro finite element ( $\mu\text{FE}$ ) models allows a highly accurate estimation of patient specific bone strength and fracture risk [23].

However, these methods assess the current fracture risk, but do not take into account the dynamic mechanobiology of the bone tissue and that bones change their structure and properties over time. In order to better estimate future fracture risk of a bone, we would need to translate the bone microstructure in a future state, which would greatly improve the identification of patients at high risk of fractures. Estimating the future state of the bone microstructure, however, is complicated as there is uninterrupted turnover and reorganization of the bone matrix happening in the process known as bone remodeling [24]. Guided by mechanosensitive osteocytes, bone forming osteoblasts and bone resorbing osteoclasts continuously renew the structure and adapt it to withstand the most prevalent daily loads [25]. This mechanical regulation leads to the optimized orientation of the trabecula in healthy bone [26]. The mechanical feedback is described by the mechanostat theory which postulates that tissue adaptation is a consequence of the magnitude of a local mechanical signal [27]. Experimental evidence to support these findings has been found *in vivo* for animals [28,29] and humans [30]. While the mechanoregulation allows the bone to adapt to new loading patterns in healthy bone and maintain the mechanical stability [31], in the case of osteoporosis, however, the fragile equilibrium is shifted towards disproportional net resorption weakening the bone.

Computer predictions of microstructural changes of the bone are classified as bone remodeling simulations. In the past years, several attempts of mechanically driven remodeling of trabecular bone have been presented [31–34]. Remodeling simulations based on  $\mu\text{CT}$  derived human bone geometries have been restricted to biopsies [33,34], but accurate strength assessment necessitates whole bone microstructural analysis [35,36]. Thus, if we want to use remodeling simulations for fracture prediction, we need to overcome the barriers currently preventing bone remodeling simulations of whole bones.

#### 1.1.4 *In silico* bone biology in augmented vertebrae

Computational modeling of bone augmentation in the spine has so far mainly been focused on strength prediction [18,37–44]. Up to now, no models on *in silico* prediction of mechanobiology in augmented spines have been published, possibly because of the difficulty to simulate the biological effects of the treatment. Thermal necrosis due to the cement polymerization is known to occur [9,45]. Also, a large amount of

the bone marrow, which plays a crucial role in bone biology is removed [46]. There is still debate whether there are any biological processes going on in the augmented part of the bone, but experimental research reported that bone is viable and bone remodeling occurs [47–50]. However, experimental methods are invasive, studies with animals or humans are costly and can usually only cover a short time period. With computational models we could avoid these issues and potentially improve our understanding of the long-term biology of augmented bone.

## 1.2 Thesis aims

Large-scale simulations predicting future remodeling processes of whole human bones give new perspectives both in fracture risk assessment as well as in treatment planning. The global aim of this thesis was to develop a framework capable of performing large-scale simulations of load-adaptive bone remodeling in human vertebrae. In the last years, technological development made high resolution imaging of large bone structures, such as whole vertebrae, possible. We aimed to investigate the potential of using large-scale microstructural imaging in combination with powerful computational systems to assess changes in the microstructure and the mechanical stability as well as to test the possible outcome to augmentation treatment.

Specifically, the following three aims were defined:

- Aim 1: Development of large-scale simulations of load-adaptive bone remodeling in whole human vertebrae.** Today, bone remodeling simulations with mechanical feedback are limited to human biopsies or small animal bones. The main reasons are limitations in computational resources as well as challenges with the definition of accurate boundary conditions to calculate the mechanical signals for such models. We therefore aim to enhance a previously proposed bone remodeling framework to run bone adaptation simulations of large-scale whole human vertebrae. They will include the calculation of local mechanical stimuli in bones under physiological load by means of  $\mu$ FE. In addition, bone remodeling will run on high-resolution human trabecular bone for the calculation of long-term effects. The stability for long-term simulations as well as the mechanisms of local trabecular realignment will be assessed.
- Aim 2: Simulations of osteoporotic bone loss in native whole human vertebrae.** The main concern in fracture risk prediction are not healthy bones, but bones affected by osteoporosis. We therefore aim to realistically simulate postmenopausal osteoporotic bone loss in long-term simulations of load-

adaptive bone remodeling in whole human vertebrae. This will include investigation of the model parameters and the development of adequate assumptions for the imbalance in bone turnover. The model will be evaluated against experimental results both visually and quantitatively.

**Aim 3: Simulations of microstructural bone adaptation in augmented vertebrae.** In order to evaluate the potential of preventive bone augmentation, the bone remodeling framework developed in the previous aims will be used to show advantages and threads of simulated cement augmentation compared to native bone. We will investigate different augmentation strategies as well as the influence of the time point of the intervention. We will assess whether patterns of bone formation and resorption can be identified and try to give recommendations for possible preventive bone augmentation.

Altogether, this research will show the potential of in silico bone adaptation of human vertebrae in native and treated human bones. It will provide computational tools for simulations of mechanobiology in whole bones and eventually help better predicting fracture risk and improve treatment planning of vertebroplasty.

## 1.3 Thesis outline

This thesis is structured into 5 chapters. While the character of chapter 1, 2 and 5 is on an overview level, deeper focus is provided in chapter 3 and 4.

**Chapter 1:** This chapter presents the motivation, specific aims and the outline of the thesis.

**Chapter 2:** In this chapter, the reader is introduced into the current state of computational modeling of bone augmentation in the spine. In a literature review, the socioeconomic burden of vertebral fractures is described in detail and advantages and threats of bone augmentation are discussed. It is reported, how the bone augmentation procedure is analyzed by means of computer simulations. In addition, an overview of strength prediction models in the spine is given, summarizing approaches from continuum-models to microstructural models. In a final section, computational modeling for in silico prediction of mechanobiology is reviewed, with a focus on augmented spines.

**Chapter 3:** This method chapter describes how the framework for large-scale simulations of load-adaptive bone remodeling in whole human vertebrae was set

up and evaluated in multiple studies.  $\mu$ FE analysis for the high-resolution human bone scans is set up and a bone loading estimation algorithm incorporated into the framework. This allows large-scale simulations of load-adaptive bone remodeling in whole human vertebrae with the estimated physiological loading. Healthy bone adaptation is simulated on two whole human vertebrae for the duration of 10 years revealing realistic homeostatic bone adaptation. On artificial trabeculae, the mechanisms of local trabecular realignment of the algorithm is evaluated in a well-controlled environment. The necessary image resolution of the  $\mu$ FE model is assessed on trabecular subvolumes. Finally, the effect of various boundary conditions on the preservation of the microstructure is investigated and re-adaptation of the microstructure shown.

**Chapter 4:** The methods described in the previous chapter are applied to two cases of large-scale simulations of load-adaptive bone remodeling. In a first part, osteoporotic bone loss is simulated in whole human vertebrae. Starting from homeostatic bone remodeling, five model parameter sets for osteoporotic bone loss are proposed and evaluated on a single vertebra. The best fitting parameter set to experimental results is chosen to simulate osteoporotic bone loss from the age of 50 to 80 years in a group of seven whole vertebrae. In a second part, the model is applied to clinical scenarios of preventive bone augmentation to investigate long-term effects of the intervention. We investigate the effects of the time-point of bone augmentation as well as the augmentation in the long-term on bone morphometry and mechanical stability. Specific attention is given to stress-shielding or stress-raisers and the influence on the whole organ mechanical stability.

**Chapter 5:** In this final chapter, the work of the thesis is synthesized and major findings summarized. The additional value for the community is discussed, but limitations are addressed at the same time. The chapter is concluded with an outlook on future work.

## References

- [1] P. Sambrook and C. Cooper. Osteoporosis. *Lancet*, 367(9527):2010–8, 2006.
- [2] C. Holroyd, C. Cooper, E. Dennison. Epidemiology of osteoporosis. *Best Pract Res Clin Endocrinol Metab*, 22(5):671–85, 2008.

- [3] United-Nations. Population ageing and development. *Department of Economic and Social Affairs, Population Division, New York, NY 10017, USA, www.unpopulation.org*, 2012.
- [4] J. A. Kanis and O. Johnell. Requirements for dxa for the management of osteoporosis in europe. *Osteoporos Int*, 16(3):229–38, 2005.
- [5] O. Johnell and J. Kanis. Epidemiology of osteoporotic fractures. *Osteoporos Int*, 16 Suppl 2:S3–7, 2005.
- [6] O. Johnell and J. A. Kanis. An estimate of the worldwide prevalence and disability associated with osteoporotic fractures. *Osteoporos Int*, 17(12):1726–33, 2006.
- [7] M. Kleerekoper, A. R. Villanueva, J. Stanciu, D. S. Rao, A. M. Parfitt. The role of three-dimensional trabecular microstructure in the pathogenesis of vertebral compression fractures. *Calcif Tissue Int*, 37(6):594–7, 1985.
- [8] R. S. Weinstein and S. Majumdar. Fractal geometry and vertebral compression fractures. *J Bone Miner Res*, 9(11):1797–802, 1994.
- [9] M. P. Bostrom and J. M. Lane. Future directions. augmentation of osteoporotic vertebral bodies. *Spine (Phila Pa 1976)*, 22(24 Suppl):38S–42S, 1997.
- [10] M. C. Nevitt *et al.* The association of radiographically detected vertebral fractures with back pain and function: a prospective study. *Ann Intern Med*, 128(10):793–800, 1998.
- [11] L. Alvarez *et al.* Percutaneous vertebroplasty: functional improvement in patients with osteoporotic compression fractures. *Spine (Phila Pa 1976)*, 31(10):1113–8, 2006.
- [12] G. C. Anselmetti *et al.* Pain relief following percutaneous vertebroplasty: results of a series of 283 consecutive patients treated in a single institution. *Cardiovasc Intervent Radiol*, 30(3):441–7, 2007.
- [13] J. D. Barr, M. S. Barr, T. J. Lemley, R. M. McCann. Percutaneous vertebroplasty for pain relief and spinal stabilization. *Spine (Phila Pa 1976)*, 25(8):923–8, 2000.
- [14] P. A. Hulme, J. Krebs, S. J. Ferguson, U. Berlemann. Vertebroplasty and kyphoplasty: a systematic review of 69 clinical studies. *Spine (Phila Pa 1976)*, 31(17):1983–2001, 2006.

- [15] C. A. Klazen *et al.* Vertebroplasty versus conservative treatment in acute osteoporotic vertebral compression fractures (vertos ii): an open-label randomised trial. *Lancet*, 376(9746):1085–92, 2010.
- [16] R. Buchbinder *et al.* A randomized trial of vertebroplasty for painful osteoporotic vertebral fractures. *N Engl J Med*, 361(6):557–68, 2009.
- [17] D. F. Kallmes *et al.* A randomized trial of vertebroplasty for osteoporotic spinal fractures. *N Engl J Med*, 361(6):569–79, 2009.
- [18] G. Baroud, J. Nemes, P. Heini, T. Steffen. Load shift of the intervertebral disc after a vertebroplasty: a finite-element study. *Eur Spine J*, 12(4):421–6, 2003.
- [19] P. A. Hulme, S. K. Boyd, P. F. Heini, S. J. Ferguson. Differences in endplate deformation of the adjacent and augmented vertebra following cement augmentation. *Eur Spine J*, 18(5):614–23, 2009.
- [20] C. H. Yen, M. M. Teng, W. H. Yuan, Y. C. Sun, C. Y. Chang. Preventive vertebroplasty for adjacent vertebral bodies: a good solution to reduce adjacent vertebral fracture after percutaneous vertebroplasty. *AJNR Am J Neuroradiol*, 33(5):826–32, 2012.
- [21] J. A. Kanis *et al.* Assessment of fracture risk and its application to screening for postmenopausal osteoporosis - synopsis of a who report. *Osteoporosis International*, 4(6):368–381, 1994.
- [22] R. Krug, A. J. Burghardt, S. Majumdar, T. M. Link. High-resolution imaging techniques for the assessment of osteoporosis. *Radiol Clin North Am*, 48(3):601–21, 2010.
- [23] W. Pistoia *et al.* Estimation of distal radius failure load with micro-finite element analysis models based on three-dimensional peripheral quantitative computed tomography images. *Bone*, 30(6):842–8, 2002.
- [24] E. F. Eriksen, F. Melsen, E. Sod, I. Barton, A. Chines. Effects of long-term risedronate on bone quality and bone turnover in women with postmenopausal osteoporosis. *Bone*, 31(5):620–5, 2002.
- [25] D. B. Burr. Targeted and nontargeted remodeling. *Bone*, 30(1):2–4, 2002.
- [26] J. Wolff. The classic: on the inner architecture of bones and its importance for bone growth. 1870. *Clin Orthop Relat Res*, 468(4):1056–65, 2010.



- [27] H. M. Frost. Bone’s mechanostat: a 2003 update. *Anat Rec A Discov Mol Cell Evol Biol*, 275(2):1081–101, 2003.
- [28] F. A. Schulte *et al.* Local mechanical stimuli regulate bone formation and resorption in mice at the tissue level. *PLoS One*, 8(4):e62172, 2013.
- [29] T. Sugiyama *et al.* Bones’ adaptive response to mechanical loading is essentially linear between the low strains associated with disuse and the high strains associated with the lamellar/woven bone transition. *J Bone Miner Res*, 27(8):1784–93, 2012.
- [30] P. Christen *et al.* Bone remodelling in humans is load-driven but not lazy. *Nat Commun*, 5:4855, 2014.
- [31] R. Ruimerman, P. Hilbers, B. van Rietbergen, R. Huiskes. A theoretical framework for strain-related trabecular bone maintenance and adaptation. *Journal of Biomechanics*, 38(4):931–941, 2005.
- [32] T. Adachi, K. Tsubota, Y. Tomita, S. J. Hollister. Trabecular surface remodeling simulation for cancellous bone using microstructural voxel finite element models. *Journal of Biomechanical Engineering-Transactions of the Asme*, 123(5):403–409, 2001.
- [33] P. Christen *et al.* Patient-specific bone modelling and remodelling simulation of hypoparathyroidism based on human iliac crest biopsies. *J Biomech*, 45(14):2411–6, 2012.
- [34] P. Mc Donnell, N. Harrison, M. A. Liebschner, P. E. Mc Hugh. Simulation of vertebral trabecular bone loss using voxel finite element analysis. *J Biomech*, 2009.
- [35] A. J. Fields, S. K. Eswaran, M. G. Jekir, T. M. Keaveny. Role of trabecular microarchitecture in whole-vertebral body biomechanical behavior. *J Bone Miner Res*, 24(9):1523–30, 2009.
- [36] E. Perilli *et al.* Failure strength of human vertebrae: prediction using bone mineral density measured by dxa and bone volume by micro-ct. *Bone*, 50(6):1416–25, 2012.
- [37] Y. Chevalier *et al.* Cement distribution, volume, and compliance in vertebroplasty: some answers from an anatomy-based nonlinear finite element study. *Spine (Phila Pa 1976)*, 33(16):1722–30, 2008.

- [38] T. S. Keller, V. Kosmopoulos, I. H. Lieberman. Vertebroplasty and kyphoplasty affect vertebral motion segment stiffness and stress distributions: a microstructural finite-element study. *Spine (Phila Pa 1976)*, 30(11):1258–65, 2005.
- [39] V. Kosmopoulos and T. S. Keller. Damage-based finite-element vertebroplasty simulations. *Eur Spine J*, 13(7):617–25, 2004.
- [40] V. Kosmopoulos, T. S. Keller, C. Schizas. Early stage disc degeneration does not have an appreciable affect on stiffness and load transfer following vertebroplasty and kyphoplasty. *Eur Spine J*, 18(1):59–68, 2009.
- [41] M. A. Liebschner, W. S. Rosenberg, T. M. Keaveny. Effects of bone cement volume and distribution on vertebral stiffness after vertebroplasty. *Spine (Phila Pa 1976)*, 26(14):1547–54, 2001.
- [42] A. Polikeit, L. P. Nolte, S. J. Ferguson. The effect of cement augmentation on the load transfer in an osteoporotic functional spinal unit: finite-element analysis. *Spine (Phila Pa 1976)*, 28(10):991–6, 2003.
- [43] V. N. Wijayathunga *et al.* Development of specimen-specific finite element models of human vertebrae for the analysis of vertebroplasty. *Proc Inst Mech Eng H*, 222(2):221–8, 2008.
- [44] L. Zhang, G. Yang, L. Wu, B. Yu. The biomechanical effects of osteoporosis vertebral augmentation with cancellous bone granules or bone cement on treated and adjacent non-treated vertebral bodies: a finite element evaluation. *Clin Biomech (Bristol, Avon)*, 25(2):166–72, 2010.
- [45] H. Deramond, N. T. Wright, S. M. Belkoff. Temperature elevation caused by bone cement polymerization during vertebroplasty. *Bone*, 25(2 Suppl):17S–21S, 1999.
- [46] T. Hirano and K. Iwasaki. Bone-marrow plays a role in bone metabolism - histomorphometry of iliac bone in postmenopausal women. *Calcified Tissue International*, 51(5):348–351, 1992.
- [47] C. W. Kim, J. Minocha, C. E. Wahl, S. R. Garfin. Response of fractured osteoporotic bone to polymethylacrylate after vertebroplasty: case report. *Spine J*, 4(6):709–12, 2004.
- [48] N. Kobayashi *et al.* Histological and radiographic evaluation of polymethylmethacrylate with two different concentrations of barium sulfate in a sheep vertebroplasty model. *J Biomed Mater Res A*, 75(1):123–7, 2005.

- [49] J. Krebs *et al.* Effect of vertebral cement augmentation with polymethylmethacrylate on intervertebral disc and bone tissue. *J Biomed Mater Res B Appl Biomater*, 2011.
- [50] D. Togawa, T. W. Bauer, I. H. Lieberman, S. Takikawa. Histologic evaluation of human vertebral bodies after vertebral augmentation with polymethylmethacrylate. *Spine (Phila Pa 1976)*, 28(14):1521–7, 2003.



## Chapter 2

### Background



## 2.1 Computational modelling of bone augmentation in the spine

Sandro D. Badilatti<sup>1</sup>, Gisela A. Kuhn<sup>1</sup>, Stephen J. Ferguson<sup>1</sup> and Ralph Müller<sup>1</sup>

<sup>1</sup>Institute for Biomechanics, ETH Zurich, 8093 Zurich, Switzerland

### published as:

S. D. Badilatti, G. A. Kuhn, S. J. Ferguson and R. Müller. Review Article - Computational modelling of bone augmentation in the spine. *J Orthop Transl*, 2015

Reprinted with permission and in compliance with the publisher copyright policy.

### Abstract:

Computational models are gaining importance not only for basic science, but also for the analysis of clinical interventions and to support clinicians prior to intervention. Vertebroplasty has been used to stabilize compression fractures in the spine for years, yet there are still diverging ideas on the ideal deposition location, volume, and augmentation material. In particular, little is known about the long-term effects of the intervention on the surrounding biological tissue. This review aims to investigate computational efforts made in the field of vertebroplasty from the augmentation procedure to strength prediction and long-term in silico bone biology in augmented human vertebrae. While there is ample work on simulating the augmentation procedure and strength prediction, simulations predicting long-term effects are lacking. Recent developments in bone remodelling simulations have the potential to show adaptation to cement augmentation and, thus, close this gap.

### Keywords:

Bone Remodelling, Computational Biology, Finite Element Analysis, Spinal Fractures, Vertebroplasty

### 2.1.1 Introduction

Demographic changes are among the most important challenges for our society in the 21st century. Advancements in modern medicine have reduced mortality rates and many members of our society are expected to reach old age. While there are about

810 million persons aged 60 years or older today, by 2050 this number is expected to surpass two billion [1]. As a consequence, the number of workers available to support one elderly person will decrease from eight to four in only 40 years [1]. If we want to ensure access to effective healthcare for the elderly population, we will be forced to control and reduce emerging costs. A key element will be the focus on the management of age-related diseases.

A particularly widespread disease among the elderly is osteoporosis - an illness that is characterized by a reduced bone mass and a concomitant increased fracture risk [2]. The morbidity of all osteoporotic bone fractures is substantial and the severe cases in the spine and hip are also coupled with elevated mortality [3]. Osteoporosis is a major problem for healthcare systems because these fractures are frequent and often need extensive treatment. Recent estimates show that osteoporotic fractures cost the European Union €36 billion every year, and these costs are expected to more than double by 2050 [4].

A significant share of the financial burden is due to vertebral fractures. Estimates of clinically diagnosed vertebral fractures show that the lifetime risk of vertebral fractures at the age of 50 can be more than 15% in women [5]. Worldwide, more than 1.4 million vertebral fractures are estimated to occur every year [6] - that is one fracture every 23 seconds. The yearly cost for osteoporotic fractures in the spine sum up to a total of €719 million in Europe alone [4]. Research in novel treatment options for spine fractures might therefore not only help reducing pain and impairments for patients, but also support controlling rising costs in general healthcare.

Vertebral compression fractures, mostly occurring in weak osteoporotic bone, are painful [7]. It is assumed that, in particular, the deterioration of the trabecular microstructure in the course of the disease leads to an increased fracture risk [8,9]. Patients typically need bed rest and are treated with medication [10]. However, advances in biomedical engineering give hope for a more widespread use of new intervention approaches that will help to reduce the period of bed rest, pain and the need for pharmacologic treatment or even ideally prevent fractures. A particular potential lays in bone augmentation procedures such as vertebroplasty because of the minimally invasive nature of these approaches. Vertebroplasty is an intervention where bone cement is injected percutaneously through a cannula into the fractured vertebral body to restore its mechanical stability [11]. With advancements in fracture risk assessment [12], potentially weak vertebrae can be detected and targeted prior to fracture. Thus, we hope in the future to use vertebroplasty to also prevent fractures by augmenting vertebral bodies that were previously defined as fragile.



Despite vertebroplasty being a straight-forward intervention, the close location of the vertebral bodies to vital organs and the spinal cord demands the reduction of side effects to an absolute minimum. Bone augmentation stabilizes the spine and leads to functional improvements [13,14]. In addition, pain relief is reported in most cases [13–17], although some studies could not confirm greater pain relief compared to conservative treatments [18,19]. The immediate complications reported with vertebroplasty are mainly connected to cement leakage [14], but it remains unclear what the long-term impact of the intervention is. A strong but controversial concern with bone augmentation in the long term is the occurrence of fractures in adjacent vertebrae due to the increased stiffness of the augmented vertebra [20,21].

Like in many other biomedical branches, the increased capability of computational tools opens new doors for the investigation of bone augmentation. Such tools allow not only studying the mechanisms of disorders, but also surgical treatments. Initially, computational models in musculoskeletal applications were based on idealised, simplified structures. Today, these models are typically based on image-derived geometries from computer tomography (CT) or magnetic resonance imaging and can thus be individualised to the specific patient [22]. In recent years, finite element (FE) analysis in particular has become a frequently used versatile, general purpose simulation tool. Not only does it allow a detailed description of the mechanical load transfer in the spine before and after vertebroplasty, but such simulations have the potential to predict optimal augmentation patterns and cement distribution for individual treatment planning. Advanced *in silico* experiments modelling the biology of the bone, can help to better understand the long-term risks and outcomes of augmentation interventions. This review aims to describe the efforts made in computational modelling of bone augmentation in the spine, focusing on the clinical intervention itself, the biomechanical situation after the treatment, and predictions of the long-term outcome.

### 2.1.2 Computational modelling of the bone augmentation procedure

Vertebroplasty is a minimally invasive intervention to restore and stabilize fractured vertebrae by augmenting the bone with cement, typically polymethylmethacrylate (PMMA). The bone cement is injected under local anaesthesia percutaneously through the back of the patient by means of a large-bore needle or cannula, directly into the vertebral body. The injection is monitored in real time by fluoroscopic guidance in order to assure deposition in the proper location as well as to avoid cement leakage. It is important to keep the patient resting during the subsequent

cement hardening period of about one hour [11, 23].

More advanced imaging techniques could allow not only a more precise deposition of the cement, but combined with computational methods they have the potential to help the surgeon in the planning of the intervention for each patient by predicting the best position of the needle for the cement placement and by defining the optimal filling volume. Moreover, such simulations would also help to select or develop cements optimized for a specific intervention.

A simple approach on the organ scale to define the incision point and angle for the injection needle is described by Kobayashi et al. [24]. Although it does not directly require computational tools, the method follows an algorithm and aims to target the middle of the cement deposition area and thus the needle position. On a horizontal CT scan at the level of the pedicles, the target is determined as the anterior one-third point along the median line. Incision point and angle are then derived by simulating the needle passing through the pedicle. The method assists treatment planning and allows a single incision for the bone augmentation.

A computational model of vertebroplasty including the needle incision and the cement injection is presented by Chui [25]. The model is designed for a virtual training setup and includes visual as well as haptic feedback. In order to be rendered in real-time, it is kept relatively simple, but still considers structures at tissue level. The resistance for the needle insertion is calculated in two phases; the cortical bone as a linear elastic material, the cancellous bone with the highly computationally efficient discrete element method, where trabeculae are simplified as single beams. The cement injection procedure [26] is based on a rheological model simulating bone cement flow through a branching-pipe network mimicking the trabecular network. The pressure drop in cement during injection is modelled with an improved version of the Hagen-Poiseuille law supplemented with a time and shear-rate dependent power law. It allows an accurate and fast estimation of the injection pressure during the virtual intervention training.

A few years earlier, Baroud and Yahia [27] established an FE rheological model to characterize the behaviour of cement flow. A modified power law was implemented, capable of modelling not only the pseudoplastic (shear rate dependent viscosity), but also the rheopectic (time dependent viscosity) behaviour of bone cements. The FE model was simulated as flow through an axi-symmetric tube and showed good agreement when compared to an analytical solution; however the simulation was limited to predicting the extravertebral flow, i.e. the cement flow through the cannula only.

The potential for patient-specific simulation of vertebroplasty was demonstrated in

preliminary work by Teo and colleagues [28], in which clinical computer tomography (CT) scan data was used to define the overall vertebral geometry and isotropic permeability of the trabecular bone. Permeability, assumed to vary proportionally with bone porosity, is a principal determinant of cement spreading velocity in a porous bone bed.

More elaborate models of the bone augmentation procedure have been described by Widmer [29–31]. The cement injection is simulated with a model taking into account both the cement flow and the displacement of the bone marrow in the porous trabecular network [29]. The cement dispersion is approximated with the “volume of fluid method“, a numerical method moving the object surface on a mesh by conserving both mass and volume. The fluid dynamics is governed by Darcy’s equation, relating cement flow rate to applied pressure differential through the permeability proportionality constant. The model was verified on spherical domains and was able to reproduce flow patterns with a known analytical solution. In follow-up work [30], the relationship between the permeability and structural parameters of trabecular bone was investigated. With a sufficiently high imaging resolution, permeability maps can be derived directly from the morphometrical parameters of the bone structure [31] and the cement injection can be simulated with the previously mentioned methods (Figure 2.1). When upscaling the pore-scale solution to continuum-scale, via a regression model built on morphometrical parameters available in clinical images, the validity of Widmer’s method for the prediction of the cement deposition pattern was shown [32]. With his multi-scale approach, it was possible to set up and validate a framework for the accurate simulation of cement spreading during bone augmentation, in a patient-specific fashion (Figure 2.2).

### 2.1.3 Computational modelling for strength prediction

#### Modelling the spine

The determination of mechanical strength of the spine after cement augmentation is a main focus both in *ex vivo* as well as in *in silico* experiments. During the intervention, the porous structure of cancellous bone is filled with a material differing in many ways from the extruded bone marrow. The load transfer will be changed not only within the augmented vertebra, but also throughout the whole spine. Although the reconstitution of strength or stiffness is unlikely the only determinant of a successful intervention, it gives a good idea on the degree of the increased stability as well as an indication about possible threads of overloading the adjacent vertebrae.

Also, here FE is typically used to predict the with model sizes ranging from

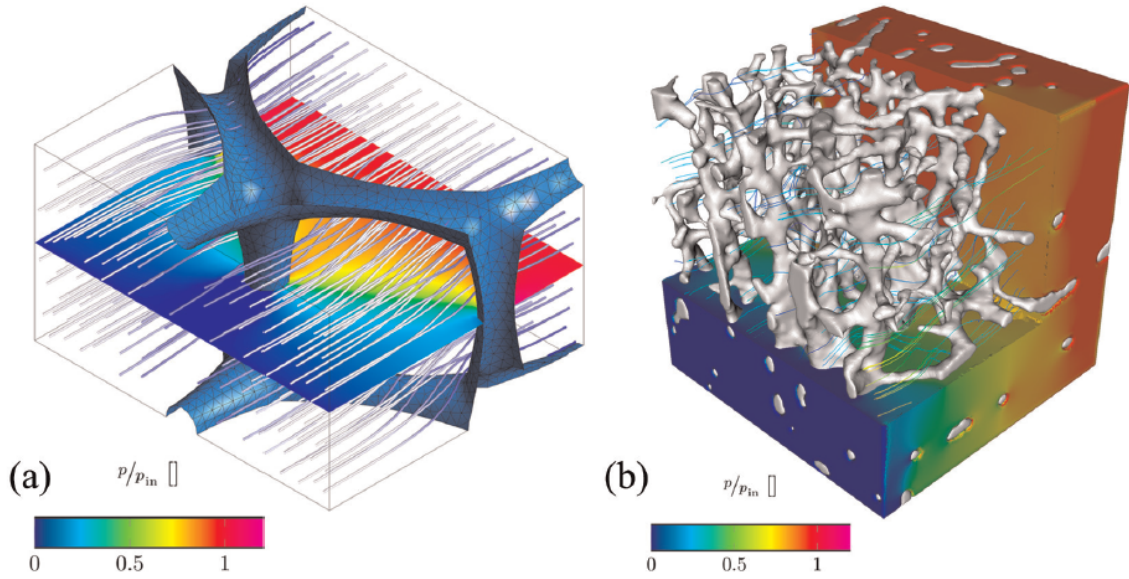


Figure 2.1: (a) Streamlines of the fluid virtually flowing through the unit cell and (b) a representative trabecular bone sample. (Figure reproduced from Widmer et al. [31] according to the guidelines of the publisher).

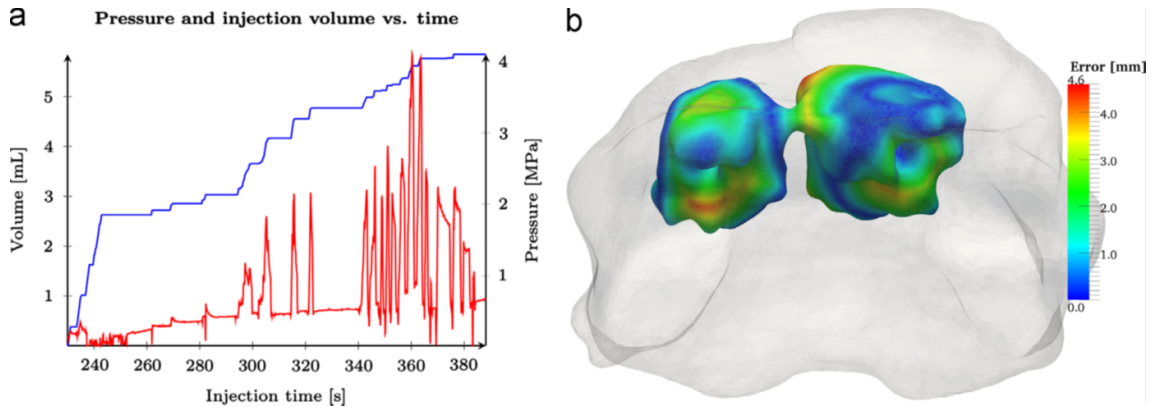


Figure 2.2: (a) demonstrates typical pressure and injection volume curves of a PMMA-based bone cement injection using the motor-driven delivery device. The recorded cement volume profile was subsequently used to drive the continuum-scale model. During the progress of the injection, the cement hardens and a higher injection pressure is needed to force the cement into the vertebral body. (b) Segmented experimental cement cloud colored by the prediction error of the continuum-scale model. The principal source of error is uncertainty in the location of the cannula during the in-vitro experiments. (Figure reproduced with permission from Widmer et al. [32]).

single vertebral slices, to larger volumes such as whole vertebrae with and without endplates or even multiple vertebral segments of the spine [33,34] and (Figure 2.3).

Although performing tests only on the level of a vertebral body may oversimplify the complex load transfer in the spine, it is difficult to accurately mimic the forces acting on multiple segments [33]. FE models are typically separated into either continuum models, where the microstructure is approximated by integrating the mechanical behaviour into large continuum elements, or micro FE models, where the mesh is fine enough to represent the bone microarchitecture, becoming more and more the state of the art in strength prediction [12].

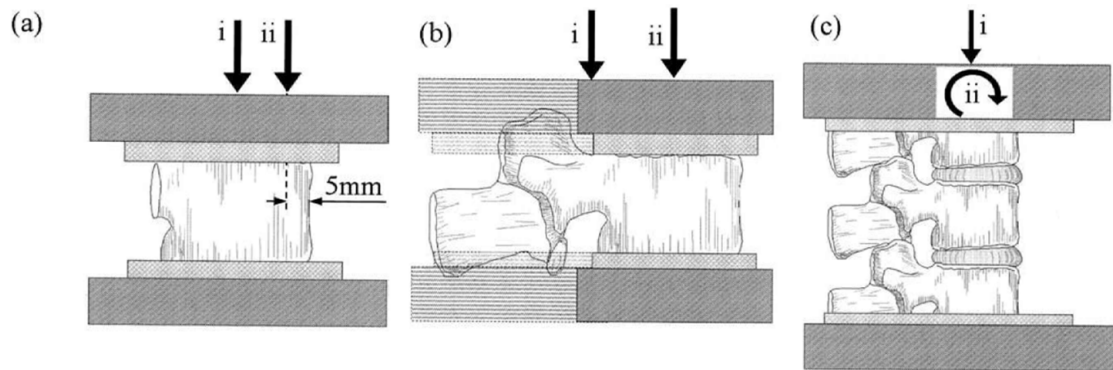


Figure 2.3: Methods of specimen test-up showing (a) a single vertebral body with (i) central and (ii) off set loading, (b) a single vertebra with loading applied to (i) the whole upper surface or (ii) only the vertebral endplate and (c) a multisegment unit under (i) compression and (ii) bending (Figure reproduced with permission from Wilcox [34]).

The increased accuracy of computational tools developed in the last decades, from increased imaging resolution to more detailed modelling of mechanics, leads to considerable advantages over classical mechanical testing, especially in the spine. Not only is the availability of testing material expensive and limited, the potential degradation of *ex vivo* samples raises questions about their relevance. The preparation phase and inadequate conservation may change the mechanical properties [33]. In addition, *in silico* experiments allow the use of a single sample to investigate several augmentation volumes, patterns and properties of the augmentation material without having to deal with variation from multiple samples [34] - a particular advantage when assessing the success of the intervention against untreated cases.

The geometry for the FE models is typically generated from CT images. Classical CT imaging is normally sufficient for the generation of the relatively rough mesh of continuum-scale FE. Some of the used material models however require structural information that is gathered from a sub-mesh resolution. Micro FE models have a mesh enough fine to represent the trabecular structure. In order to generate models from real bone, high resolution imaging techniques are needed. Where currently

micro FE models of human bone are typically generated from *ex vivo* micro-CT measurements, the development of high-resolution peripheral quantitative CT allows *in vivo* imaging of the trabecular structure of human bone and the subsequent generation of micro FE meshes [35].

### Continuum models

Continuum FE models vary in the complexity of the used material models. Liebschner and colleagues [36] used models where the geometry of vertebral bodies was derived from CT scans and converted to 20-noded brick elements. Different material models were used for cortical and cancellous bone. The cortical shell was modelled as an isotropic material with a constant modulus derived from experiments. The cancellous bone was modelled with changing moduli in the axial direction, in a linear relation to the mineral content. Baroud and colleagues [37] proposed a model of a whole spinal unit including two vertebrae and the enclosed intervertebral disk. Similar to the previous model, the endplates and cortical shell were simulated as linear-elastic materials, whereas the cancellous bone was simplified to be isotropic linear elastic, with different moduli for the non-augmented bone and for the bone cement composite. Eight linear elastic layers represented the annulus while the nucleus was modelled as a non-linear incompressible solid. The whole spinal unit model was extended by Polikeit et al. [38] in a model including not only two vertebral bodies and the endplates but also the facets and ligaments. The mesh was finer than that of the previous models, and the bone and cartilage elements were chosen as linear, homogeneous and isotropic, whereas the fibres were modelled as tension-only truss elements. The facet joints were modelled as non-bonded elements with friction. Baroud et al. and Polikeit et al. were able to show with these multi-segment models that augmentation not only alters the properties of the treated vertebra, but through stiffening of this structure, an altered load transfer through the flexible intervertebral disc to the adjacent vertebra results. A similar model using linear elastic tetrahedral elements was presented by Zhang et al. [39] again including two vertebrae with pedicles, ligaments and friction facet joints as well as the endplates. With this model, Zhang and colleagues highlighted also that load is shared between the vertebral bodies (85%) and the posterior processes (15%), and that this load sharing can be altered through augmentation, which was previously reported in an experimental study [40]. A model allowing damage accumulation was presented by Kinzl et al. [41]. The elements of the homogenised bone are considered as a damageable spring and allow the model of both the elastic and nonlinear phase of the augmented vertebrae under load. Similarly, Tarsuslugil et al. [42] considers both

intact and damaged model elements. In this work, however, the damaged elements are defined in a previously performed mechanical test. Yet another aspect of bone augmentation is considered in the presented model of a whole vertebra by Purcell et al. [43]. Some augmentation procedures push the trabecular structures out of the augmentation volume leading to a region of more compact trabecular bone at the edge. In this model, the element nodes adjacent to the augmentation cement are thus considered as compacted bone elements with an increased modulus.

While still a continuum FE model, the model of Wijayathunga et al. [44] represents a step towards a micro-FE model. Although relatively fine, the mesh does not entirely resolve the microstructure. This structure is however represented by directly integrating and converting the greyscale values to material properties within the elements. In addition, a nonlinear elastic perfectly plastic material model was chosen. The complexity of the material model was further increased in a study by Chevalier et al. [45], where trabecular bone elasticity was represented in the continuum elements with a stiffness tensor taking into account the anisotropy of the axial and transverse directions and the local bone volume fraction.

### Microstructural models

Continuum FE models were developed to overcome the simplification of the geometry of the simulated tissue, but require complex material models. Today, both high-resolution imaging techniques as well as the improvements of computational power and algorithms allow the direct representation of the microstructure in micro-FE models. Because the real bone geometry is used, isotropic material properties are normally sufficient to adequately model the mechanical behaviour. Keller and colleagues [46] present a two-dimensional micro-FE model to investigate different augmentation patterns. The geometry was derived from a micro-CT cross-section of a vertebral body at  $146\text{ }\mu\text{m}$  resolution. For simplicity reasons, sagittal symmetry was assumed and only half the vertebra was modelled. The geometry was mirrored on top to create two adjacent vertebrae with an enclosed intervertebral disc. Bone, marrow, cartilage and bone cement elements were modelled with corresponding material properties. Later, the model was extended [47] to account for the intervertebral disc degeneration in the process of the degeneration of the whole motion segment and included several augmentation patterns for vertebroplasty (Figure 2.4). The reduced disc mobility was simulated by increasing the stiffness of the nucleus to the value of the surrounding annulus. In another, earlier project [48], the resolution was increased to  $83\text{ }\mu\text{m}$  and a whole section of a vertebra was used without mirroring.

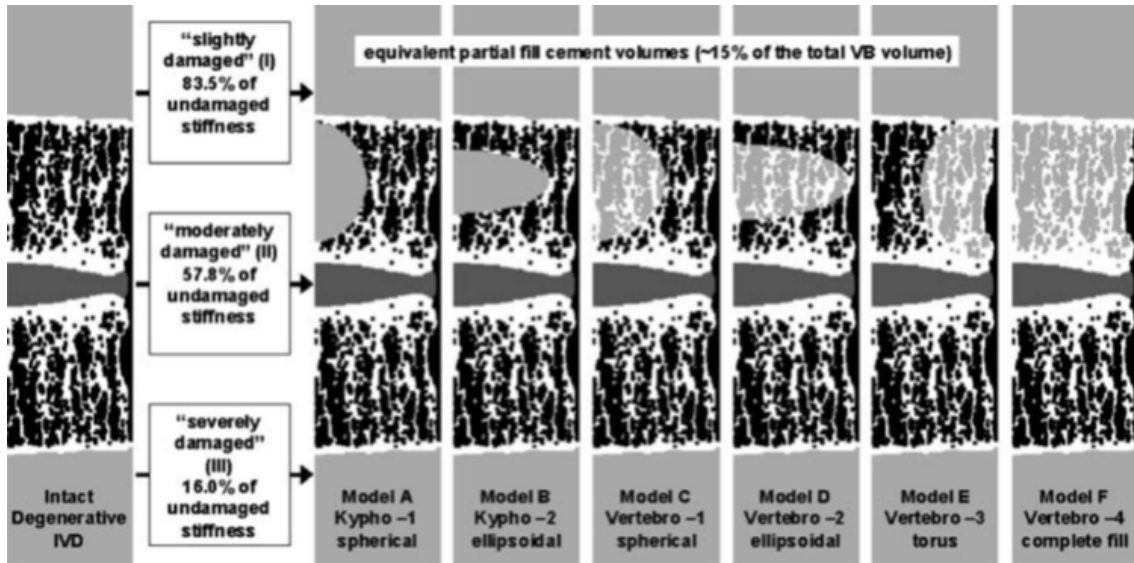


Figure 2.4: An intact axi-symmetric degenerative intervertebral disk microstructural FE motion segment model (left) is evaluated at three bone damage levels (I, II, III) to determine the effectiveness of each of the six cement augmentation strategies (models A - F). PMMA cement in regions above and below the superior and inferior vertebral bodies was added to mimic in vitro experimental validation test conditions. (Figure reproduced with permission from Kosmopoulos et al. [47]).

### Augmentation volumes

While the procedure for the geometry generation is generally standardized, simulations of augmented bone have been performed with a variety of different approaches. Several simulations include a prior simulation of bone fracture [36, 46–49]. Models including fracture simulation are performed in two or more loading cycles [36, 46–48]. In the adaptation cycles, the vertebrae are loaded and the moduli of bone elements exceeding a compressive load threshold are reduced to represent micro-damage of the trabecular structure. The deterioration levels vary from single [36] to multiple [46–48] stages of degradation. Instead of fracture, osteoporosis was also modelled by reducing the elastic moduli of the entire cancellous bone by 66% and the cortical shell by 33% [38].

In order to predict strength after augmentation, the geometry and material properties of the augmented cement volume have to be defined. The augmentation volume is often created artificially in order to test different augmentation shapes and levels of augmentation [38, 39, 46–49] as shown in Figure 2.5. Purcell et al. [43] used a horizontally oriented barrel model to represent the augmentation volume. Similarly, Polikeit [38] modelled the cement as vertically oriented barrels to simulate bi- and



unipedicular augmentation. The partial augmentation filled up about one third of the vertebral body. In addition, full augmentation was modelled by replacing the cancellous bone elements with PMMA. As a whole spinal unit was modelled, effects of augmentation on the superior and inferior endplate could be investigated. The approach of complete filling was also used by Zhang [39] but extended to change the properties of the augmentation material and therefore allowing optimization of the augmentation cement. Additionally, different augmentation patterns were modelled in the studies by Keller and Kosmopoulos [46,47]. For this, the augmentation volume was kept constant at 15% of the total vertebral body volume. Augmentation patterns included elliptic filling with and without contact to the endplates, a model with a torus geometry connecting the superior and inferior endplate as well as complete filling. Augmentation was modelled by replacing bone marrow within the augmentation volume with cement but keeping the trabecular structures. In addition, the model was used to investigate the effects of cement stiffness on the stiffness of the whole augmented vertebra. In a similar study, Kosmopoulos [48] simulated six different degrees of augmentation filling with a spherical shape ranging from 12% to 100% filling of the interior vertebral body. In addition, real augmentation volumes derived from micro-CT data directly were also used [41,42,45].

Both *ex vivo* as well as *in silico* strength is typically predicted using axial compression loading. Fractures of osteoporotic bone, however, often occur because of non-characteristic loading due to unexpected impacts. Zhang and colleagues [39] simulated different combined loading scenarios including pure axial loading, axial loading and forward moment as well as axial loading and backward moment.

### Model validation

Typically, the validation of the predictive models is a very difficult task. In the work of Kinzl et al. [41], each of the 41 models was validated with mechanical testing of the real underlying augmented specimens showing small deviations in strength and apparent stiffness. Also the FE results were comparable to the pressure measurements on sensitive films. Wijayathunga and colleagues [44] created eleven models directly from human samples and validated the results by comparison with mechanical tests of the real samples under loading to failure up to 25% reduction of initial height. The model parameters were fitted to three samples and the predictive power was determined for four non-augmented and four augmented models. Validation of the simulations showed good agreement with experimental test for the non-augmented bones, but models overestimated stiffness and strength in the augmented case. Chevalier and colleagues [45] used twelve vertebral bodies that

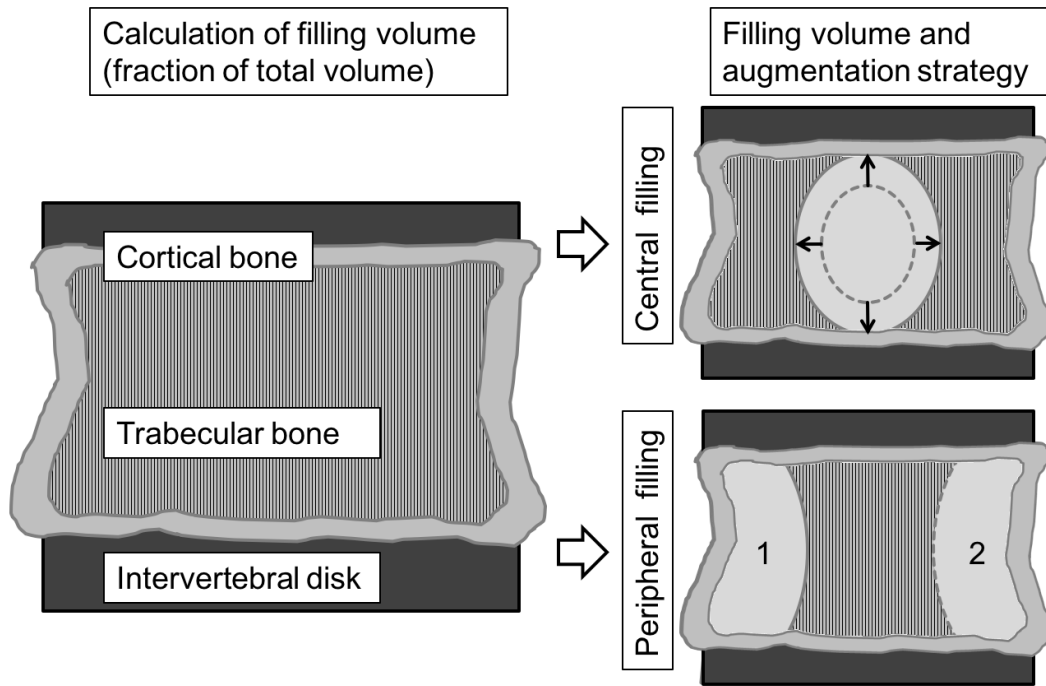


Figure 2.5: Typical procedure for the definition of the simulated augmentation volumes: first, the filling volume is defined as a fraction of the total vertebral body volume. Then, the shape of the augmentation volume is defined depending on the augmentation strategy.

were scanned prior to axial compression to fracture. After fracture, the vertebrae were augmented and rescanned. FE models were developed for both non-augmented and augmented samples and the stiffness compared. In addition, cements of different stiffness were tested *in silico*. They concluded that optimal augmentation was achieved with a compliant cement, completely bridging from superior to inferior endplate.

While continuum models suggest that already a small fill volume is enough to restore the stability of the vertebral body to the pre-fracture state [36], increasing the mesh resolution reveals that significant stiffening was observed only for vertebrae where cement was deposited through the whole height of the body [45]. Full augmentation increases the stiffness to more than in the pre-fracture state [37]. The cement deposition pattern appears to be of great importance for the fracture stabilization. The models suggest that symmetric placement of small amounts of cement might be more appropriate [36]. The most effective strategy to repair stiffness with a partial augmentation seemed to be using a torus shaped geometry connecting superior and inferior endplates [46].

Cement augmentation changes the load transfer in the spine by reducing the bulge of the endplates and increasing the pressure in the intervertebral disk [37,38], which increases the stress under load in cancellous and cortical bone [38] as well as increasing stresses in the endplates [39,45] of the adjacent vertebra, potentially provoking subsequent fractures. However, the augmentation of the vertebral body successfully reduces the number of highly stressed trabeculae in the cancellous bone in both damaged and undamaged bone, if the degree of filling is high enough [48]. The facet joints were less loaded after augmentation which led to a load shift towards the anterior column [38]. Osteoporosis and augmentation had little effect on the internal pressure of the disk [39], and the cement modulus had almost no influence on the apparent stiffness unless the vertebral body was completely filled. Where available, validation showed good agreement with models, but cement stiffness was overestimated [44].

While the proposed models greatly simplify the system, the benefits of all approaches are the multitude of simulations that can be performed. However, no three-dimensional  $\mu$ FE of augmented cancellous bone have been published so far. The two-dimensional structure analysis is not equally representative for the load transmission. Most models simplify the microstructure mechanics in complex material models. A particular difficulty lies in the bone and cement composite region of the continuum models.

### 2.1.4 Computational modelling for *in silico* prediction of bone biology in augmented spines

#### Bone adaptation

We know that the bone microstructure does not represent random orientations of the rod- and plate-like trabeculae, but that their alignment is very well oriented to withstand the forces of daily loading [50]. While the principle geometry of the bones is mostly genetically determined, the mechanics at the organ and tissue level regulate the microstructural adaptation [51]. The trabecular orientation is a result of the remodelling cycle, where different bone cells are involved in the renewal of the bone tissue: bone forming osteoblasts and bone resorbing osteoclasts constantly rebuild the bone matrix and may be motivated by osteocytes embedded within the bone matrix sensing a mechanical signal [52]. While bone remodelling simply leads to bone turnover, mechanically driven remodelling leads to bone adaptation. Possible triggers for bone adaptation are electromagnetic fields, bone deformation or strain, fluid flow, vibration, damage or any combinations of these [51]. While the complexity and

the large number of involved cells and signalling pathways makes it difficult to describe bone remodelling on the cellular level, simplified models for tissue adaptation are available. Most importantly, the mechanostat principle [53] linking mechanical strains to bone formation and resorption has been widely accepted. According to the theory, bone will be formed in regions with high mechanical strains and removed from unloaded bone structures, hence guiding the tissue structure towards an optimal form that ensures a homogeneous stress distribution. Because of its simplicity and the predictive power, this model is ideally suited for *in silico* bone adaptation.

Bone formation and resorption is well balanced in healthy bones maintaining their net volume. In osteoporosis, the balance is disturbed towards an overall loss of bone mass and a concomitant increase in fracture risk [2]. Vertebroplasty is typically used for osteoporotic patients, and changes in bone density have to be taken into account for a long-term prediction of the treatment success. Bone is dynamic and constantly adapting to the changing needs in load transfer. While assessing the mechanical strength of augmented bone might give a good insight into the immediate postoperative stability, it is questionable, whether the strength of the cement and bone composite remains the same in the long-term. Augmentation changes the load transfer and will inevitably lead to under- and overloaded bone sites, as is also known from metal implants. *In silico* biology has the potential to significantly increase the success in the prediction of the intervention. In combination with accurate fracture risk assessment [12,54], it could give better insight into the micromechanical changes of augmented bone and lead to a better understanding of the augmentation approach as a whole.

A variety of approaches to simulate bone remodelling have been proposed, ranging from organ-level to tissue-level to cell-level [55,56]. Organ-level approaches do not resolve the trabecular microstructure and are not suited for the assessment of long-term stiffness and stability. Cell-level bone adaptation simulations model the action of single cells and typically do not look at structural influences of the whole bone stability. The focus for *in silico* bone adaptation in augmented bones lies thus on tissue-level models.

### Non-targeted bone remodelling

A microstructural bone remodelling model was introduced by Müller [57]. The algorithm sequentially applies Gaussian filtration and thresholding and models long-term architectural changes due to osteoporotic bone loss. It could potentially be used for a generic analysis of the long-term fracture risk in augmented bone; however, the lack of a mechanical feedback would not take into account the biological response

to bone augmentation. Because the trabeculae are primarily oriented along a single principal loading direction, Gerhard and colleagues [55] suggested the compression of the filter in the principal loading direction, and hence considering some of the adaptation of the bone to the loading. Nevertheless, the model cannot account for the changes of loading in the local microarchitecture around and within the augmentation material.

### **Bone remodelling with mechanical signal**

Microstructural remodelling simulations of whole bones are challenging because of the computational cost and few cases have been reported so far. Wang and colleagues [58] presented a remodelling simulation of a cross section of an artificially generated vertebra. The model includes modelling of micro-damage as well as adaptive remodelling with strain energy density (SED) as the mechanical signal. The model was used to show mechanisms of bone loss and the collateral deterioration of mechanical strength. Nevertheless, the reduction of the model to two dimensions is a drastic limitation making the model less suitable for simulations of bone adaptation in the context of osteoporosis and bone augmentation.

Boyle and Kim [59] used space topology optimization on a three-dimensional random trabecular structure to create a realistic trabecular distribution of the proximal human femur. The method reorients structures in order to uniform the strain energy of the system. Although the model was used to investigate Wolff's law and started with a randomly generated architecture, it was able to show adaptation to changed loading. A limitation of the model is that space topology keeps bone volume constant and hence cannot recreate the bone deterioration due to bone loss.

An iterative mechanical feedback loop for three-dimensional bone remodelling was proposed by Ruimerman [60]. This approach is based on a previously developed model of tissue adaptation [61], where formation and resorption are considered as separate events. Similar to the mechanostat principle, formation is mechanically driven (local strain energy density levels) with more deposition for a higher mechanical signal. Bone resorption, however, is modelled as a stochastic process that is happening randomly on the bone surface. The model was able to generate reasonably realistic trabecular structures when compared to pig samples. In a recent study [62], the model was applied to human iliac crest biopsies to simulate increase in bone mass (Figure 2.6). Appropriate tuning of the settings may allow simulations of long-term adaptation of augmented osteoporotic bone.

Another three-dimensional bone adaptation algorithm was introduced by Adachi [63]. Following the mechanostat principle, the model uses stress gradients to define

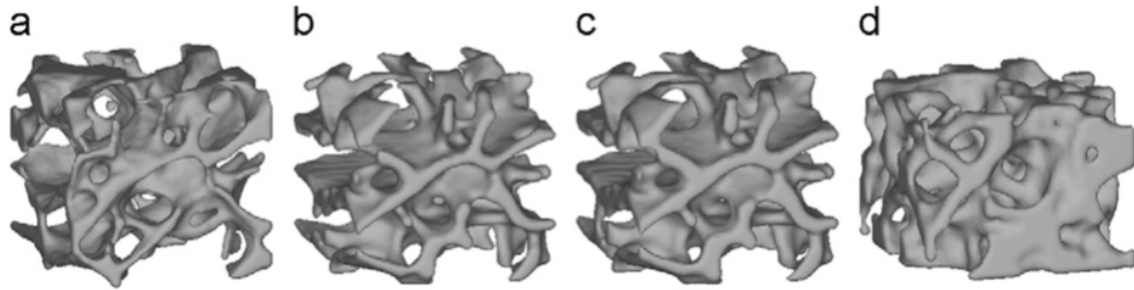


Figure 2.6: Bone micro-architecture of the initial (a), adapted (b), and simulated hypoparathyroidism with 140% osteocyte mechanosensitivity (c), and clinical hypoparathyroidism (d) biopsies. (Figure reproduced with permission from Christen et al. [62]).

sites of bone formation and resorption, as well as regions of quiescent bone. The procedure is repeated until an equilibrium state is reached and showed smooth morphological changes on the trabecular level. Although using a simple formulation of the bone remodelling algorithm, adaptation of real canine cortical bone to different loading conditions could be simulated. The model was subsequently applied on an artificial human proximal femur, under different loading conditions, which led to characteristic patterns of trabecular bone found in humans [64].

Cancellous bone deterioration is simulated in a model described by Mc Donnell [65]. In this model, not only voxels with low principal strains are resorbed, but also the very highly loaded voxels to simulate micro-crack formation. The model was run on specimens of human vertebral trabecular bone and showed the structural degradation of the microarchitecture following bone loss (Figure 2.7). This model could be particularly interesting for the long-term prediction of augmented bone, as it is able to simulate the formation of possible micro-cracks due to the changed loading environment.

Whole mouse vertebrae have been simulated in a remodelling algorithm presented by Schulte and colleagues [66]. The model is based on a mechanostat approach with SED as a mechanical signal determining locations of bone formation and resorption. Real *in vivo* micro-CT measured data has been used allowing an extensive validation of the static and dynamic changes in morphometric parameters. In later work [67], the model was applied to large datasets and extended to simulate the effects of additional loading and pharmaceutical treatment regimens.

In order to overcome some of the computational challenges linked with three-dimensional microstructural bone adaptation of human bones, efforts are made in the direction of multiscale approaches where the idea is to run the FE on a macroscopic level only [68]. Another possibility is to simulate the local changes of bone mass

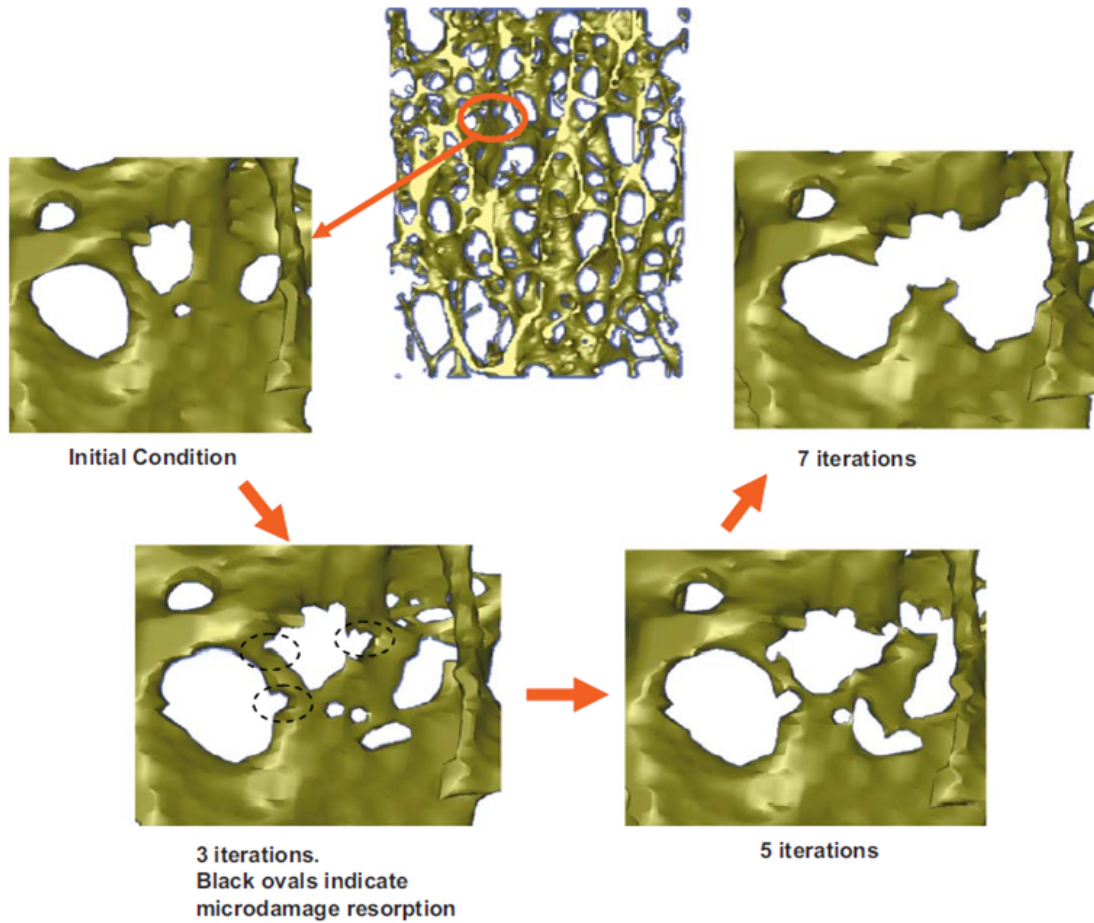


Figure 2.7: Close up view of progression of microdamage resorption and perforation of vertical trabeculae. (Figure reproduced with permission from Mc Donnell et al. [65]).

by integrating structural information at multiple scales and analytically define the consequences on the mechanical stability [69]. At the same time, the previously described Schulte model has been adapted to run datasets of whole human bone [70]. Homeostatic bone adaptation has been simulated on two datasets of whole human vertebrae at high resolution. Having crossed the technical challenge to run simulations on such large volumes, bone remodeling models have the potential to be used to investigate microstructural changes of the trabecular bone due to cement augmentation.

As far as the authors are aware of, no simulations of bone adaptation after bone augmentation have been published so far. Tarala and colleagues [71] have presented an organ level model of bone adaptation after total hip replacement. Looking at bone augmentation, similar to this work the special interest would be in regions of bone loss due to stress shielding. With the necessary simulation tools available,

simulating the evolution of the microstructure of the augmented vertebrae should be feasible in the future in order to get better insight into the long-term effectiveness of vertebroplasty.

### 2.1.5 Conclusions

Vertebroplasty is a promising minimally invasive approach to stabilize fractured vertebrae and may be used to prevent vertebral fractures in the future. Although pain reduction has been reported consistently [13–17], the biological mechanisms leading to pain reduction are still unclear and the mechanical effectiveness is controversial, with strong potential for improvement. Computational tools have thus a great potential to give better insight into the augmentation procedure, the stability after augmentation and the long-term consequences on bone biology.

In particular the work of Widmer [29–32] give a clear description of the injection patterns during vertebroplasty. This multiscale approach cannot only be used to predict augmentation volumes for individual vertebrae and help deciding where the augmentation material should be injected, but it can also be used to design new augmentation materials with better characteristics in the filling process.

Computational modelling of augmentation in the spine has primarily focused in the stability of the vertebra after augmentation. While most studies use organ-scale models, microstructural models for strength prediction have traditionally been limited to two dimensions. However, advances in computational power and parallelization approaches allow today a three-dimensional analysis of the bone microstructure. There is huge potential in the use of such tools for analysing the changed biomechanics after augmentation to make fracture assessment more accurate and improve treatment planning.

Multiple microstructural bone adaptation models have been proposed and show realistic morphological changes on real trabecular bone volumes. The high computational cost is the main factor why most models are limited to small volumes. Recent developments in bone remodelling simulations, however, are able to simulate microstructural bone adaptation in whole human bones. These models have the potential to show adaptation to cement augmentation in the bone. Not only could this give insight in the biological processes after the intervention, but also help to better predict the long-term effectiveness of bone augmentation in the stabilization of fragile bone.



## Acknowledgements

The authors gratefully acknowledge funding from the European Union (VPHOP FP7-ICT2008-223865).

## References

- [1] United-Nations. Population ageing and development. *Department of Economic and Social Affairs, Population Division, New York, NY 10017, USA, www.unpopulation.org*, 2012.
- [2] S. R. Cummings and L. J. Melton. Epidemiology and outcomes of osteoporotic fractures. *Lancet*, 359(9319):1761–7, 2002.
- [3] C. Holroyd, C. Cooper, E. Dennison. Epidemiology of osteoporosis. *Best Pract Res Clin Endocrinol Metab*, 22(5):671–85, 2008.
- [4] J. A. Kanis and O. Johnell. Requirements for dxa for the management of osteoporosis in europe. *Osteoporos Int*, 16(3):229–38, 2005.
- [5] O. Johnell and J. Kanis. Epidemiology of osteoporotic fractures. *Osteoporos Int*, 16 Suppl 2:S3–7, 2005.
- [6] O. Johnell and J. A. Kanis. An estimate of the worldwide prevalence and disability associated with osteoporotic fractures. *Osteoporos Int*, 17(12):1726–33, 2006.
- [7] M. C. Nevitt *et al.* The association of radiographically detected vertebral fractures with back pain and function: a prospective study. *Ann Intern Med*, 128(10):793–800, 1998.
- [8] M. Kleerekoper, A. R. Villanueva, J. Stanciu, D. S. Rao, A. M. Parfitt. The role of three-dimensional trabecular microstructure in the pathogenesis of vertebral compression fractures. *Calcif Tissue Int*, 37(6):594–7, 1985.
- [9] R. S. Weinstein and S. Majumdar. Fractal geometry and vertebral compression fractures. *J Bone Miner Res*, 9(11):1797–802, 1994.
- [10] M. P. Bostrom and J. M. Lane. Future directions. augmentation of osteoporotic vertebral bodies. *Spine (Phila Pa 1976)*, 22(24 Suppl):38S–42S, 1997.
- [11] T. S. Eckel and W. Olan. Vertebroplasty and vertebral augmentation techniques. *Tech Vasc Interv Radiol*, 12(1):44–50, 2009.

- [12] D. Christen, D. J. Webster, R. Mueller. Multiscale modelling and nonlinear finite element analysis as clinical tools for the assessment of fracture risk. *Philos Transact A Math Phys Eng Sci*, 368(1920):2653–68, 2010.
- [13] L. Alvarez *et al.* Percutaneous vertebroplasty: functional improvement in patients with osteoporotic compression fractures. *Spine (Phila Pa 1976)*, 31(10):1113–8, 2006.
- [14] P. A. Hulme, J. Krebs, S. J. Ferguson, U. Berlemann. Vertebroplasty and kyphoplasty: a systematic review of 69 clinical studies. *Spine (Phila Pa 1976)*, 31(17):1983–2001, 2006.
- [15] G. C. Anselmetti *et al.* Pain relief following percutaneous vertebroplasty: results of a series of 283 consecutive patients treated in a single institution. *Cardiovasc Intervent Radiol*, 30(3):441–7, 2007.
- [16] J. D. Barr, M. S. Barr, T. J. Lemley, R. M. McCann. Percutaneous vertebroplasty for pain relief and spinal stabilization. *Spine (Phila Pa 1976)*, 25(8):923–8, 2000.
- [17] C. A. Klazen *et al.* Vertebroplasty versus conservative treatment in acute osteoporotic vertebral compression fractures (vertos ii): an open-label randomised trial. *Lancet*, 376(9746):1085–92, 2010.
- [18] R. Buchbinder *et al.* A randomized trial of vertebroplasty for painful osteoporotic vertebral fractures. *N Engl J Med*, 361(6):557–68, 2009.
- [19] D. F. Kallmes *et al.* A randomized trial of vertebroplasty for osteoporotic spinal fractures. *N Engl J Med*, 361(6):569–79, 2009.
- [20] I. Legroux-Gerot *et al.* Long-term follow-up of vertebral osteoporotic fractures treated by percutaneous vertebroplasty. *Clin Rheumatol*, 23(4):310–7, 2004.
- [21] A. A. Uppin *et al.* Occurrence of new vertebral body fracture after percutaneous vertebroplasty in patients with osteoporosis. *Radiology*, 226(1):119–24, 2003.
- [22] S. S. Blemker *et al.* Image-based musculoskeletal modeling: applications, advances, and future opportunities. *J Magn Reson Imaging*, 25(2):441–51, 2007.
- [23] J. M. Mathis *et al.* Percutaneous vertebroplasty: a developing standard of care for vertebral compression fractures. *AJNR Am J Neuroradiol*, 22(2):373–81, 2001.

- [24] K. Kobayashi *et al.* Unilateral transpedicular percutaneous vertebroplasty using puncture simulation. *Radiat Med*, 24(3):187–94, 2006.
- [25] C.-K. Chui *et al.* Haptics in computer-mediated simulation: Training in vertebroplasty surgery. *Simulation Gaming*, 37(4):438–451, 2006.
- [26] Z. Lian, C. K. Chui, S. H. Teoh. A biomechanical model for real-time simulation of pmma injection with haptics. *Comput Biol Med*, 38(3):304–12, 2008.
- [27] G. Baroud and F. B. Yahia. A finite element rheological model for polymethylmethacrylate flow: analysis of the cement delivery in vertebroplasty. *Proc Inst Mech Eng H*, 218(5):331–8, 2004.
- [28] J. Teo, S. C. Wang, S. H. Teoh. Preliminary study on biomechanics of vertebroplasty: a computational fluid dynamics and solid mechanics combined approach. *Spine (Phila Pa 1976)*, 32(12):1320–8, 2007.
- [29] R. P. Widmer and S. J. Ferguson. A mixed boundary representation to simulate the displacement of a biofluid by a biomaterial in porous media. *J Biomech Eng*, 133(5):051007, 2011.
- [30] R. P. Widmer and S. J. Ferguson. On the interrelationship of permeability and structural parameters of vertebral trabecular bone: a parametric computational study. *Comput Methods Biomech Biomed Engin*, 2012.
- [31] R. P. Widmer and S. J. Ferguson. A comparison and verification of computational methods to determine the permeability of vertebral trabecular bone. *Proc Inst Mech Eng H*, 227(6):617–28, 2013.
- [32] R. P. Widmer Soyka, A. Lopez, C. Persson, L. Cristofolini, S. J. Ferguson. Numerical description and experimental validation of a rheology model for non-newtonian fluid flow in cancellous bone. *Journal of the Mechanical Behavior of Biomedical Materials*, 27(0):43–53, 2013.
- [33] M. A. Adams. Mechanical testing of the spine. an appraisal of methodology, results, and conclusions. *Spine (Phila Pa 1976)*, 20(19):2151–6, 1995.
- [34] R. K. Wilcox. The biomechanics of vertebroplasty: a review. *Proc Inst Mech Eng H*, 218(1):1–10, 2004.
- [35] T. L. Mueller *et al.* Mechanical stability in a human radius fracture treated with a novel tissue-engineered bone substitute: a non-invasive, longitudinal as-

- assessment using high-resolution pqt in combination with finite element analysis. *J Tissue Eng Regen Med*, 5(5):415–20, 2011.
- [36] M. A. Liebschner, W. S. Rosenberg, T. M. Keaveny. Effects of bone cement volume and distribution on vertebral stiffness after vertebroplasty. *Spine (Phila Pa 1976)*, 26(14):1547–54, 2001.
- [37] G. Baroud, J. Nemes, P. Heini, T. Steffen. Load shift of the intervertebral disc after a vertebroplasty: a finite-element study. *Eur Spine J*, 12(4):421–6, 2003.
- [38] A. Polikeit, L. P. Nolte, S. J. Ferguson. The effect of cement augmentation on the load transfer in an osteoporotic functional spinal unit: finite-element analysis. *Spine (Phila Pa 1976)*, 28(10):991–6, 2003.
- [39] L. Zhang, G. Yang, L. Wu, B. Yu. The biomechanical effects of osteoporosis vertebral augmentation with cancellous bone granules or bone cement on treated and adjacent non-treated vertebral bodies: a finite element evaluation. *Clin Biomech (Bristol, Avon)*, 25(2):166–72, 2010.
- [40] N. Farooq, J. C. Park, P. Pollintine, D. J. Annesley-Williams, P. Dolan. Can vertebroplasty restore normal load-bearing to fractured vertebrae? *Spine (Phila Pa 1976)*, 30(15):1723–30, 2005.
- [41] M. Kinzl *et al.* An experimentally validated finite element method for augmented vertebral bodies. *Clin Biomech (Bristol, Avon)*, 28(1):15–22, 2013.
- [42] S. M. Tarsuslugil *et al.* Experimental and computational approach investigating burst fracture augmentation using PMMA and calcium phosphate cements. *Ann Biomed Eng*, 42(4):751–62, 2014.
- [43] P. Purcell *et al.* A parametric finite element analysis of the compacted bone cement interface following balloon kyphoplasty. *Proc Inst Mech Eng H*, 228(1):89–97, 2014.
- [44] V. N. Wijayathunga *et al.* Development of specimen-specific finite element models of human vertebrae for the analysis of vertebroplasty. *Proc Inst Mech Eng H*, 222(2):221–238, 2008.
- [45] Y. Chevalier *et al.* Cement distribution, volume, and compliance in vertebroplasty: some answers from an anatomy-based nonlinear finite element study. *Spine (Phila Pa 1976)*, 33(16):1722–30, 2008.

- [46] T. S. Keller, V. Kosmopoulos, I. H. Lieberman. Vertebroplasty and kyphoplasty affect vertebral motion segment stiffness and stress distributions: a microstructural finite-element study. *Spine (Phila Pa 1976)*, 30(11):1258–65, 2005.
- [47] V. Kosmopoulos, T. S. Keller, C. Schizas. Early stage disc degeneration does not have an appreciable affect on stiffness and load transfer following vertebroplasty and kyphoplasty. *Eur Spine J*, 18(1):59–68, 2009.
- [48] V. Kosmopoulos and T. S. Keller. Damage-based finite-element vertebroplasty simulations. *Eur Spine J*, 13(7):617–25, 2004.
- [49] V. Kosmopoulos and T. S. Keller. Finite element modeling of trabecular bone damage. *Comput Methods Biomech Biomed Engin*, 6(3):209–16, 2003.
- [50] J. Wolff. The classic: on the inner architecture of bones and its importance for bone growth. 1870. *Clin Orthop Relat Res*, 468(4):1056–65, 2010.
- [51] C. R. Jacobs, S. Temiyasathit, A. B. Castillo. Osteocyte mechanobiology and pericellular mechanics. *Annu Rev Biomed Eng*, 12:369–400, 2010.
- [52] R. B. Martin. Toward a unifying theory of bone remodeling. *Bone*, 26(1):1–6, 2000.
- [53] H. M. Frost. Bone’s mechanostat: a 2003 update. *Anat Rec A Discov Mol Cell Evol Biol*, 275(2):1081–101, 2003.
- [54] M. Viceconti, E. Schileo, F. Taddei, S. Martelli, D. Testi. Personalised multi-scale models for risk fracture prediction. *Osteoporos Int*, (21):1067–1071, 2010.
- [55] F. A. Gerhard, D. J. Webster, G. H. van Lenthe, R. Mueller. In silico biology of bone modelling and remodelling: adaptation. *Philosophical Transactions of the Royal Society a-Mathematical Physical and Engineering Sciences*, 367(1895):2011–2030, 2009.
- [56] D. Webster and R. Mueller. In silico models of bone remodeling from macro to nano-from organ to cell. *Wiley Interdiscip Rev Syst Biol Med*, 2010.
- [57] R. Mueller. Long-term prediction of three-dimensional bone architecture in simulations of pre-, peri- and post-menopausal microstructural bone remodeling. *Osteoporos Int*, 16 Suppl 2:S25–35, 2005.
- [58] C. Wang, C. Zhang, J. Han, H. Wu, Y. Fan. Simulated evolution of the vertebral body based on basic multicellular unit activities. *J Bone Miner Metab*, 2010.

- [59] C. Boyle and I. Y. Kim. Three-dimensional micro-level computational study of wolff's law via trabecular bone remodeling in the human proximal femur using design space topology optimization. *J Biomech*, 2010.
- [60] R. Ruimerman, P. Hilbers, B. van Rietbergen, R. Huiskes. A theoretical framework for strain-related trabecular bone maintenance and adaptation. *Journal of Biomechanics*, 38(4):931–941, 2005.
- [61] R. Huiskes, R. Ruimerman, G. H. van Lenthe, J. D. Janssen. Effects of mechanical forces on maintenance and adaptation of form in trabecular bone. *Nature*, 405(6787):704–6, 2000.
- [62] P. Christen *et al.* Patient-specific bone modelling and remodelling simulation of hypoparathyroidism based on human iliac crest biopsies. *J Biomech*, 45(14):2411–6, 2012.
- [63] T. Adachi, K. Tsubota, Y. Tomita, S. J. Hollister. Trabecular surface remodeling simulation for cancellous bone using microstructural voxel finite element models. *Journal of Biomechanical Engineering-Transactions of the Asme*, 123(5):403–409, 2001.
- [64] K. Tsubota *et al.* Computer simulation of trabecular remodeling in human proximal femur using large-scale voxel fe models: Approach to understanding wolff's law. *J Biomech*, 42(8):1088–94, 2009.
- [65] P. Mc Donnell, N. Harrison, M. A. Liebschner, P. E. Mc Hugh. Simulation of vertebral trabecular bone loss using voxel finite element analysis. *J Biomech*, 2009.
- [66] F. A. Schulte *et al.* Strain-adaptive in silico modeling of bone adaptation - a computer simulation validated by in vivo micro-computed tomography data. *Bone*, 52(1):485–92, 2013.
- [67] A. Levchuk *et al.* The clinical biomechanics award 2012 - presented by the european society of biomechanics: large scale simulations of trabecular bone adaptation to loading and treatment. *Clin Biomech (Bristol, Avon)*, 29(4):355–62, 2014.
- [68] R. Hambli, H. Katerchi, C. L. Benhamou. Multiscale methodology for bone remodelling simulation using coupled finite element and neural network computation. *Biomech Model Mechanobiol*, 2010.

- [69] M. Colloca *et al.* A multiscale analytical approach for bone remodeling simulations: linking scales from collagen to trabeculae. *Bone*, 64:303–13, 2010.
- [70] S. D. Badilatti, P. Christen, A. Levchuk, I. Parkinson, R. Mueller. Large-scale microstructural simulation of load-adaptive bone remodeling in whole human vertebrae. *Biomech Model Mechanobiol*, published online, 2015.
- [71] M. Tarala, D. Janssen, N. Verdonchot. Balancing incompatible endoprosthesis design goals: A combined ingrowth and bone remodeling simulation. *Med Eng Phys*, 2010.





## Chapter 3

Development of large-scale  
simulations of load-adaptive bone  
remodeling in whole human  
vertebrae



## 3.1 Simulations of healthy bone adaptation in whole human vertebrae

Sandro D. Badilatti<sup>1</sup>, Patrik Christen<sup>1</sup>, Alina Levchuk<sup>1</sup>, Javad Hazrati Marangalou<sup>2</sup>, Bert van Rietbergen<sup>2</sup>, Ian Parkinson<sup>3</sup> and Ralph Müller<sup>1</sup>

<sup>1</sup>Institute for Biomechanics, ETH Zurich, 8093 Zurich, Switzerland

<sup>2</sup>Orthopaedic Biomechanics, Department of Biomedical Engineering, Eindhoven University of Technology, 5600 MB Eindhoven, The Netherlands

<sup>3</sup>SA Pathology and University of Adelaide, Adelaide, 5005 South Australia, Australia

### published as:

S. D. Badilatti, P. Christen, A. Levchuk, J. H. Marangalou, B. van Rietbergen, I. Parkinson and R. Müller. Large-scale microstructural simulation of load-adaptive bone remodeling in whole human vertebrae. *Biomech Model Mechanobiol*, 2015

Reprinted with permission and in compliance with the publisher copyright policy.

### Abstract:

Identification of individuals at risk of bone fractures remains challenging despite recent advances in bone strength assessment. In particular, the future degradation of the microstructure and load adaptation has been disregarded. Bone remodeling simulations have so far been restricted to small volume samples. Here, we present a large-scale framework for predicting microstructural adaptation in whole human vertebrae. The load-adaptive bone remodeling simulations include estimations of appropriate bone loading of three load cases as boundary conditions with micro finite element analysis. Homeostatic adaptation of whole human vertebrae over a simulated period of ten years is achieved with changes in bone volume fraction (BV/TV) of less than 5%. Evaluation on subvolumes shows that simplifying boundary conditions reduces the ability of the system to maintain trabecular structures when keeping remodeling parameters unchanged. By rotating the loading direction, adaptation towards new loading conditions could be induced. This framework shows the possibility of using large-scale bone remodeling simulations towards a more accurate prediction of microstructural changes in whole human bones.

**Keywords:**

Bone Adaptation, Bone Remodeling Simulations, Human Vertebra, Bone Loading Estimation, Micro Finite Element Modeling

### 3.1.1 Introduction

The weakening of bone tissue due to osteoporotic bone loss increases the risk of bone fractures in elderly people. Most frequently, such fractures affect the forearm, the hip or the spine [1] and affected patients not only suffer pain but have increased morbidity and mortality [2]. Recovery periods often take weeks and months and necessitate bed rest, causing increased costs for our ageing societies [3]. While preventive approaches with medication and exercise can help maintain bone quality [4,5], the key to successfully controlling fracture numbers is to identify the individuals at risk and provide them with focused preventive treatment.

The current practice for estimating fracture risk is to assess bone mass with dual-energy X-ray absorptiometry (DXA) [6], but its prediction capability is limited by the fact that DXA provides an areal density measure and gives no information about the bone microarchitecture [7–9]. New techniques such as high-resolution peripheral quantitative computed tomography (HR-pQCT) allow the three-dimensional resolution of trabecular structures from patients, thus potentially leading to a more precise analysis of bone strength [10]. In combination with micro finite element ( $\mu$ FE) models, a high accuracy bone specific fracture risk assessment can be achieved [11]. While *in vivo* measurements at high resolution are still limited to peripheral bones such as the wrist, improvements in imaging techniques might allow scanning of the bone microstructure in other locations in the future.

$\mu$ FE models are used to investigate the mechanical behavior of bones, including their stability, from high-resolution computer tomography images which represent a time point of the bone in the present or past. Bone, however, is a highly dynamic tissue with a turnover and rebuilding of the internal structures in a process known as bone remodeling [12,13]. Not only is the matrix renewed in the process, the structure is continuously being adapted to meet the needs of its load bearing function [14]. A complete fracture risk assessment should therefore not only take a snapshot of the present bone structure, but also predict the evolution of its microstructure and the implications for the future mechanical stability of the organ.

Computer simulations using predictive models of bone adaptation could forecast the future of a bone's microstructure and describe the mechanical stability at a later time point [15]. The existence of load-adaptive bone adaptation has been described more than a century ago by comparing the trabecular structures of long bones to

the calculated principal stress lines of bent beams [16]. Whole-body forces cause mechanical strains down to the cellular level, where the mechanical excitation is translated into a stimulus for local matrix formation or resorption, eventually resulting in tissue adaptation of the whole organ [17]. In his “mechanostat” theory, Frost directly links the mechanical signal to bone tissue adaptation [18]. A mechanical stimulus is sensed by the cells, and tissue is only preserved if the signal is within a certain range, referred to as “lazy zone” [19]. If the signal does not reach a minimal magnitude, tissue is removed - if it exceeds the range, new bone tissue is added. Evidence for local mechanoregulation has been found *in vivo*, where sites of bone formation and resorption could be linked to different levels of mechanical strain in animals [20,21] and humans [22].

Many simulations of bone adaptation of  $\mu$ CT derived real bone structures have been published in recent years [23–26]. While the studies initially explored the adaptation mechanism [23,27], the simulations are now shifting towards modeling bone degeneration and diseases [24–26]. So far, simulated volumes are limited to either small animal bones or to sub-regions of large bones. Accurate calculation of failure loads however ideally includes trabecular microarchitecture for the bone as a whole [9,28]. Bone remodeling simulations for the evaluation of bone strength at a future time point should therefore represent the whole bone structures. While such studies have been performed in animal studies [29], these are still lacking in humans. This is mostly due to the high computational costs associated with these analyses [30], and limitation of the *in vivo* assessment of microstructural bone for whole organs [23,31]. In addition, even for sites for which the microstructure can be assessed *in vivo*, only limited possibilities for validation exists [31].

In whole bone as well as subvolume remodeling simulations, the direct translation of local mechanical stimuli into structural changes leads to high sensitivity for the applied external boundary conditions, where inaccurate loading will lead to unnatural adaptation. A reverse engineering approach has recently been developed, capable of estimating the history of the loading conditions for an individual bone, by starting from its trabecular orientation [32,33]. Bone has the tendency to adapt the microstructure towards uniform tissue loading [20,22]; hence its structure holds information about forces previously acting on the structure. In this so called bone loading estimation algorithm, this phenomenon is used to solve the linear combination of possible external loads that leads to the most uniform bone tissue loading. However, the herewith estimated loads do not lead to a perfectly uniform load distribution in the bone [32] and therefore still allow further adaptation to the externally applied forces.

So far, the potential of combining these recently developed tools and technologies including high resolution imaging of whole bones, large-scale  $\mu$ FE and individual bone loading history has not been exploited. In this paper, the principal goal is to integrate these into a unified bone remodeling framework. For this purpose, we divide the work into five aims.

**Aim 1:** Framework integration. On  $\mu$ CT derived whole human bones we will simulate bone adaptation with exaggerated bone turnover and investigate the system stability for long-term simulations. The focus is on linking the necessary technologies and testing the framework with large-scale samples. In particular, the convergence time of the used  $\mu$ FE solver is sensitive to changes of the bone microstructure and the framework must allow smooth simulations of bone adaptation also in the long-term.

**Aim 2:** Simulating healthy bone adaptation. a) On whole human vertebrae, we find remodeling parameters to simulate realistic bone adaptation of healthy bone, that is with balanced formation and resorption only marginally changing total bone mass for the duration of 10 simulated years. b) We evaluate the local functioning of the parameter set in a well-controlled environment based on previously published models of synthetic single X, Y and Z shaped trabeculae, where the local load adaptation of trabeculae can be tested [23].

**Aim 3:**  $\mu$ FE image resolution. On a cubic trabecular subvolume (14.5 mm length), we investigate the influence of the sample image resolution on the mechanical signal (strain energy density (SED)) distribution calculated from  $\mu$ FE. We will run  $\mu$ FE analysis of the trabecular cube at different resolutions and compare histograms of the SED distribution at reduced resolutions with the histogram of the highest resolution. Bone remodeling algorithms with mechanical feedback are sensitive to the local mechanical stimuli. Because of the massive size of the large-scale datasets used for whole human bones, the resolution that can be used in simulations is constrained both by the remodeling simulations and the  $\mu$ FE. Downscaling and thus reducing the image resolution, however, might cause a smoothing of the local SED values.

**Aim 4:** Effects of various boundary conditions. On a cubic trabecular subvolume (13.1 mm length) we look at the influence of using advanced versus simple boundary conditions by simulating bone adaptation to different loading configurations with decreasing complexity. Besides the image resolution, the other main factor influencing the local mechanical stimuli are the applied boundary conditions. The implementation of the bone load estimation into the remodeling framework allows the definition of more physiological bone loading compared to previous remodeling simulations. Highest complexity of loading configurations means three load cases

including axial loading and shear forces in both orthogonal directions. Because each load case is calculated separately, we investigate if a reduction of the number of load cases to axial loading only is sufficient.

**Aim 5:** Re-adaptation of the microstructure. On a cubic trabecular subvolume (13.1 mm length) we investigate the ability of the algorithm to readapt the microstructure to new loading directions. The subvolume is subjected to axial compressive loading in a first loading scenario. In a second scenario, the compressive force is rotated by 30°. In a third scenario, the non-rotated compressive force is used first, and rotated after half the simulation duration. Comparison of the scenarios will be done by looking at the principal axis of trabecular orientation.

### 3.1.2 Materials and Methods

#### Micro-computed Tomography and Bone Microstructure

Bone microstructure was derived from two micro-computed tomography ( $\mu$ CT) datasets of cadaveric human vertebral bodies. An overview of the used datasets and volumes for the aims is given in Table 3.1.

Aim 1: The dataset used in the integration part ( $D_1$ ) includes two L1 vertebrae from a previous study [34] scanned at the Department of Biomedical Engineering of the Eindhoven University of Technology ( $\mu$ CT 80, Scanco Medical AG, Bassersdorf, Switzerland) with a resolution of 41  $\mu$ m and Gaussian-filtered (sigma= 0.9 voxel, support= 1 voxel).

Aim 2a): A second dataset ( $D_2$ ) of two vertebral bodies measured at 17.4  $\mu$ m resolution was used in the healthy whole bone adaptation simulations. It consists of L2 vertebrae scanned at SA Pathology and the University of Adelaide (SkyScan 1076 in vivo, SkyScan, Kontich, Belgium) with approval to use the samples for research purposes granted by the Human Research Ethics Committee at the Royal Adelaide Hospital, South Australia. The  $D_2$  scans were downsampled with voxel averaging and interpolation to 43.5  $\mu$ m.

Together, the  $D_1$  and  $D_2$  datasets led to four similarly sized volumes of about 1200x900x700 voxels. All bones were aligned along the z-axis, thresholded (135/1000 of the maximum greyscale value for  $D_1$ , 189/1000 for  $D_2$ ) for binarization and component-labelled to remove unconnected parts. Each dataset includes one low bone volume fraction vertebra ( $D_{1L}$ : 8.6% and  $D_{2L}$ : 9.1% BV/TV) and one high bone volume fraction vertebra ( $D_{1H}$ : 10.6% and  $D_{2H}$ : 16.9% BV/TV).

Aim 2b): In addition to the real bone geometries, three artificial 403 voxel cubes (resolution: 43.5  $\mu$ m, length: 1.74 mm) were designed representing single human

Table 3.1: Datasets and volumes overview

Aim	Dataset	Volume	Resolution	Load Scenario (Load Cases)	# of Iterations
1	D <sub>1</sub>	whole vertebrae	42 $\mu\text{m}$	LS <sub>I</sub> (LC <sub>1</sub> , LC <sub>2</sub> , LC <sub>3</sub> )	10
2a	D <sub>2</sub>	whole vertebrae	43.5 $\mu\text{m}$	LS <sub>I</sub> (LC <sub>1</sub> , LC <sub>2</sub> , LC <sub>3</sub> )	10
2b	artificial	single trabeculae	43.5 $\mu\text{m}$	LS <sub>III</sub> (LC <sub>3</sub> )	50
3	D <sub>2L</sub>	subvolume 840 <sup>3</sup>	17.4-87.0 $\mu\text{m}$	LS <sub>I</sub> (LC <sub>1</sub> , LC <sub>2</sub> , LC <sub>3</sub> )	20
				LS <sub>I</sub> (LC <sub>1</sub> , LC <sub>2</sub> , LC <sub>3</sub> )	20
4	D <sub>2L</sub>	subvolume 300 <sup>3</sup>	43.5 $\mu\text{m}$	LS <sub>II</sub> (LC <sub>2</sub> , LC <sub>3</sub> )	20
				LS <sub>III</sub> (LC <sub>3</sub> )	20
				LS <sub>I</sub> (LC <sub>1</sub> , LC <sub>2</sub> , LC <sub>3</sub> )	20
5	D <sub>2L</sub>	subvolume 300 <sup>3</sup>	43.5 $\mu\text{m}$	LS <sub>IV</sub> (LC <sub>1</sub> , LC <sub>2</sub> , LC <sub>3ROT</sub> )	20
				LS <sub>V</sub> (LC <sub>1</sub> , LC <sub>2</sub> , LC <sub>3</sub> , LC <sub>3ROT</sub> )	20



trabeculae (Trabecular thickness:  $150\ \mu\text{m}$ ) using characteristic X, Y and Z shapes as introduced earlier [23].

Aim 3: For the investigation of the resolution influence, a cubic 8403 subvolume of  $14.5\ \text{mm}$  length from  $D_{2L}$  was downsampled from  $17.4\ \mu\text{m}$  to  $34.8\ \mu\text{m}$  (2.0 x), to  $43.5\ \mu\text{m}$  (2.5 x), to  $52.2\ \mu\text{m}$  (3.0 x) to  $69.6\ \mu\text{m}$  (4.0 x) and to  $87.0\ \mu\text{m}$  (5.0 x).

Aim 4 and 5: A cubic subvolume from the center of the previously downsampled  $D_{2L}$  of 3003 voxel (resolution:  $43.5\ \mu\text{m}$ , length:  $13.1\ \text{mm}$  length) was extracted for the analysis of the boundary conditions and the re-adaptation to the rotated load.

Standard static morphometry parameters bone volume fraction (BV/TV), surface density (BS/TV), degree of anisotropy (DA), trabecular thickness (Tb.Th), trabecular separation (Tb.Sp) and trabecular number (Tb.N) were calculated for all volumes and time steps (IPL v5.15, Scanco Medical AG, Bassersdorf, Switzerland). In Aim 5, the angle  $\Theta_Z$  was calculated from the scalar product of the z-axis vector and the vector of the principal direction of trabecular orientation as determined by mean intercept length and calculated in IPL.

## Bone Remodeling Simulation

Bone remodeling was simulated using an extension of a framework developed and validated earlier for the simulation of bone remodeling in mouse bone [26]. Adaptation is based on Frost's mechanostat theory and simulated by moving the bone surface according to a previously defined mechanosensitive cell signal. Bone apposition occurs above a signal formation threshold and leads to thickening, while a cell signal below the resorption threshold leads to bone removal. In our model, SED was used since it has been shown to be linked to sites of bone remodeling in animals [20] and humans [22] as well as it is a reasonable substitute for strain-rate [30]. The cell signal is calculated by integrating  $\mu\text{FE}$  derived SED values within the sensing radius of osteocytes ( $\sigma=43.5\ \mu\text{m}$ , defined by design and comparable to what has been reported elsewhere [35]). The framework includes automated preprocessing, load estimation and iterative remodeling (Figure 3.1). The preprocessing step generates the initial geometry and the input files for the  $\mu\text{FE}$  analyses. The  $\mu\text{FE}$  analysis for the first bone adaptation iteration includes a bone load estimation step where boundary conditions are defined. Once set, the same boundary conditions are kept constant for all following bone adaptation iterations. By design, one iteration represents one year of bone adaptation. For Aim 1 and Aim 2a, the whole vertebrae,  $n=10$  iterations were performed in order to limit computational cost. For Aims 4 and 5 on subvolumes the duration was doubled to  $n=20$  iterations so that more pronounced changes were achieved. For Aim 2b, the single trabeculae,  $n=50$  iterations

were chosen analogous to the previous study [23] and Table 3.1.

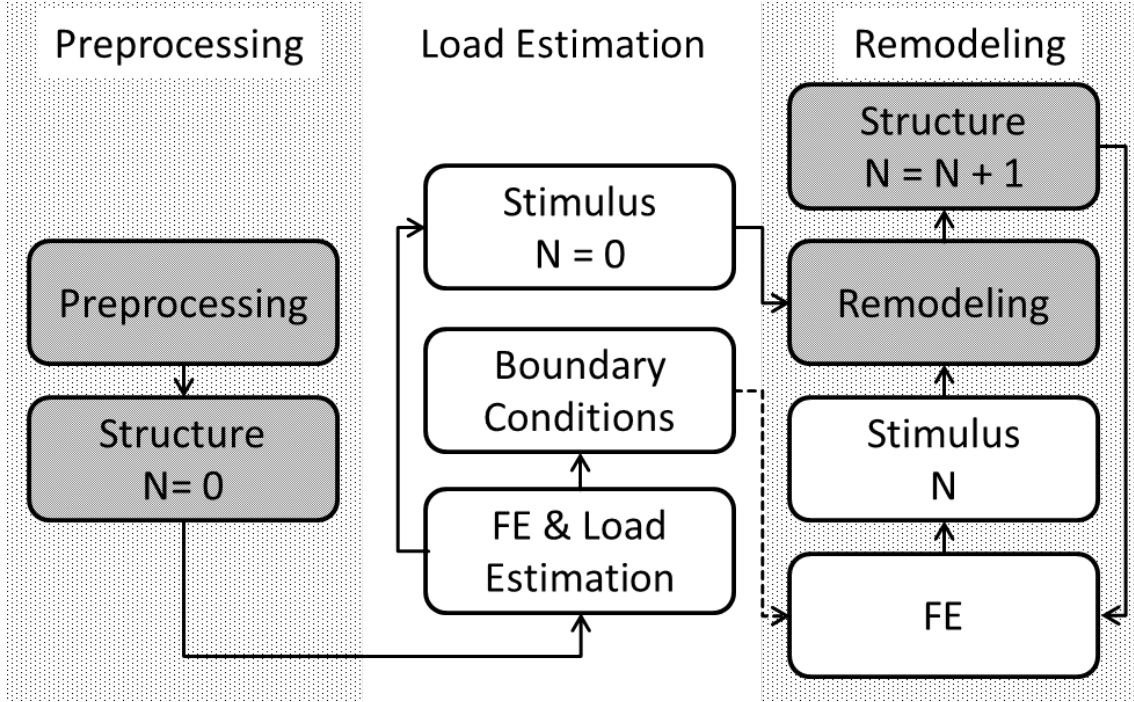


Figure 3.1: Bone remodeling framework. Simulations begin with a preprocessing step where input files for FE and remodeling are generated. The subsequent load estimation routine calculates boundary conditions for the loading scenarios. The iterative bone remodeling calculates the adapted bone structure and feeds this information back into the FE. Gray boxes represent calculations on the local cluster, white boxes calculations on the supercomputer.

Simulations were performed on two platforms: all processing parts including the remodeling and data analysis were performed on a local cluster (HP Integrity BL89c i2), the  $\mu$ FE and load estimation steps on the Monte Rosa cluster (Cray XE6) at the Swiss National Supercomputing Centre (CSCS, Lugano, Switzerland) on maximally 1024 CPUs. The duration for a single iteration of a whole bone takes up to 8 h (6 h  $\mu$ FE analysis plus 2 h remodeling simulation).

### $\mu$ FE setup and load estimation

All FE simulations were performed with a state of the art linear  $\mu$ FE solver that includes automated meshing [36]. The boundary conditions for the bone loading were applied to soft pads that were artificially generated at the end plates with an elastic modulus of 0.2 GPa mimicking a material in the range of the intervertebral disk [37, 38], thus replicating natural load transfer through the endplates of the

vertebral body. Binary  $\mu$ FE with an elastic modulus of 6.8 GPa and grey scale  $\mu$ FE with an exponential increase of the elastic modulus with increasing density according to previously published results [39] were tested in Aim 1 (D<sub>1</sub>). For the subsequent Aims, grey scale  $\mu$ FE was used allowing models of up to 365 million elements for the whole bone datasets to be analyzed.

For the simulations with advanced boundary conditions (Aims 1, 2a, 4 and 5), we defined three load cases: shear force in the x-direction representing sideward bending (LC<sub>1</sub>), shear force in the y-direction representing forward bending (LC<sub>2</sub>) and axial compressive loading (LC<sub>3</sub>). All loads were applied on the top nodes only, with the bottom nodes being fixed. 1000 N loads were applied for all whole vertebrae load cases [40,41] (Aim 1 and Aim 2a), for the subvolumes we used 100 N loading (Aim 4 and Aim 5) and the single trabeculae (Aim 2b, axial compressive loading only) were loaded with 10 N. A target value of 0.02 MPa for the tissue strain energy density was chosen [35,42] representing physiological tissue loading as shown in strain-gauge measurements [43].

#### Remodeling parameter selection

In previous mouse studies [26, 29], remodeling parameters could be deduced from the experiments or gathered from the literature. As these values are not available for human tissue, another systematic approach was used. In a first step, SED values calculated from the FE model were listed in histograms. The formation and resorption thresholds ( $P_{upp}$  and  $P_{low}$ ) define the eroding and mineralizing surface in our model. Between samples, a large variation of these surfaces is reported [29]. In addition, the influence of formation and resorption thresholds is not linear, but has a large influence on the resulting bone mass that is difficult to define *a priori*. In this work, these parameters were arbitrarily chosen so that the lower 25% of the surface elements were assigned to resorption ( $P_{low}$ ) and the upper 25% to formation ( $P_{upp}$ ). For this study, the resorption rate ( $\tau_{low}$ ) of the mechanostat curve was defined such that the saturation level ( $u_{max}$ ) was just reached:

$$\tau_{low} = u_{max}/P_{low} \quad (3.1)$$

As mentioned previously, we used parameters simulating exaggerated bone turnover for the framework integration test. For the other simulations, we used a parameter set optimized to minimize changes in BV/TV. While osteoporotic bone shows an average relative changes of more than 1% per year [12, 31, 44], changes of healthy bone are in average less than 0.5% [45]. In our study, the goal was to reach a

healthy homeostatic balance ( $\Delta BV/TV < 0.5\%$  average relative change per year) of the bone tissue. The time step per iteration was set to one year in order to capture the long-term behavior of the microstructure. The model parameters used are listed in Table 3.2.

### **Loading scenarios**

With the previously mentioned three loading cases, we were able to create different loading scenarios (Table 3.1). The whole bones and the subvolumes used for the resolution study (Aim 3) were subjected to three load cases, loading scenario 1 ( $LS_I$ ) with  $LC_1$ ,  $LC_2$  and  $LC_3$ . The subvolume used in Aim 4 was subjected to changing loading scenarios with three load cases ( $LS_I$ ), two load cases (loading scenario 2 ( $LS_{II}$ ) with  $LC_2$  and  $LC_3$ ) and one load case representing pure axial loading (loading scenario 3 ( $LS_{III}$ ) with  $LC_3$ ). Because we used SED as a mechanical signal for bone remodeling, we considered the shear forces in the x and the y direction as symmetric, representing the mechanical stimulus for a rotation of the volume, such as forward and sideward bending. First, the shear in the x direction was removed ( $LS_{II}$ ), then shear in the y direction ( $LS_{III}$ ).

In Aim 5 we investigated the ability of the remodeling framework to reorient a trabecular network by forcing a reorientation towards a specific loading direction. Firstly, for this purpose the axial compressive force ( $LC_3$ ) in  $LS_I$  was rotated by  $30^\circ$  in the frontal plane ( $LC_{3ROT}$ ) leading to a new rotated scenario  $LS_{IV}$  and the results compared to the non-rotated case after 20 iterations. Secondly, a separate simulation was performed, where adaptation was simulated for 10 iterations ( $LS_I$  with  $LC_3$ ) and then rotated by  $30^\circ$  ( $LS_{IV}$  with  $LC_{3ROT}$ ) for additional 10 iterations leading to a late rotation loading scenario ( $LS_V$ ).

The artificial X, Y and Z trabeculae were subjected to pure axial compressive loading ( $LC_3$ ).

### **3.1.3 Results**

In the attempt of testing the computational utilization of the remodeling framework and bone load estimation for large-scale samples, adaptation with exaggerated bone turnover was accomplished for 2 whole vertebrae with 10 iterations each. Figure 3.2 shows the solving duration for the axially loaded  $\mu FE$  model of the whole vertebra  $D_{1H}$  with even load distribution on the soft pad. While solving time increases for the binary files, it is reduced in the grayscale models. Although solving time for the grayscale model takes 4 times longer to solve initially, this trend is inverted with

Table 3.2: Model parameters for the bone remodeling algorithm

Parameter	Variable name	Unit	Aim 1	Aim 2, Aim 4 and Aim 5
Sample resolution		$\mu\text{m}$	42 <sup>1)</sup> (Scanco $\mu\text{CT}$ 80)	43.5 <sup>1,2)</sup> (ScyScan 1076 <i>in vivo</i> )
Osteocyte influence distance	$\sigma$	$\mu\text{m}$ (voxel)	42 (1) <sup>3)</sup>	43.5 (1) <sup>3)</sup>
Bone formation rate per SED	$\tau_{\text{upp}}$	$\mu\text{m}/\text{year}/\text{MPa}$	0.2 <sup>4)</sup>	1 <sup>4)</sup>
Bone resorption rate per SED	$\tau_{\text{low}}$	$\mu\text{m}/\text{year}/\text{MPa}$	22.22 <sup>3)</sup>	4.2857 <sup>3)</sup>
Formation threshold	$P_{\text{upp}}$	MPa	0.04 <sup>3)</sup>	0.012 <sup>3)</sup>
Resorption threshold	$P_{\text{low}}$	MPa	0.0018 <sup>3)</sup>	0.0028 <sup>3)</sup>
Saturation level	$u_{\text{max}}$	mm/year	0.04 <sup>3)</sup>	0.012 <sup>5)</sup>

1) Scanner setting

2) Resized pixel size from 17.4  $\mu\text{m}$ 

3) By design

2) Optimized by matching BV/TV

2) Optimized by eye

increasing iteration steps.

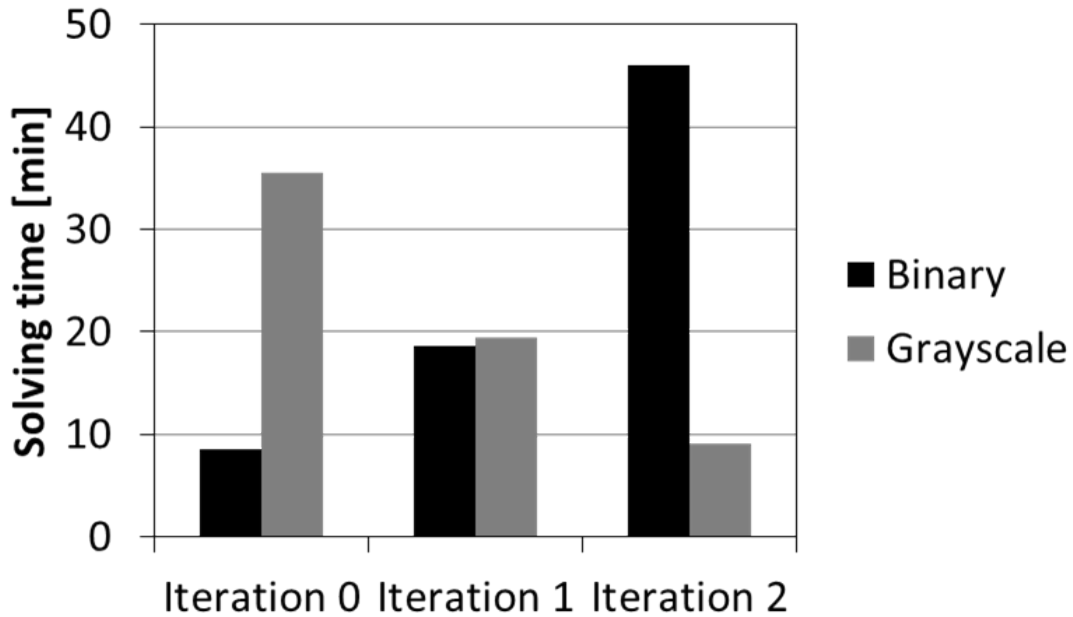


Figure 3.2: Solving time of the  $\mu$ FE analysis for the axial loading of the whole bone model  $D_{1H}$ . Solving time is increasing for binarized models, while grey scale models reduce solving duration.

For the whole bone datasets ( $D_1$  and  $D_2$ ), loads estimate were between 141 N and 791 N for  $LC_1$ , between 60 N and 563 N for  $LC_2$  and between 179 N and 2127 N for  $LC_3$  (Figure 3.3). The smallest contribution (max. 24%) to the uniform tissue loading comes from forward bending ( $LC_2$ ) while axial loading ( $LC_3$ ) contributes at least 47% to the total loading. Load estimations of  $D_{2H}$  were the highest for all load cases.

Aim 2a: The changes of morphometric indices are shown in Figure 3.4. Bone volume fraction continually decreases in  $D_{2L}$  while it initially increases for  $D_{2H}$ . Both samples show a similar decrease in  $BV/TV$  from the fifth year onwards.  $D_{2L}$  shows a loss of 4.5% relative to its original value in bone volume fraction. Different patterns between the samples were observed in the trabecular thickness (Tb.Th). While it increased during the simulated period for  $D_{2L}$ , it decreased in  $D_{2H}$ . Changes were less than 4% for both samples. Trabecular number Tb.N decreased for both samples between 3.2% and 9.9%. The degree of anisotropy (DA) increases by 3.8% in  $D_{2H}$  and by 5.7% in  $D_{2L}$  respectively. Compressive stiffness in the z-direction increased for both samples; 16.3% for  $D_{2H}$  and 25.1% in  $D_{2L}$ , with saturation during the simulation period.

Aim 2b: The adaptation of the single trabeculae under compressive loading for

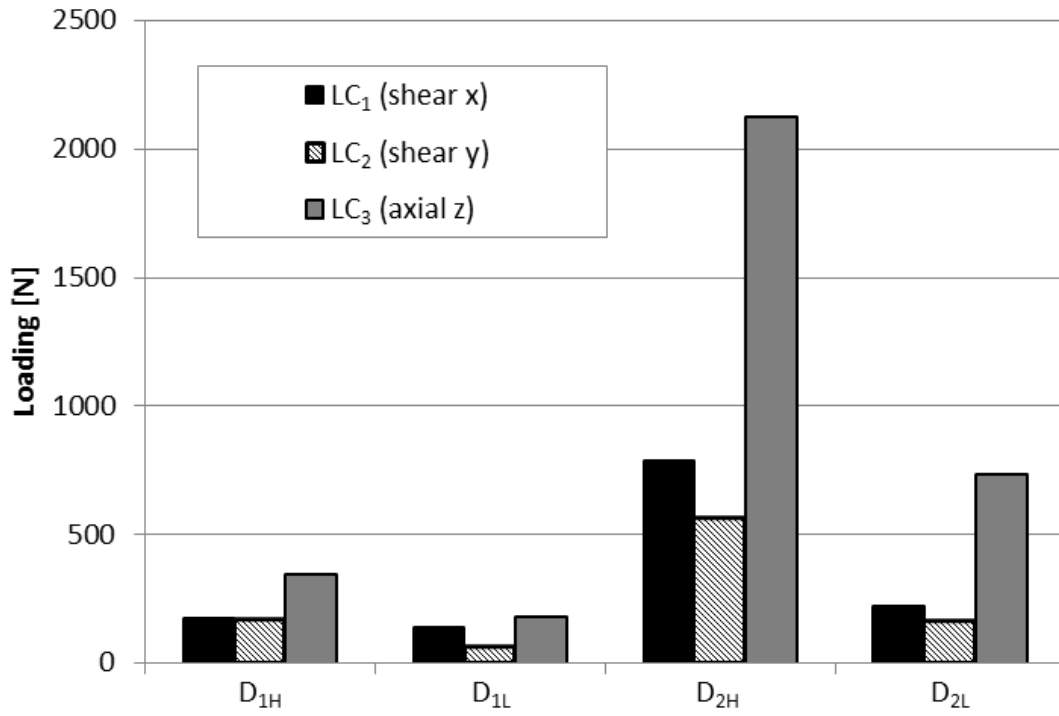


Figure 3.3: Bone load estimation for the human whole bone samples. Forward bending (LC<sub>2</sub>) contributed the least, axial loading (LC<sub>3</sub>) the most to the uniform tissue loading. For the sample with the highest BV/TV (third sample), the highest loading conditions were estimated.

the three different configurations is shown in Figure 3.5. The simulations show smooth morphological changes and a rotation of the structures towards the loading direction. The X shaped trabecula separates towards a double H-shaped trabecula. The bifurcation of Y-shaped trabecula moves towards the edge. The most dynamic behavior can be seen with the Z-shaped trabecula. The main trabecular strut moves towards the center faster than the subsequent absorption of the lateral structures.

Aim 3: Normalized histograms of the SED distribution from the  $\mu$ FE results of the trabecular subvolume at different resolutions are shown in Figure 3.6. The structures were subjected to advanced boundary conditions (LS<sub>I</sub>). The frequency of the obtained values remains relatively stable for values larger than 0.012 MPa. For values lower than 0.012 MPa, however, increasing voxel sizes shift the frequency from values between 0.004-0.012 MPa to values below 0.004 MPa. The frequency distribution only minimally changes for voxel sizes from 17.4  $\mu$ m to 43.5  $\mu$ m, but increasingly changes with increasing voxel sizes as compared to the 17.4  $\mu$ m baseline.

Aim 4: A section of the trabecular subvolume used for the testing of the boundary conditions is shown in Figure 3.7. Visual inspection revealed that LS<sub>I</sub> conserved

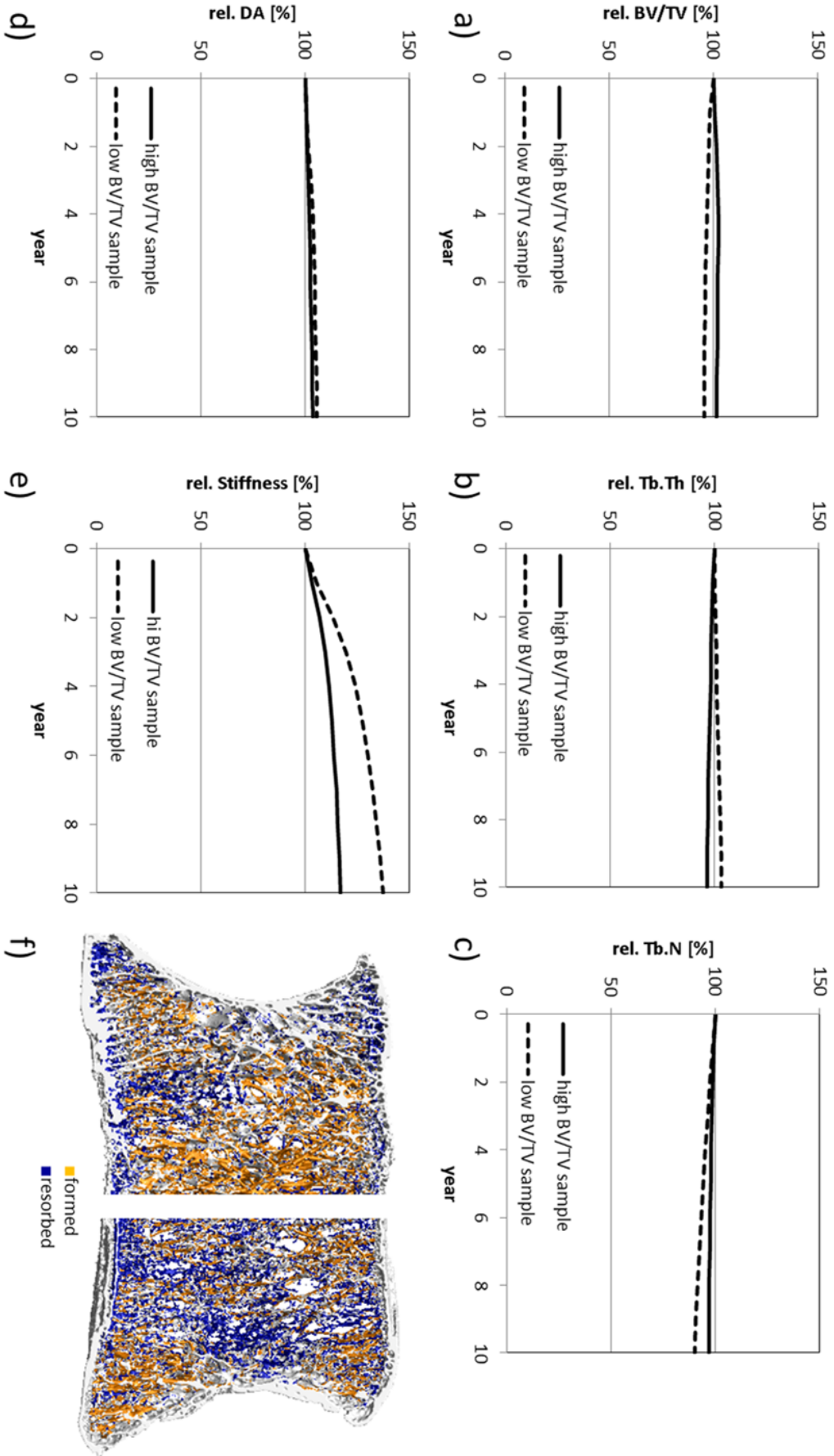


Figure 3.4: Course of bone morphometric indices for  $D_2$  over time. The solid line denotes the high BV/TV sample and the dashed line the low BV/TV sample. a) rel. BV/TV, b) rel. Tb.Th, c) rel. Tb.N, d) rel. DA, e) rel. Stiffness f) sites of bone formation and resorption for the high BV/TV sample left and low BV/TV sample right.



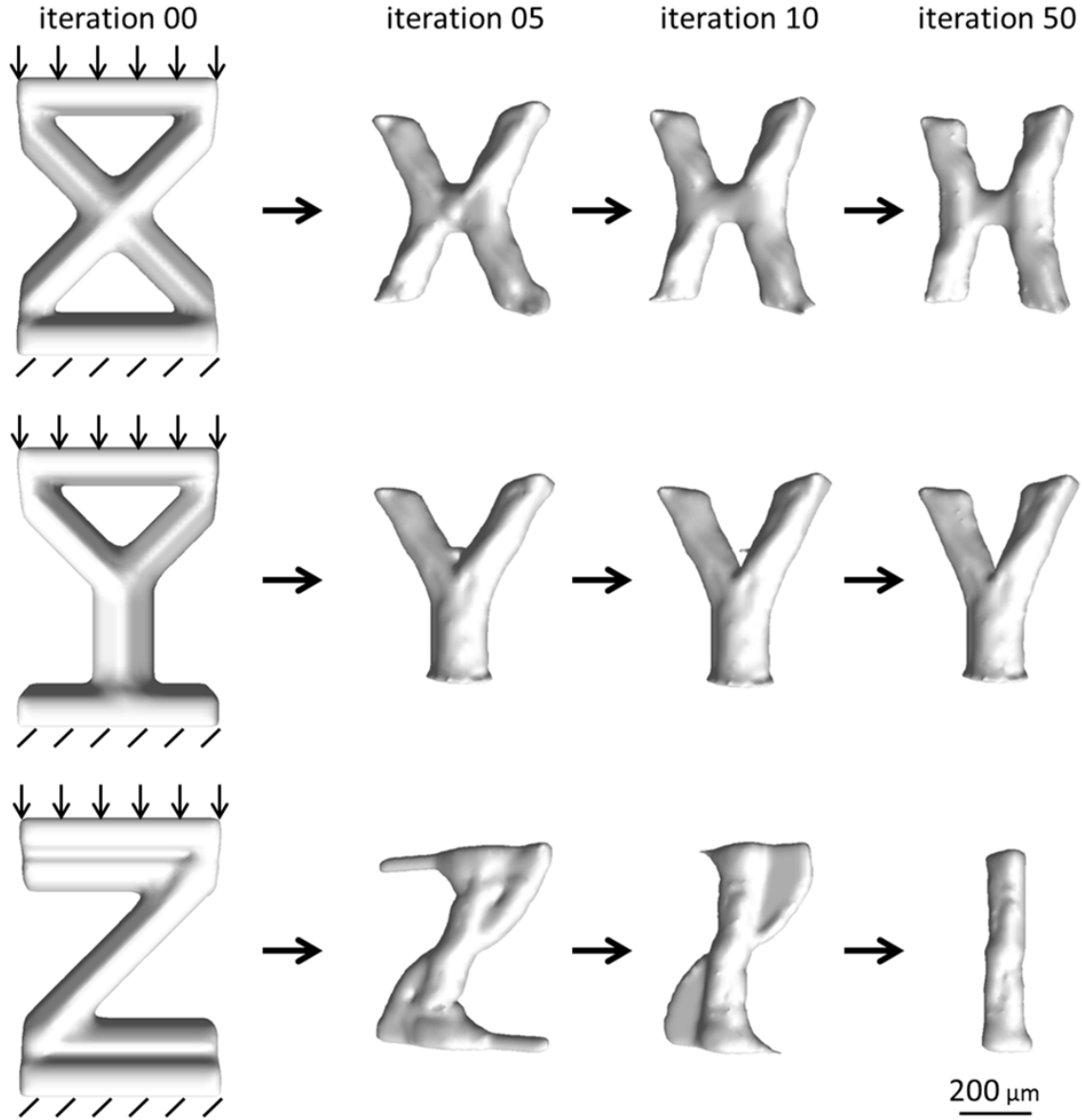


Figure 3.5: Adaptation of single trabeculae to uniaxial compressive loading.

the initial structures to a large degree, whereas the removal of shear loading in x-direction ( $LS_{II}$ ) and removal of both shear load cases ( $LS_{III}$ ) led to more pronounced adaptation and visible changes of the trabeculae. In particular, a high number of trabeculae oriented perpendicularly to the direction of axial compressive loading were removed in the simulations. Bone morphometric indices and the difference to the initial structure are listed in Table 3.3. Bone volume fraction decreased for all loading scenarios (-14.1% with  $LS_I$ , -23.2% with  $LS_{II}$  and -40.6% with  $LS_{III}$ ). Changes from the baseline of other parameters ranged from 0.34% (BS/BV) to 18.9% (Tb.Sp) in  $LS_I$  and from 2.84% (BS/BV) to 34.8% (DA) in  $LS_{III}$ .

Aim 5: The effects of rotation of the axial compressive force and the re-adaptation

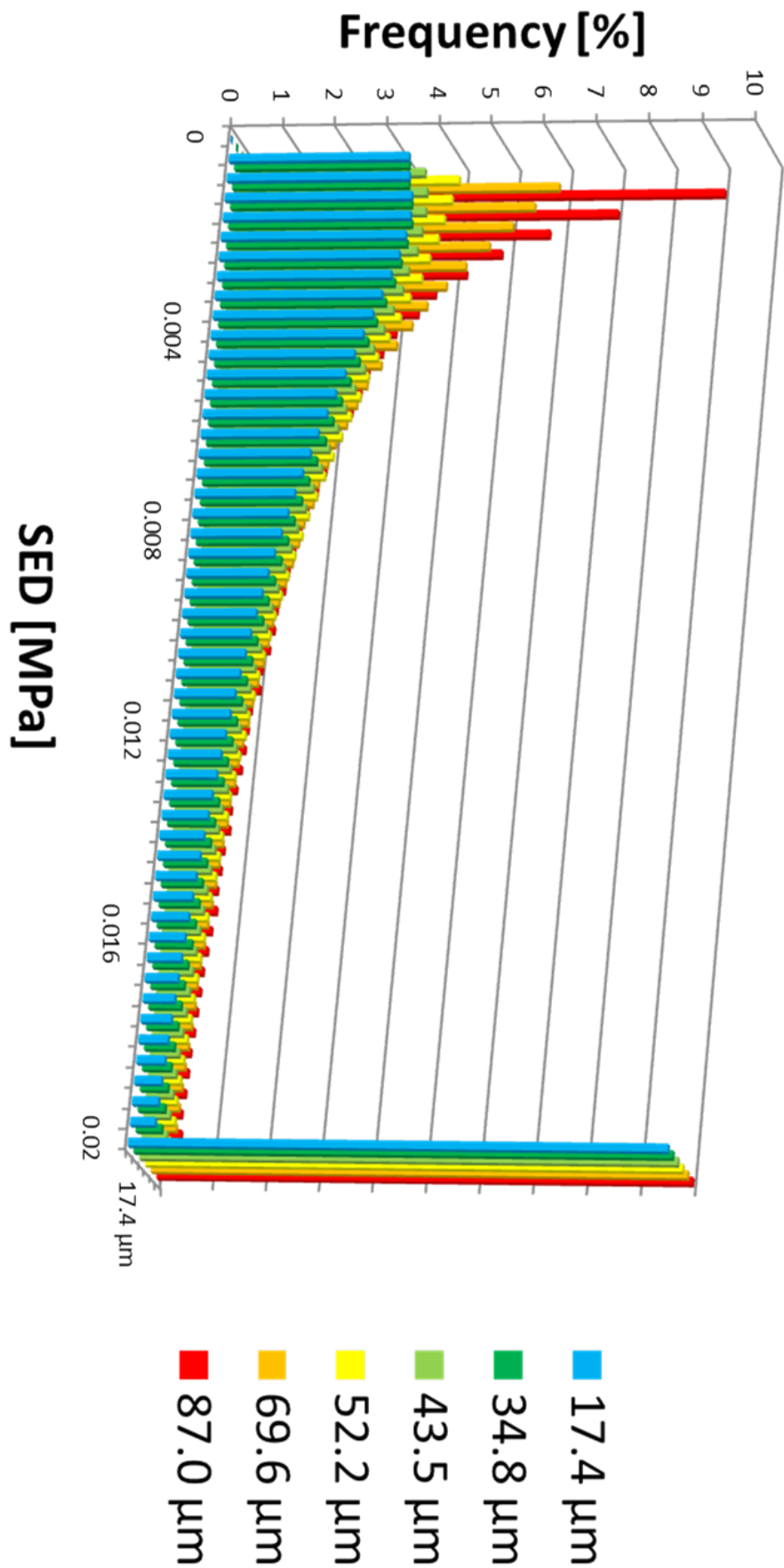


Figure 3.6: SED frequency for different resolutions. While upscaling up to 43.5  $\mu\text{m}$  does maintain the distribution pattern, further upscaling increases the frequency of small SED values in particular.

Table 3.3: Bone morphometric indices for the different loading scenarios tested in Aim 4 on the D<sub>L2</sub> subvolume

	BV/TV [%]	$\Delta$ BV/TV [%]	BS/TV [1/mm]	$\Delta$ BS/TV [%]	DA [-]	$\Delta$ DA [%]	Tb.Th [mm]	$\Delta$ Tb.Th [%]	Tb.Sp [mm]	$\Delta$ Tb.Sp [%]	Tb.N [-]	$\Delta$ Tb.N [%]
Initial value	7.90	0.00	18.73	0.00	1.41	0.00	0.18	0.00	1.04	0.00	0.92	0.00
LS <sub>I</sub>	6.79	-14.06	18.79	0.34	1.62	14.79	0.18	0.54	1.24	18.87	0.78	-15.05
LS <sub>II</sub>	6.07	-23.21	19.23	2.68	1.72	21.57	0.18	1.44	1.26	21.23	0.77	-16.81
LS <sub>III</sub>	4.69	-40.56	19.26	2.84	1.90	34.75	0.19	6.88	1.38	32.49	0.70	-23.81

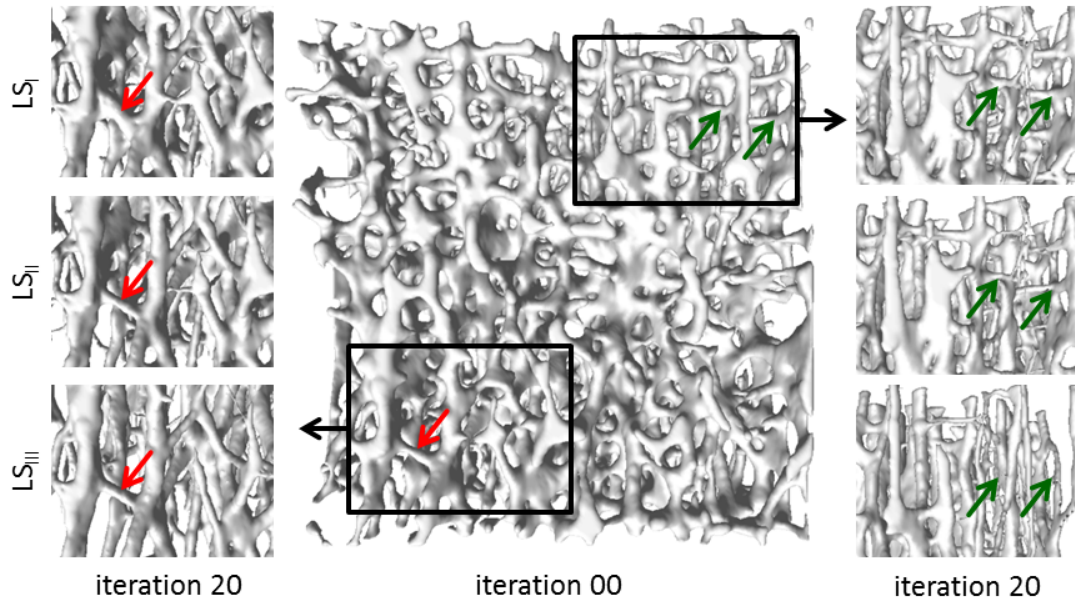


Figure 3.7: Adaptation of trabecular bone with different number of load cases. In the center, a 13 mm cube before remodeling simulations is shown, the extracts on the sides show remodeled bone after 20 simulated years. In the left section a thickening of a trabecula for the 3 load cases sample can be observed (red arrows). The right section shows increasing structural deterioration with decreasing load cases (green arrows).

to the irregular force are shown in Figure 3.8. The angle between the principal direction of trabecular orientation and the z-axis  $\Theta_Z$  is decreasing from  $1.75^\circ$  to  $0.71^\circ$  for  $LS_I$ . The rotation of axial load by  $30^\circ$  ( $LS_{IV}$ ) leads to an increase of  $\Theta_Z$  by  $1.05^\circ$ . Late rotation ( $LS_V$ ) not only reversed the orientation but almost reached the reorientation of the early rotation  $LS_{IV}$ . BV/TV was reduced for both  $LS_I$  and  $LS_{IV}$  simulations, while the reorientation in the late loading  $LS_V$  led to a transitory increase in the morphometric index. The underlying changes of the SED-distribution are shown in Figure 3.9. The distribution of the not rotated  $LS_I$  is similar at iteration 10 and iteration 20, showing a stable remodeling state. Rotation  $LS_V$  shifts the distribution towards higher levels causing increased bone formation. The subsequent bone adaptation moves the SED-distribution back towards the non-rotated stable remodeling state.

### 3.1.4 Discussion

In this paper, we presented a framework for large-scale microstructural simulation of load-adaptive bone remodeling in whole human vertebrae. It included microstruc-

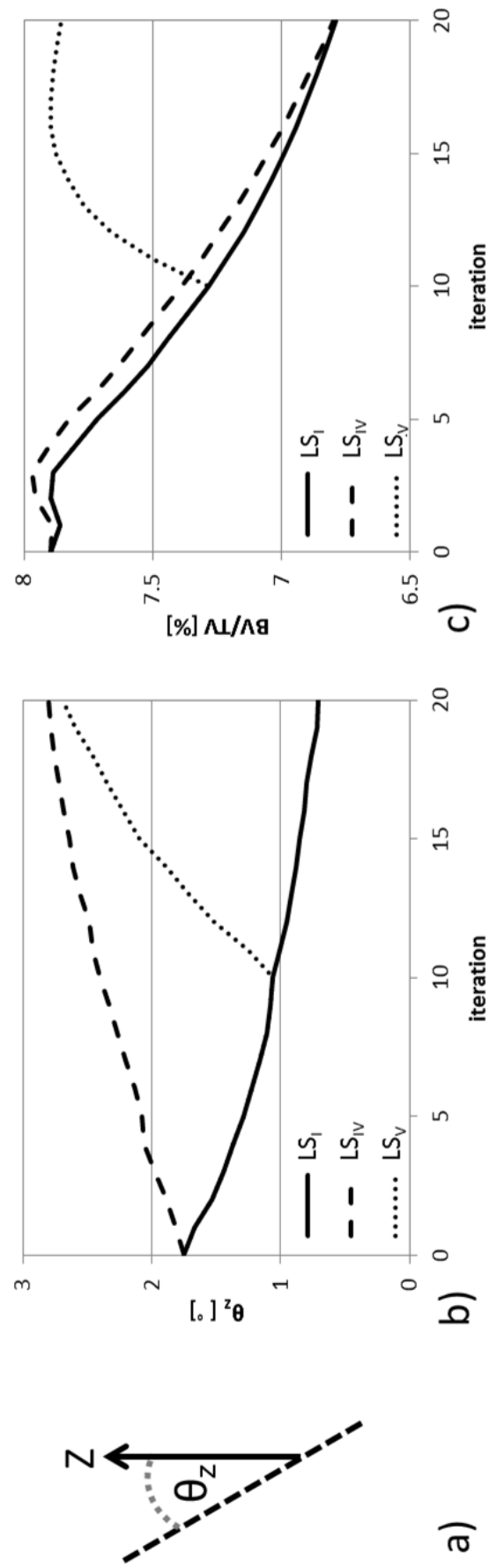


Figure 3.8: Rotation of axial force. a)  $\theta_z$  is the angle between the principal direction of trabecular orientation (dashed line) and the z-axis. Changes during adaptation simulations in b) trabecular orientation and c) bone volume fraction.

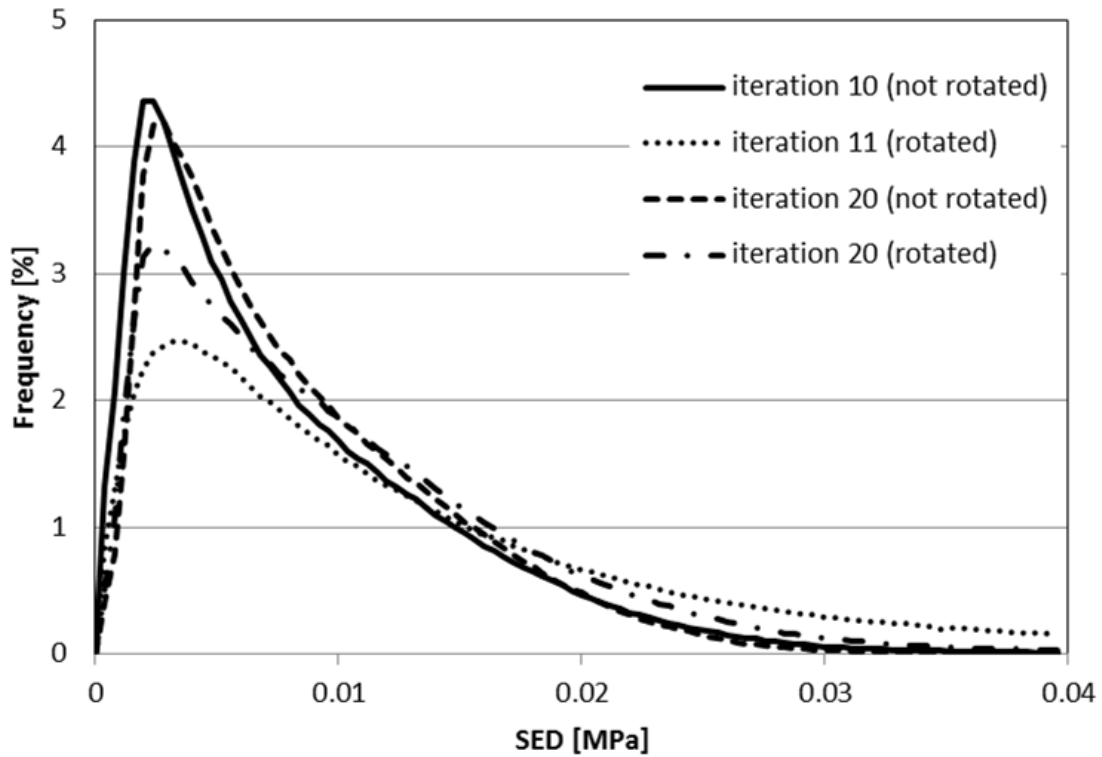


Figure 3.9: SED frequency for  $LS_I$  and  $LS_V$ . The distributions at iteration 10 (not rotated) and iteration 20 (not rotated) are similar. The load rotation (iteration 11 rotated) increases the internal SED and alters the distribution. Nine iterations of bone adaptation shifts the distribution back towards the initial distribution (iteration 20 rotated).

tural analysis of load distribution by means of FE as well as bone remodeling on high-resolution datasets. In addition, the framework included the calculation of complex boundary conditions with multiple load cases.

The bone load estimation was performed prior to the remodeling simulations and defined the boundary conditions for the subsequent adaptation. In line with experimental measurements in the lumbar spine [46, 47], the largest share of the estimated loads (Figure 3.3) was the axial load, accounting for half the load or more in all cases. Between samples, axial loading varied the most but remained in the physiological range below fracture levels [48, 49]. The largest forces were estimated for the sample with the highest bone volume fraction (16.9% BV/TV). If we consider bones with higher bone mass healthy [44, 45], this means healthy samples may be adapted to higher loads in daily life compared to osteoporotic bones.

With variations in bone volume fraction of less than 1.1% per year for the high BV/TV sample and 1.7% for the low BV/TV (Figure 3.4), and similar decreases in bone mass from year 5 onwards, the simulations represent homeostatic adaptation of human bone [12, 44, 45]. Other bone structural indices match the reported values [50] and do not exceed a maximal change of 9.9% (Tb.N of low BV/TV sample) over the simulated 10 years of bone adaptation.

During the bone load estimation the loading conditions leading to the most uniform SED distribution are defined. The resulting strain field however remains inhomogeneous [33] and allows further adaptation of the microstructure to the applied loads. This is reflected in the observed apparent stiffness of the bone along the axial loading force. Although keeping the total bone mass almost constant, stiffness is increased for both samples (Figure 3.4e). The structural adaptation leading to this increase is however a poor indicator for overall fracture risk. It is hypothesized that fractures occur not because of the loading to which the trabecular structure is well adapted to, but rather due to infrequent impact false loading [37].

While the remodeling parameters were designed to reach homeostatic adaptation of the whole bones, these simulations alone were not able to show the true potential of the presented framework. The conservation of the structures is not *a priori* given by the algorithm, but rather a consequence of the use of appropriate boundary conditions. Additional simulations were performed to show the adaptive behavior of the algorithm under known conditions and in synthetic environments (Aims 2b, 4 and 5).

A first verification (Aim 2b) of the algorithm with testing basic remodeling mechanisms was performed with the single trabeculae adaptation. The rotation and adaptation pattern matches the study by Adachi et al. [23]. A minor deviation in

the remodeling can however be seen in the z-shaped trabecula. In our study, the lateral bone resorption is lagging behind the formation of new bone towards the center. In the first few steps, even bone deposition is found in these regions. This is a consequence of using symmetric SED values for the cell signal compared to the strain gradients used by Adachi and colleagues.

The  $\mu$ FE analysis in Aim 3 of a trabecular subvolume at different resolutions subjected to advanced boundary conditions showed only minimal changes in the SED distribution for voxel sizes ranging from 17.4  $\mu\text{m}$  to 43.5  $\mu\text{m}$ . We are therefore confident, that the image resolution used for the remodeling simulations of D<sub>2</sub> or a subvolume is a reasonable compromise to minimize computational costs without major loss of the local mechanical signal quality. However, resizing to lower resolution overestimates the bone quality [51]. This has to be born in mind as it is possibly influencing the quality at the microstructure of remodeling simulations performed on datasets directly measured at a resolution of around 43.5  $\mu\text{m}$ .

The study part investigating the calculated boundary conditions demonstrated the conservation potential of the advanced boundary conditions. Simple reduction of the number of load cases led to increased deterioration in the trabecular structure. The difference is detectable by eye (Figure 7 and Online Resource 4) and calculation of structural parameters showed that while the 3 load case simulations showed moderate changes of maximally 18.9% (Tb.Sp) during the simulated 20 years, changes were on average 2.65 times more severe in the 2 load cases simulation and 4.94 times more severe in the single load case simulation. It was shown in a previous study that a further increase in the number of load cases will not add further to the load estimation outcome [33].

In addition to the conservation of the bone structures with appropriate loading conditions, the rotation of the axial load force in the simulations of the subvolume showed the ability of the bone adaptation algorithm not only to resorb or maintain existing structures, but also to adapt the structure to a new artificially defined load case. In agreement with Ruimerman and colleagues [27], this reorientation comes along with a temporary increase in bone volume.

Finally, a few limitations of the study should be addressed. In order to reach realistic bone adaptation, a significant lazy zone was defined, where the tissue is maintained in the current status and no bone is added or removed. This phenomenon has been reported previously and is in agreement with the inhomogeneity found in the load distribution [33]. Recent research however does not support a remodeling model including a lazy zone [20–22, 52] indicating a potential shift from purely deterministic remodeling models towards partially stochastic models.



Furthermore, we investigated the influence of the voxel size on the  $\mu$ FE signal, but not on the bone remodeling itself. In particular, trabecular thickness spanning over about four voxels in average is not much even when using grey scale images. Nevertheless, the used resolution allows smooth changes of the microstructure over time.

Despite these limitations, the newly developed framework allows large-scale simulations of bone remodeling of whole human vertebrae at a spatial resolution not reached before, including the adaptation of the trabecular microstructure. With progress made in imaging techniques such as HR-pQCT, human datasets with a spatial resolution in the range of our simulations will become accessible and the approach may be used for improved fracture prediction in patients.

## Acknowledgements

The authors thank Dr. Friederike Schulte for her work on the  $\mu$ CT datasets and gratefully acknowledge funding from the European Union Osteoporotic Virtual Physiological Human Project (VPHOP FP7-ICT2008-223865) and the Swiss National Supercomputing Center in Lugano, Switzerland, for computational time (CSCS ID 5372).

## References

- [1] O. Johnell and J. A. Kanis. An estimate of the worldwide prevalence and disability associated with osteoporotic fractures. *Osteoporos Int*, 17(12):1726–33, 2006.
- [2] O. Johnell and J. Kanis. Epidemiology of osteoporotic fractures. *Osteoporos Int*, 16 Suppl 2:S3–7, 2005.
- [3] J. A. Kanis and O. Johnell. Requirements for dxa for the management of osteoporosis in europe. *Osteoporos Int*, 16(3):229–38, 2005.
- [4] J. A. Kanis *et al.* European guidance for the diagnosis and management of osteoporosis in postmenopausal women. *Osteoporos Int*, 19(4):399–428, 2008.
- [5] W. Kemmler *et al.* Benefits of 2 years of intense exercise on bone density, physical fitness, and blood lipids in early postmenopausal osteopenic women: results of the erlangen fitness osteoporosis prevention study (efops). *Arch Intern Med*, 164(10):1084–91, 2004.

- [6] J. A. Kanis *et al.* Assessment of fracture risk and its application to screening for postmenopausal osteoporosis - synopsis of a who report. *Osteoporosis International*, 4(6):368–381, 1994.
- [7] A. M. Briggs *et al.* Measurement of subregional vertebral bone mineral density in vitro using lateral projection dual-energy x-ray absorptiometry: validation with peripheral quantitative computed tomography. *Journal of Bone and Mineral Metabolism*, 30(2):222–231, 2012.
- [8] E. M. Lochmuller, R. Mueller, V. Kuhn, C. A. Lill, F. Eckstein. Can novel clinical densitometric techniques replace or improve dxa in predicting bone strength in osteoporosis at the hip and other skeletal sites? *Journal of Bone and Mineral Research*, 18(5):906–912, 2003.
- [9] E. Perilli *et al.* Failure strength of human vertebrae: prediction using bone mineral density measured by dxa and bone volume by micro-ct. *Bone*, 50(6):1416–25, 2012.
- [10] R. Krug, A. J. Burghardt, S. Majumdar, T. M. Link. High-resolution imaging techniques for the assessment of osteoporosis. *Radiol Clin North Am*, 48(3):601–21, 2010.
- [11] D. Christen *et al.* Improved fracture risk assessment based on nonlinear micro-finite element simulations from hrpqt images at the distal radius. *J Bone Miner Res*, 28(12):2601–8, 2013.
- [12] E. F. Eriksen, F. Melsen, E. Sod, I. Barton, A. Chines. Effects of long-term risedronate on bone quality and bone turnover in women with postmenopausal osteoporosis. *Bone*, 31(5):620–5, 2002.
- [13] S. J. Glover, P. Garnero, K. Naylor, A. Rogers, R. Eastell. Establishing a reference range for bone turnover markers in young, healthy women. *Bone*, 42(4):623–30, 2008.
- [14] D. B. Burr. Targeted and nontargeted remodeling. *Bone*, 30(1):2–4, 2002.
- [15] M. Viceconti, E. Schileo, F. Taddei, S. Martelli, D. Testi. Personalised multi-scale models for risk fracture prediction. *Osteoporos Int*, (21):1067–1071, 2010.
- [16] J. Wolff. The classic: on the inner architecture of bones and its importance for bone growth. 1870. *Clin Orthop Relat Res*, 468(4):1056–65, 2010.

- [17] C. R. Jacobs, S. Temiyasathit, A. B. Castillo. Osteocyte mechanobiology and pericellular mechanics. *Annu Rev Biomed Eng*, 12:369–400, 2010.
- [18] H. M. Frost. Bone’s mechanostat: a 2003 update. *Anat Rec A Discov Mol Cell Evol Biol*, 275(2):1081–101, 2003.
- [19] R. Huiskes *et al.* Adaptive bone-remodeling theory applied to prosthetic-design analysis. *J Biomech*, 20(11-12):1135–50, 1987.
- [20] F. A. Schulte *et al.* Local mechanical stimuli regulate bone formation and resorption in mice at the tissue level. *PLoS One*, 8(4):e62172, 2013.
- [21] T. Sugiyama *et al.* Bones’ adaptive response to mechanical loading is essentially linear between the low strains associated with disuse and the high strains associated with the lamellar/woven bone transition. *J Bone Miner Res*, 27(8):1784–93, 2012.
- [22] P. Christen *et al.* Bone remodelling in humans is load-driven but not lazy. *Nat Commun*, 5:4855, 2014.
- [23] T. Adachi, K. Tsubota, Y. Tomita, S. J. Hollister. Trabecular surface remodeling simulation for cancellous bone using microstructural voxel finite element models. *Journal of Biomechanical Engineering-Transactions of the Asme*, 123(5):403–409, 2001.
- [24] P. Christen *et al.* Patient-specific bone modelling and remodelling simulation of hypoparathyroidism based on human iliac crest biopsies. *J Biomech*, 45(14):2411–6, 2012.
- [25] P. Mc Donnell, N. Harrison, M. A. Liebschner, P. E. Mc Hugh. Simulation of vertebral trabecular bone loss using voxel finite element analysis. *J Biomech*, 2009.
- [26] F. A. Schulte *et al.* Strain-adaptive in silico modeling of bone adaptation - a computer simulation validated by in vivo micro-computed tomography data. *Bone*, 52(1):485–92, 2013.
- [27] R. Ruimerman, P. Hilbers, B. van Rietbergen, R. Huiskes. A theoretical framework for strain-related trabecular bone maintenance and adaptation. *Journal of Biomechanics*, 38(4):931–941, 2005.

- [28] A. J. Fields, S. K. Eswaran, M. G. Jekir, T. M. Keaveny. Role of trabecular microarchitecture in whole-vertebral body biomechanical behavior. *J Bone Miner Res*, 24(9):1523–30, 2009.
- [29] A. Levchuk *et al.* The clinical biomechanics award 2012 - presented by the european society of biomechanics: large scale simulations of trabecular bone adaptation to loading and treatment. *Clin Biomech (Bristol, Avon)*, 29(4):355–62, 2014.
- [30] R. Ruimerman. Modeling and remodeling in bone tissue. *electronic, University Library, Doctoral Thesis, TU Eindhoven*, page Available: <http://alexandria.tue.nl/extra2/200510655.pdf>, 2005.
- [31] R. Mueller. Long-term prediction of three-dimensional bone architecture in simulations of pre-, peri- and post-menopausal microstructural bone remodeling. *Osteoporos Int*, 16 Suppl 2:S25–35, 2005.
- [32] P. Christen, K. Ito, A. A. Santos, R. Mueller, R. Bert van. Validation of a bone loading estimation algorithm for patient-specific bone remodelling simulations. *J Biomech*, 46(5):941–8, 2013.
- [33] P. Christen, B. van Rietbergen, F. M. Lambers, R. Mueller, K. Ito. Bone morphology allows estimation of loading history in a murine model of bone adaptation. *Biomech Model Mechanobiol*, 2011.
- [34] R. P. Widmer and S. J. Ferguson. A comparison and verification of computational methods to determine the permeability of vertebral trabecular bone. *Proc Inst Mech Eng H*, 227(6):617–28, 2013.
- [35] M. G. Mullender and R. Huiskes. Proposal for the regulatory mechanism of wolff’s law. *J Orthop Res*, 13(4):503–12, 1995.
- [36] C. Flaig and P. Arbenz. A scalable memory efficient multigrid solver for micro-finite element analyses based on ct images. *Parallel Computing*, 37(12):846–854, 2011.
- [37] J. Homminga *et al.* The osteoporotic vertebral structure is well adapted to the loads of daily life, but not to infrequent "error" loads. *Bone*, 34(3):510–6, 2004.
- [38] R. K. Wilcox *et al.* A dynamic investigation of the burst fracture process using a combined experimental and finite element approach. *Eur Spine J*, 13(6):481–8, 2004.

- [39] E. F. Morgan, H. H. Bayraktar, T. M. Keaveny. Trabecular bone modulus-density relationships depend on anatomic site. *J Biomech*, 36(7):897–904, 2003.
- [40] T. S. Keller, V. Kosmopoulos, I. H. Lieberman. Vertebroplasty and kyphoplasty affect vertebral motion segment stiffness and stress distributions: a microstructural finite-element study. *Spine (Phila Pa 1976)*, 30(11):1258–65, 2005.
- [41] A. Polikeit, L. P. Nolte, S. J. Ferguson. The effect of cement augmentation on the load transfer in an osteoporotic functional spinal unit: finite-element analysis. *Spine (Phila Pa 1976)*, 28(10):991–6, 2003.
- [42] P. Christen *et al.* Subject-specific bone loading estimation in the human distal radius. *J Biomech*, 46(4):759–66, 2013.
- [43] R. Al Nazer, J. Lanovaz, C. Kawalilak, J. D. Johnston, S. Kontulainen. Direct in vivo strain measurements in human bone—a systematic literature review. *J Biomech*, 45(1):27–40, 2012.
- [44] S. Boutroy, M. L. Bouxsein, F. Munoz, P. D. Delmas. In vivo assessment of trabecular bone microarchitecture by high-resolution peripheral quantitative computed tomography. *J Clin Endocrinol Metab*, 90(12):6508–15, 2005.
- [45] S. Khosla *et al.* Effects of sex and age on bone microstructure at the ultradistal radius: a population-based noninvasive in vivo assessment. *J Bone Miner Res*, 21(1):124–31, 2006.
- [46] N. Arjmand, A. Shirazi-Adl, B. Bazrgari. Wrapping of trunk thoracic extensor muscles influences muscle forces and spinal loads in lifting tasks. *Clin Biomech (Bristol, Avon)*, 21(7):668–75, 2006.
- [47] J. Calisse, A. Rohlmann, G. Bergmann. Estimation of trunk muscle forces using the finite element method and in vivo loads measured by telemeterized internal spinal fixation devices. *J Biomech*, 32(7):727–31, 1999.
- [48] Y. Chevalier, D. Pahr, P. K. Zysset. The role of cortical shell and trabecular fabric in finite element analysis of the human vertebral body. *J Biomech Eng*, 131(11):111003, 2009.
- [49] P. A. Hulme, S. K. Boyd, S. J. Ferguson. Regional variation in vertebral bone morphology and its contribution to vertebral fracture strength. *Bone*, 41(6):946–57, 2007.

- [50] J. Wegrzyn *et al.* Role of trabecular microarchitecture and its heterogeneity parameters in the mechanical behavior of ex vivo human l3 vertebrae. *J Bone Miner Res*, 25(11):2324–31, 2010.
- [51] D. G. Kim, G. T. Christopherson, X. N. Dong, D. P. Fyhrie, Y. N. Yeni. The effect of microcomputed tomography scanning and reconstruction voxel size on the accuracy of stereological measurements in human cancellous bone. *Bone*, 35(6):1375–82, 2004.
- [52] J. W. Dunlop, M. A. Hartmann, Y. J. Brechet, P. Fratzl, R. Weinkamer. New suggestions for the mechanical control of bone remodeling. *Calcif Tissue Int*, 85(1):45–54, 2009.

## Chapter 4

# Applications of large-scale simulations of load-adaptive bone remodeling





## 4.1 Simulations of osteoporotic bone loss in native whole human vertebrae

Sandro D. Badilatti<sup>1</sup>, Patrik Christen<sup>1</sup>, Ian Parkinson<sup>2</sup> and Ralph Müller<sup>1</sup>

<sup>1</sup>Institute for Biomechanics, ETH Zurich, 8093 Zurich, Switzerland

<sup>2</sup>SA Pathology and University of Adelaide, Adelaide, 5005 South Australia, Australia

### **in preparation as:**

Load-adaptive remodeling simulations reveal osteoporotic microstructural and mechanical changes in human vertebrae

### **Abstract:**

Osteoporosis is one of the greater medical burdens for our society and its impact is expected to increase. It is associated with low bone density and microstructural deteriorations. Treatments are available, but the critical factor is being able to define individuals at risk from osteoporotic fractures. Computational simulations investigating not only changes in the net bone tissue volume, but also changes in its microstructure where osteoporotic deteriorations occur might help to better predict the risk of fractures.

In this study, bone remodeling simulations with a mechanical feedback loop were used to predict microstructural changes due to osteoporosis, and their impact on bone fragility from 50 to 80 years of age. Starting from homeostatic bone remodeling of a group of seven vertebrae, five models mimicking different biological alterations associated with osteoporosis were developed on a single bone, leading to imbalanced bone formation and resorption with a total net loss of bone tissue. The best-matching model to findings from literature was chosen to predict postmenopausal osteoporotic bone loss in the whole group.

Thirty years of osteoporotic bone loss were predicted with changes in morphometric indices in agreement with experimental measurements, and only showing major deviations in trabecular number and trabecular spacing. In particular, although being optimized to match to the morphometric indices alone, the predicted bone loss revealed realistic changes on the organ level and on the biomechanical competence. While the osteoporotic bone was able to maintain the mechanical stability to a great extent, higher fragility towards error loads was found for the osteoporotic

bones.

**Keywords:**

Bone Adaptation, Bone Remodeling Simulations, Human Vertebra, Bone Loading Estimation, Micro Finite Element Modeling, Osteoporosis

### **4.1.1 Introduction**

Our society greatly benefits from modern medicine with reduced mortality rates allowing many to reach old age. At the same time, this desirable progress inevitably changes the demographics with the number of elderly increasing [1]. This is particularly impacting medicine and medical research, which, due to its success in life-preservation, will have to increasingly focus on age-related ailments. Next to other major age-related illnesses such as cardiovascular problems, cancer, osteoarthritis and Alzheimer's disease, osteoporosis has a great impact on the quality of life [2]. The disease is defined by a reduction of bone mass, but the clinical significance arises from the frequent subsequent bone fractures caused by deterioration of the microstructure and mostly occurring in the vertebra, the proximal femur and the wrist [3, 4]. Not only are such fractures painful and often difficult to treat, morbidity is substantial and severe cases lead to increased mortality [5]. By 2025, it is estimated that osteoporosis-related fractures will rise by almost 50% in the United States alone [6].

Osteoporosis is most commonly found in postmenopausal women, where a massive loss of bone tissue occurs within just a few years [7]. While the net bone loss can partly be inhibited by medication with bisphosphonates and parathyroid hormone [8], a crucial aspect for the successful prevention of osteoporotic bone fractures is an identification of patients at risk. Dual-energy X-ray absorptiometry is commonly used for the determination of fracture risk [9], but this technique is not able to capture the bone microstructure and thus the osteoporotic microstructural changes, although such deteriorations of the microstructure greatly affect bone strength and thus fracture risk [10, 11]. Assessment of bone microstructure is however possible with micro-computed tomography ( $\mu$ CT) in biopsies or animals, and high-resolution peripheral quantitative computed tomography (HR-pQCT) in patients, where the three-dimensional trabecular microstructure is imaged with high fidelity [12]. Feeding this image data into micro finite element ( $\mu$ FE) models then allows a highly accurate estimation of bone specific bone strength and fracture risk [13, 14].

Translating bone microstructure in a future state could even serve to predict

bone strength and thus also bone fracture risk, which would greatly improve the identification of patients at risk of fractures. But this is complicated due to the uninterrupted turnover and reorganization of the bone matrix in the process known as bone remodeling. [15, 16]. Guided by mechanosensitive osteocytes, bone forming osteoblasts and bone resorbing osteoclasts continuously renew the structure and adapt it to withstand the most prevalent daily loads [17]. This mechanical regulation leads to the optimized orientation of the trabecula in healthy bone [18]. In the case of osteoporosis, however, the fragile equilibrium is shifted towards disproportional net resorption and only the most crucial structures are conserved [19]. While this decreases mechanical stability as a whole, osteoporotic bones get particularly susceptible to non-typical loads even with magnitudes below what would normally cause a fracture in healthy bone [20]. A translation of bone microstructure should therefore account for such osteoporotic microstructural changes.

Predicting changes of the bone microstructure generally is the scope of computational bone remodeling simulations. In the past years, mechanically targeted remodeling of trabecular bone has been simulated [21–26]. Although accurate strength assessment necessitates whole bone microstructural analysis [11, 27], human remodeling simulations of micro-computed tomography ( $\mu$ CT) derived bones have mostly been restricted to biopsies [23, 24, 26], but recently the feasibility of microstructural bone remodeling simulations with mechanical feedback on whole human bones has been shown [22]. The mechanical feedback is typically modelled with algorithms based on the mechanostat theory [28]. It postulates that tissue adaptation is a consequence of the magnitude of a local mechanical signal, and supporting findings have been found *in vivo* for animals [29, 30] and humans [31]. If the signal is below a required amount, local disuse is assumed and the tissue removed. On the other hand, a signal exceeding a formation level will lead to local bone deposition. This mechanoregulation leads to the previously mentioned trabecular orientation and additionally allows the bone to adapt to new loading patterns [25]. The key difference to move from sub-volume to whole bone simulations, apart from the increased computational requirements [25], is the definition of appropriate boundary conditions for the applied loads for the mechanical signal calculation using  $\mu$ FE analysis [22]. Such realistic loading conditions are calculated by reversing the idea of bone adaptation: trabecular orientation, as it is found at any time point, is an optimization to previous loads and hence can be used to back-calculate the most prevalent external forces [32, 33]. We have recently shown, that in whole bone simulations, this bone loading estimation approach provides boundary conditions leading to realistic healthy bone remodeling [22].

The purpose of the present study is to extend this previous healthy bone remodeling simulation to simulate postmenopausal osteoporosis in whole human vertebrae to investigate the osteoporotic microstructural changes and their impact on the biomechanical competence and fracture risk. We hypothesize that if simulations of load-driven bone remodeling realistically predict microstructural changes due to bone loss, the deterministic mechanoregulation is sufficient to realistically predict changes on the organ level including the biomechanical competence and fracture prediction. To test this hypothesis, we first match changes in static morphometric indices to experimental findings and simulate bone loss over a period of 30 years. Subsequent mechanical testing and visual inspection will be used to evaluate the hypothesis. High resolution three-dimensional  $\mu$ FE models of seven vertebral bodies were generated from  $\mu$ CT images. The boundary conditions for the loading were calculated with the above mentioned bone loading estimation approach. An iterative load-driven bone remodeling framework with a parameter set defined in the previous healthy remodeling study [22] was used to simulate a control group with homeostatic changes representing healthy aging. Then, the median sample was used to analyze the effects of changes in the model parameters leading to imbalanced bone resorption and formation and a total net volume loss as observed in osteoporosis. Parameter changes include increased resorption rates, reduced cell sensitivity and reduced formation rates (Figure 4.1). Standard bone morphometric parameters were calculated for every iteration step and compared to data from human biopsies from a study on postmenopausal osteoporosis [7]. Finally, the parameter set with the best matching outcome of the changes in the morphometric parameters was subsequently used for all seven samples to simulate osteoporosis. The mechanical competence of these simulated bones was calculated using  $\mu$ FE analysis and resistance to fractures was assessed.

### **4.1.2 Results**

The simulations were performed on a group of  $\mu$ CT derived human vertebral bodies measured at a resolution of  $43.5\ \mu\text{m}$  with an average initial BV/TV of 13.8% and a large standard deviation of 3.24%, though in the same range as reported elsewhere [7, 15]. No information about the age of the samples was available and all samples were assigned to a starting age of 50 years. As morphometric parameters showed considerable differences in the bone quality already at this point, we supposed that this heterogeneous group was a good representation of the population. They showed considerable variation in bone volume fraction (BV/TV) ranging from 19.4% to 9.2% and a mean value of 13.8%. The samples were labelled in decreasing order of BV/TV

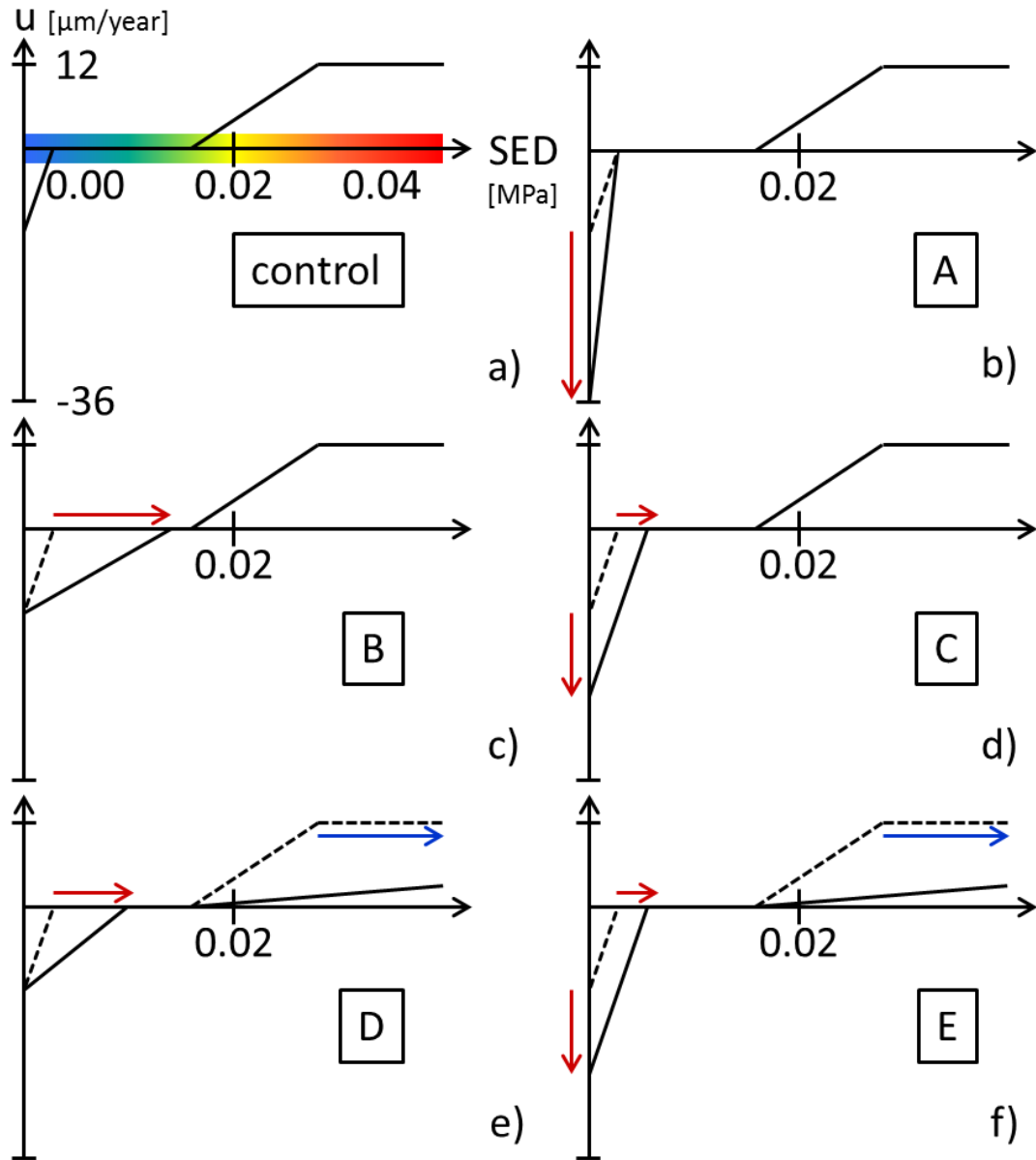


Figure 4.1: **Visualization of the mechanostat model parameters used in the remodeling simulations.** The x axis shows SED values as the mechanical signal, the y axis shows the bone growth velocity normal to the bone surface. a) Control group with no net bone loss b) set A with increased resorption saturation level c) set B with reduced cell sensitivity d) set C with increased resorption and reduced cell sensitivity e) set D with reduced formation rate and cell sensitivity and f) set E with increased resorption, reduced formation rate and cell sensitivity.

from c01 to c07 for the control group and o01 to o07 for the simulated osteoporosis group. At the first time point, corresponding to an age of 50 years, samples from the control group and osteoporotic group were identical.

As expected, the control group samples showed little change in morphometric indices over the course of the simulated 21 years (Figure 4.2). Both BV/TV and bone surface per bone volume (BS/BV) decreased by less than 1%. Changes in trabecular thickness (Tb.Th) (+0.78%) were also minor, trabecular spacing (Tb.Sp) (+2.54%) and trabecular number (Tb.N) (-2.54%) slightly greater. The largest changes were found the degree of anisotropy (DA) (+2.81%), the structure model index (SMI) (-2.81%) and the trabecular bone pattern factor (TBPf) (-3.22%) on average.

The comparison of virtual biopsies of our simulated bones and real biopsies from a previous study [34] is shown in Figure 4.4. The pre-menopausal bone (50 years) has thicker and better interconnected structures. After the simulated 30 years of bone loss, gaps between the structures arise and the single trabeculae get thinner and more strut-like, a pattern also found in the real biopsies of 80 year old subjects. On average, the samples lost 30.7% BV/TV (Figure 4.2 and Figure 4.3). While the samples with high initial bone volume (o01, o02) lost the most in absolute numbers, the relative highest bone loss occurred for the sample with the lowest initial bone volume (o07). BS/BV increased in all samples by 21.9% on average. Tb.Th decreased by 11.61% and Tb.Sp increased accordingly by 7.8%, with a decrease in Tb.N of 5.8%. The trabecular structure got more aligned as the DA increased on average by 10.0%. The change from plate to rod-like structures can be seen in Figure 4.5 and is quantitatively described by the increase of the SMI by 38.1%. The rod-like structures are formed both through perforations of bone plates or by thinning of a bulky trabecula. Finally, the TBPf, an indicator for the trabecular interconnectivity, increased by 68.8% indicating the decreased number of connections between the trabeculae. Disconnecting trabeculae are visualized in Figure 4.5.

Effects of postmenopausal osteoporosis on the trabecular bone at the organ scale are shown in Figure 4.6. The ventral slice shows loss of whole trabecular packages close to the cortex on both sides, the dorsal slice shows loss of trabecular bone towards the forearm. In the central slice, bone loss is more equally distributed.

In addition to morphometric parameters, mechanical stability was assessed for the samples of the osteoporotic group. The changes in apparent stiffness in axial compression are shown in Figure 4.7. The stiffness is reduced for all samples by 7.87% on average, but varies between samples (max. 10.84% for o05, min. 5.97% for o07). The mechanical robustness of the bones was investigated by calculating the failure load using the Pistoia criterion [14] for several load cases. Figure 4.8

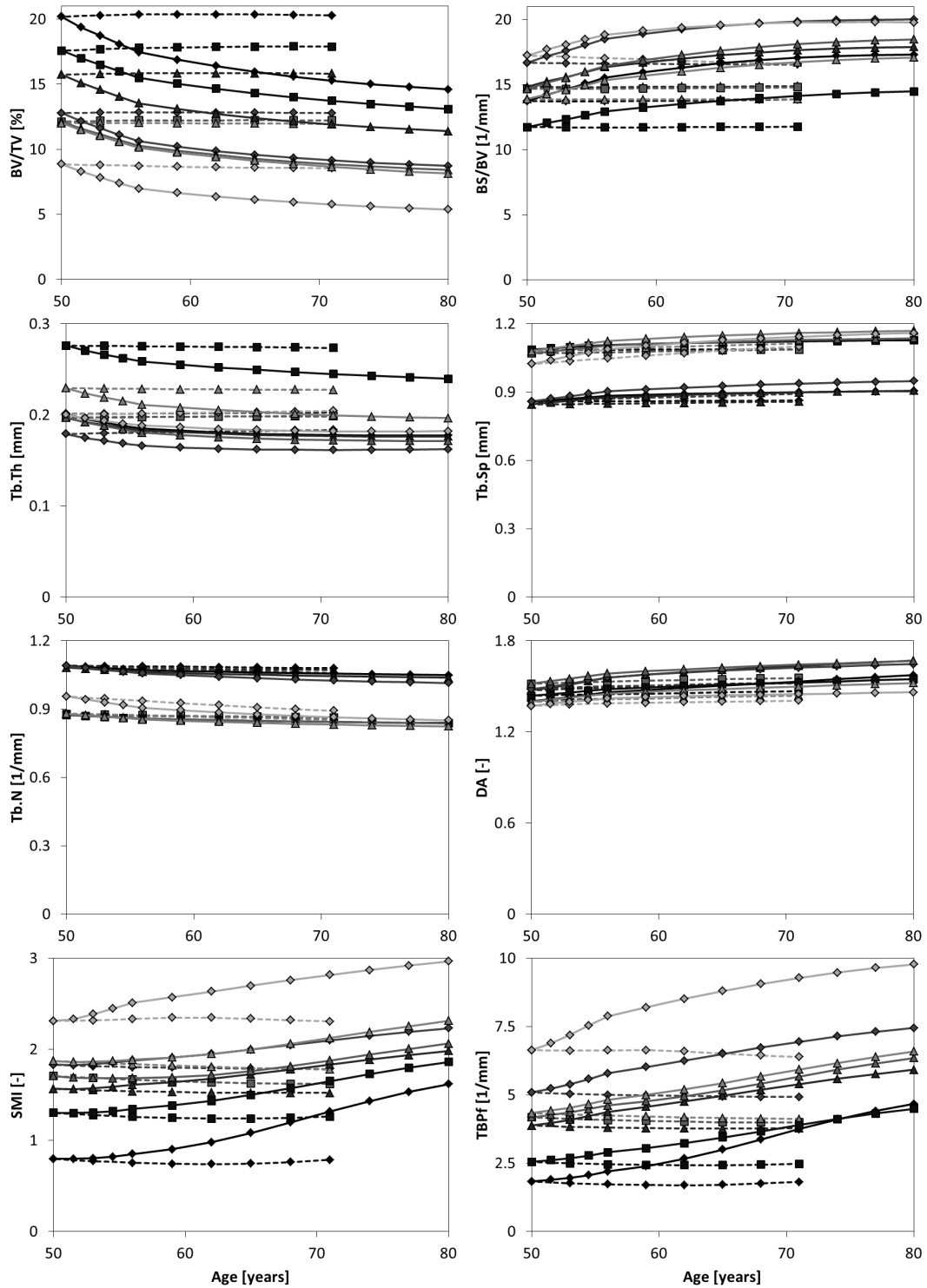


Figure 4.2: **Course of bone morphometric indices over time.** Absolute values for all samples (black c01/o01 to light gray c07/o07) and both control (dashed line) and osteoporotic group (continuous line) are shown. Calculated morphometric indices are (from top left to bottom right): BV/TV, BS/BV, Tb.Th, Tb.Sp, Tb.N, DA, SMI, TBPf.

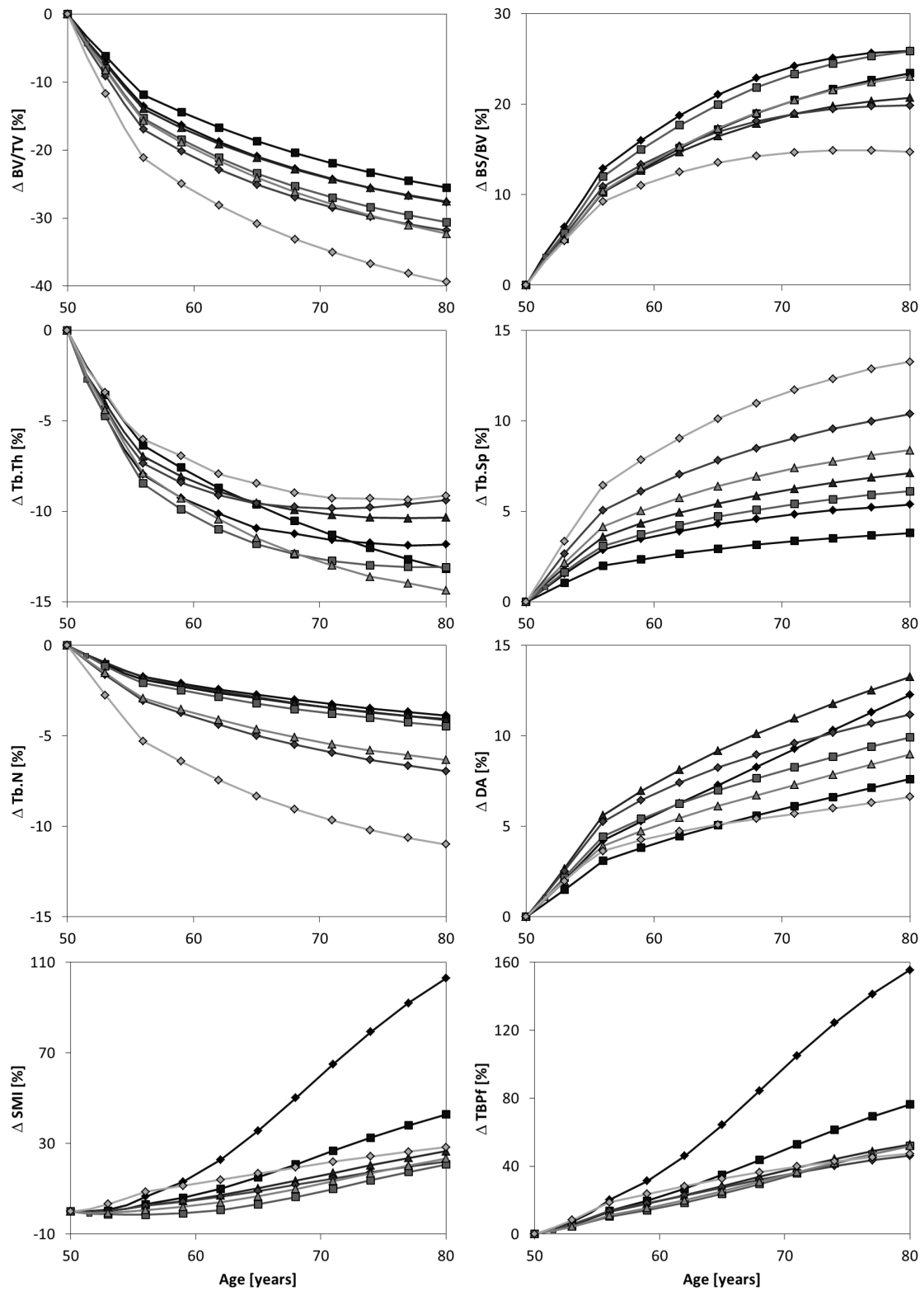


Figure 4.3: **Relative changes of bone morphometric indices for the osteoporotic group.** The samples range from o01 (black) to o07 (light gray). Calculated morphometric indices are (from top left to bottom right): BV/TV, BS/BV, Tb.Th, Tb.Sp, Tb.N, DA, SMI, TBPf.



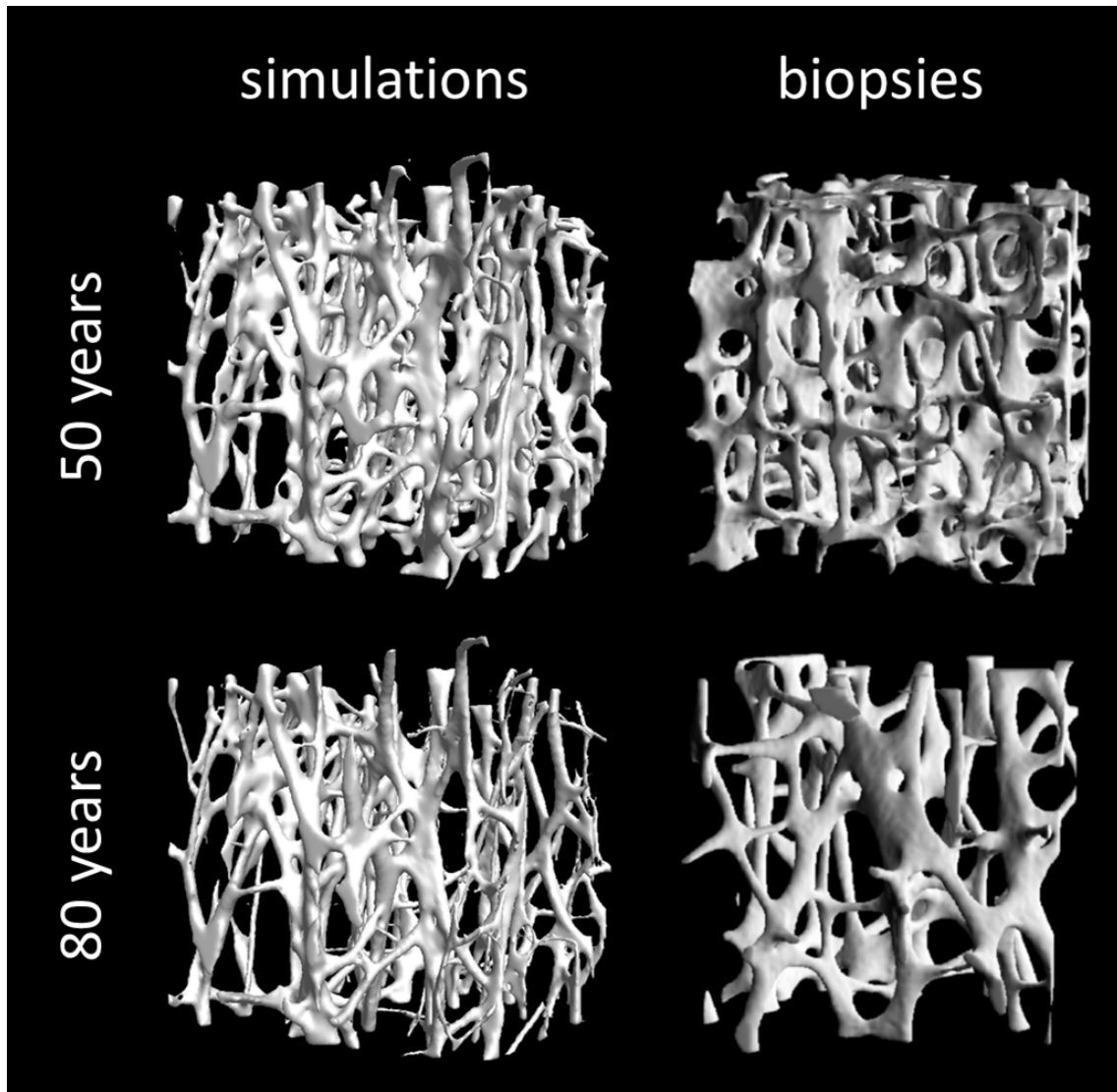


Figure 4.4: **Comparison between simulated and real trabecular bone biopsies.** In both simulated (left) and read (right) cases, the pre-menopausal case (50 years) structures are thicker and well-connected. The post-menopausal bone (80 years) shows more gaps and in general trabecular structures are thinner and strut-like. Figures from the biopsies [?] reproduced according to the guidelines of the publisher.

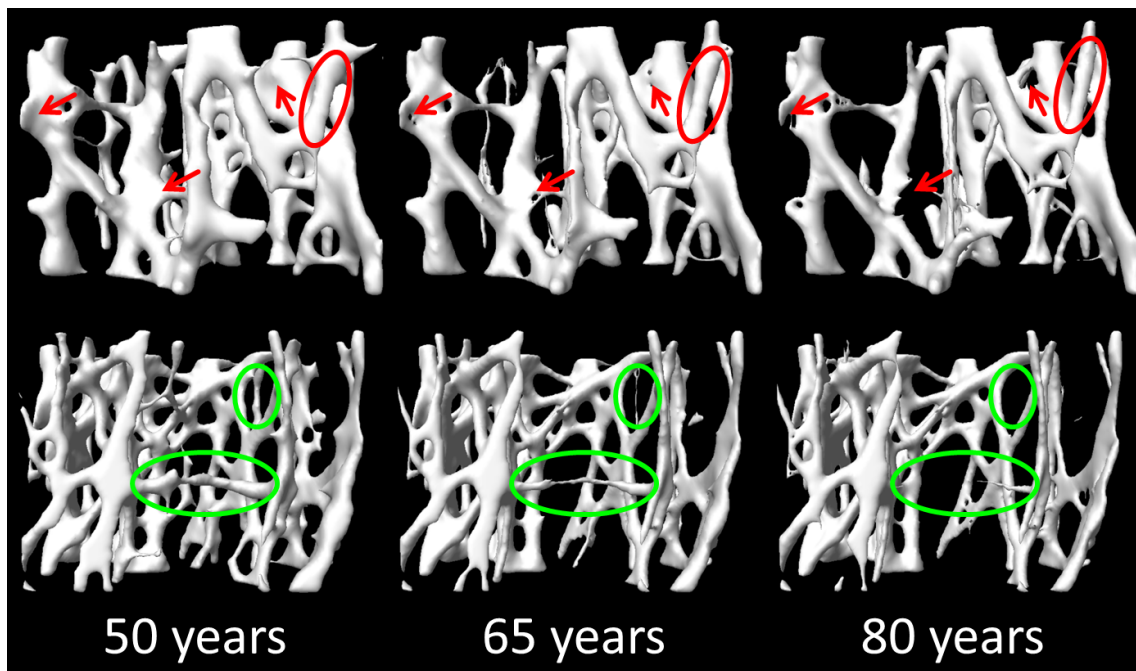


Figure 4.5: **Changes of the bone microstructure.** The structure changes from plate to rod-like structures (red) and from well-connected to disconnected structures (green). The rod-like structures are created either by perforation (arrows) or by thinning of a bulky trabecula (circle).

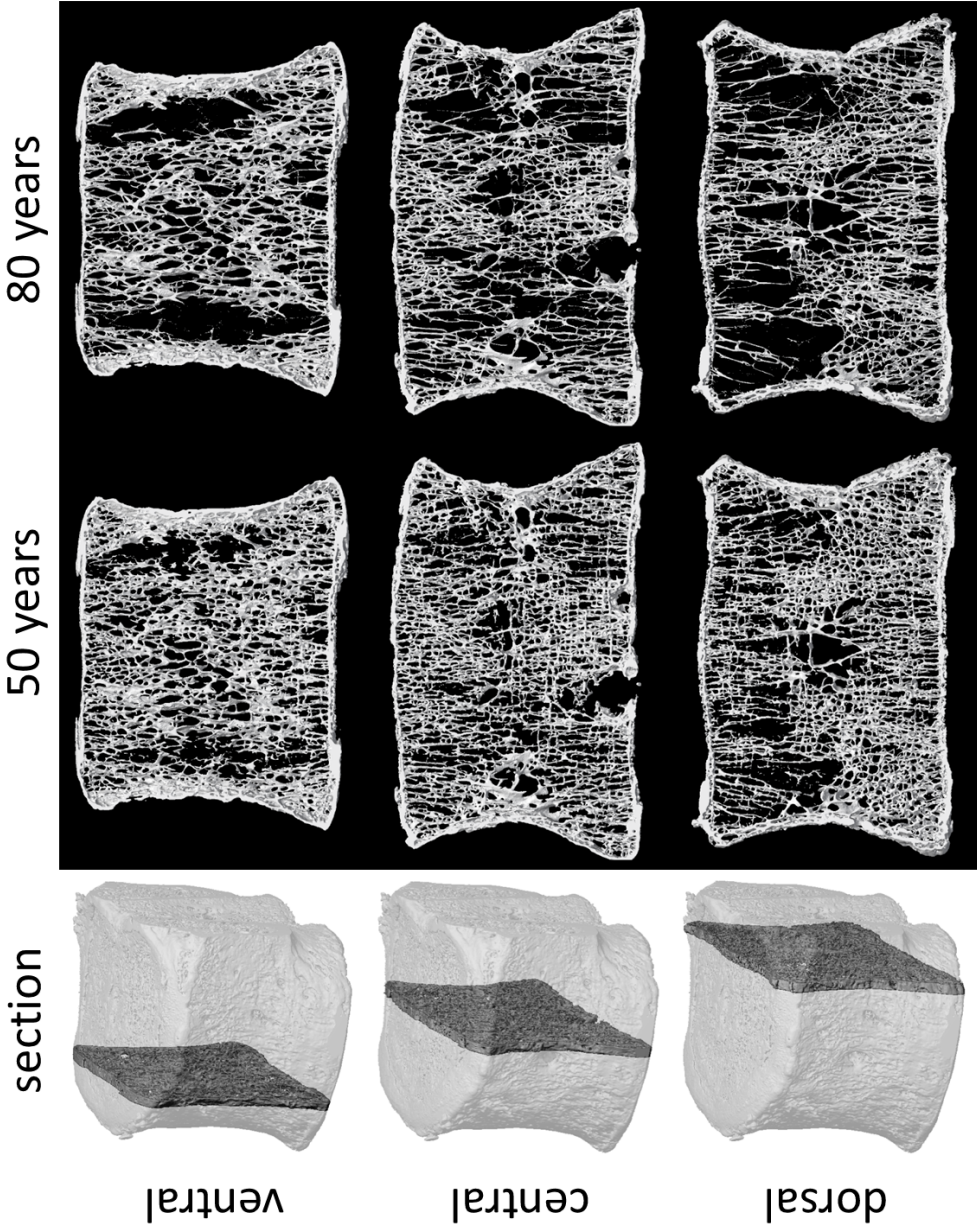


Figure 4.6: **Remodeled whole vertebrae.** Ventral (top), central (middle) and dorsal (bottom) slice of a whole vertebra before and after simulated postmenopausal osteoporosis. Loss of whole trabecular packages can be found close to the cortex in the ventral and close to the foramen in the dorsal slices.

shows the strength of all load cases that were used as boundary conditions in the bone remodeling simulations. While axial compression strength is reduced by at least 1.9% for all samples, strength towards shear loading varied between +3.94% ( $F_{ZY}$  for o02) and -5.17% ( $F_{ZX}$  for o03). The effects of simulated osteoporosis on the strength towards error loads are shown in Figure 4.9. While failure strength is lower for error loads at the age of 50 already (-13% on average,  $p$ -value  $< 0.05$ ), this effect is further increased at the age of 80 (-17%,  $p$ -value  $< 0.01$ ).

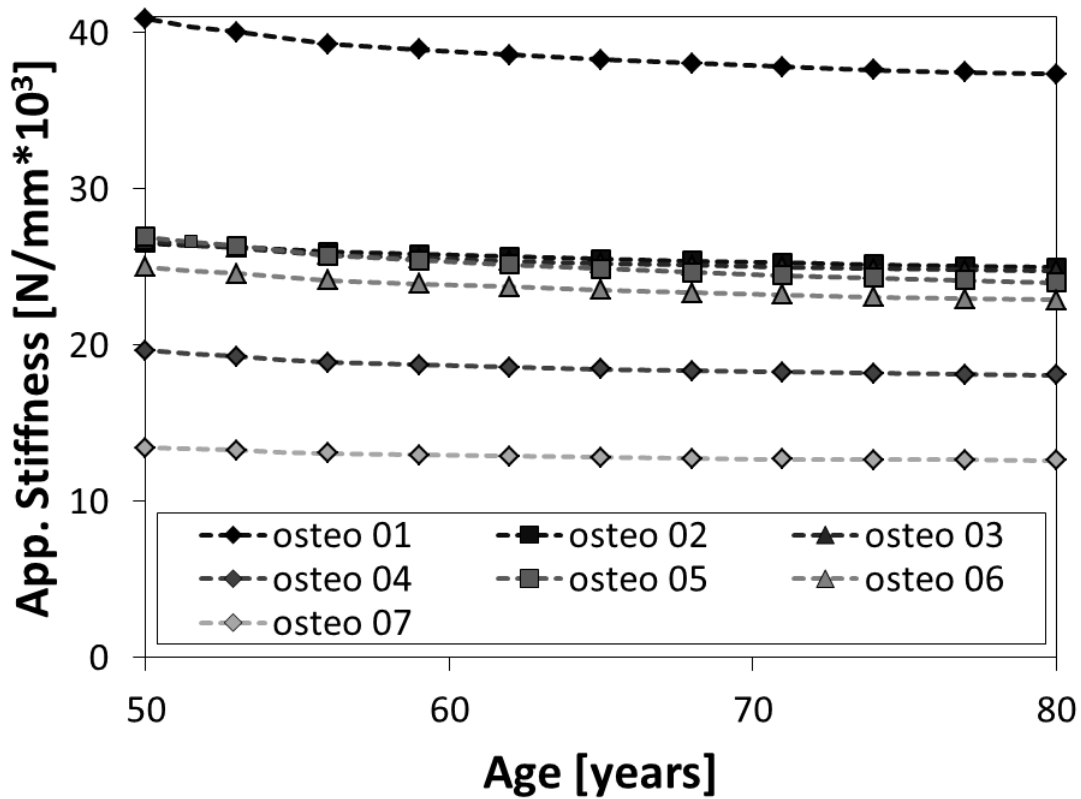


Figure 4.7: **Course of apparent stiffness over time.** Although average BV/TV was reduced during the simulated 30 years by more than 30%, the reduction in average apparent stiffness was less than 8%.

Computations included the  $\mu$ FE analysis, the remodeling algorithm and the calculation of the morphometric parameters, with  $\mu$ FE analysis run on a supercomputer and taking up the largest computational effort by far. The usage for the  $\mu$ FE is shown in Figure 4.10. The 10 iterations of the control group (Figure 4.10, top) were calculated on 32 parallel nodes with a total of 1024 cores, the 13 iterations of the osteoporosis group (Figure 4.10, bottom) on 16 parallel nodes with a total of 384 cores. Simulations for the osteoporosis group were run on a cluster with higher memory capacity, which allowed a considerable reduction of the computational time

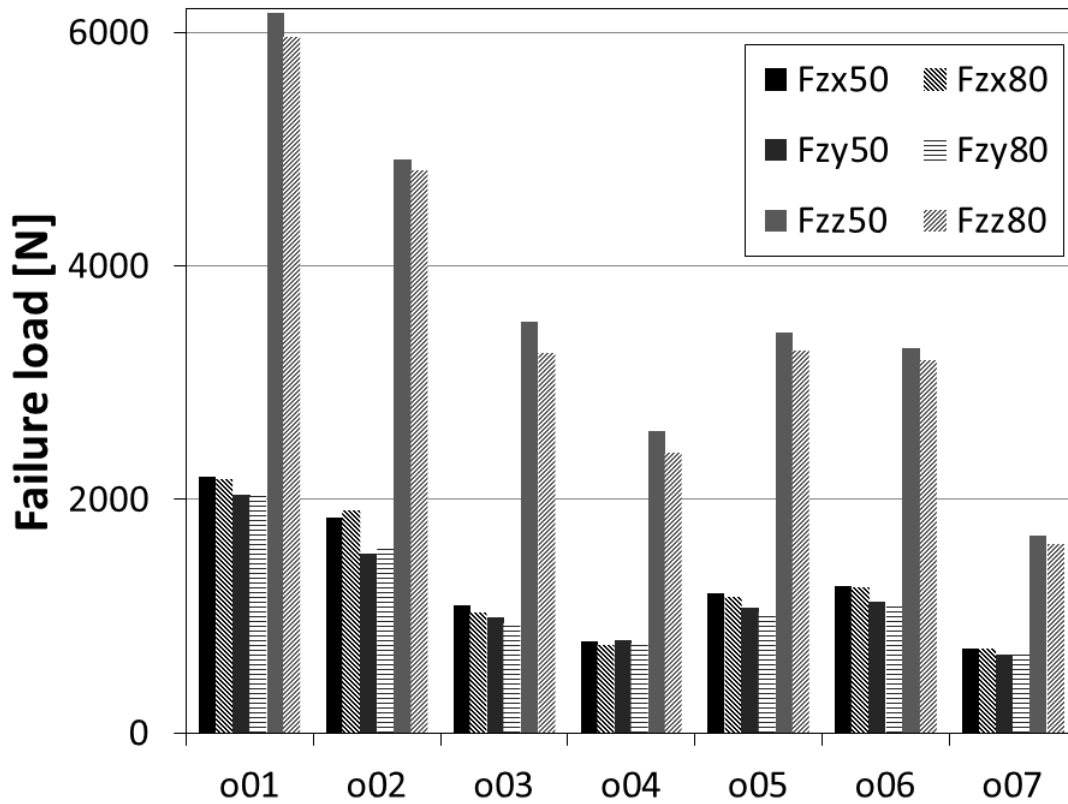


Figure 4.8: **Comparison of the Pistoia strength at the age of 50 and 80 for the three load cases.** While axial compression strength was reduced by at least 1.9% for all samples, strength towards shear loading varied between +3.94% and -5.17%.

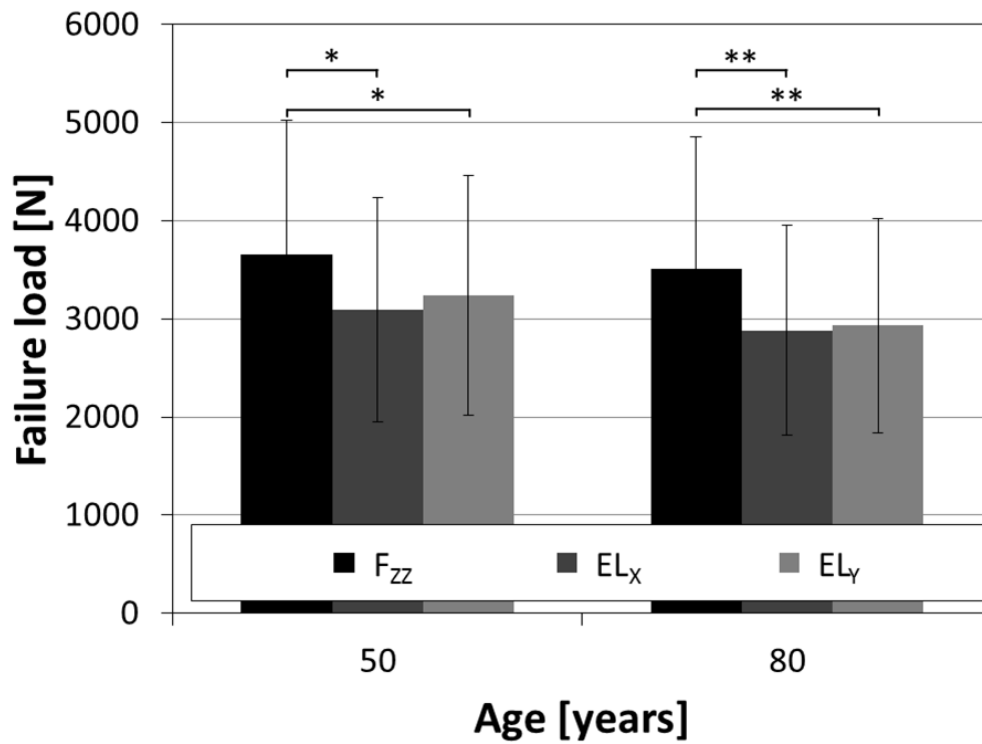


Figure 4.9: **Failure load for axial compression force and error loads.** While failure load was different with weak significance ( $p < 0.05$ ) between load cases at the age of 50, bone gets more fragile towards error loads at the age of 80 ( $p < 0.01$ ).

per sample and iteration. The average computational time for the control group was reduced by more than 50% from the first to the last iteration. This reduction did not occur in the osteoporosis simulations. Sample 04 is not shown in the osteoporosis group, because it was used for the parameter definition. In total, more than 367'000 CPU hours were used for the  $\mu$ FE analysis only (157'000 CPU hours control, 146'000 CPU hours parameter, 64'000 CPU hours osteoporosis).

The results from the bone load estimation required in the bone remodeling framework are shown in Figure 4.11. The pie chart shows the average distribution between the three load cases. The vertical compressive load  $F_{ZZ}$  contributes by far the most to the total loading for all samples (avg. 64.9%, min. 54.5%). The shear forces in the transverse axis  $F_{ZX}$  and in the sagittal axis  $F_{ZY}$  only contribute with 19.4% and 15.7% on average, and the transverse shear force is higher than the sagittal shear force in all samples. The bar chart indicates the total force for all loading cases and all samples. The average total force is 2626 N with typically higher loads for samples with higher bone mass. The maximal force is the compressive force for c01 (4441 N) the lowest - the sagittal shear force for c07 (149 N).

### 4.1.3 Discussion

The purpose of this study was to simulate postmenopausal osteoporosis on whole human vertebrae and to subsequently investigate the microstructural changes and their impact on the risk of fracture. We hypothesized that by matching microstructural morphometric indices, mechanoregulated bone remodeling simulations are sufficient to realistically predict sites of bone loss on the organ level as well as the biomechanical competence of the vertebrae in a future state. Because of the lack of *in vivo* comparison, validations of remodeling simulations are generally difficult [7]. In this study, we tried to give evidence on the realistic outcome of the simulations by investigating morphometric parameters, visualization and investigating the mechanical competence as well as comparison of the findings with values from the literature from bones gathered by  $\mu$ CT and HR-pQCT. Comparison of the morphometric indices of the simulated osteoporotic samples with osteoporotic biopsies from a previous study ([7] and Figure 4.3) showed only minor differences for most indices (results from experimental biopsies are listed in brackets): -30.7% (-38) BV/TV, +21.9% (+12) BS/BV, +9.98% (+7) DA and +38.1% (+72) SMI. More pronounced differences were found for Tb.N and Tb.Sp. Reduction in Tb.N was with -5.8% less expressed than the -32% found by Müller [7] in biopsies from the vertebra and iliac crest, but relatively close to biopsies in the tibia [35]. Accordingly, Tb.Sp increased by 7.8% only, compared to 25% in experiments. Tb.Th on the other hand was well modelled

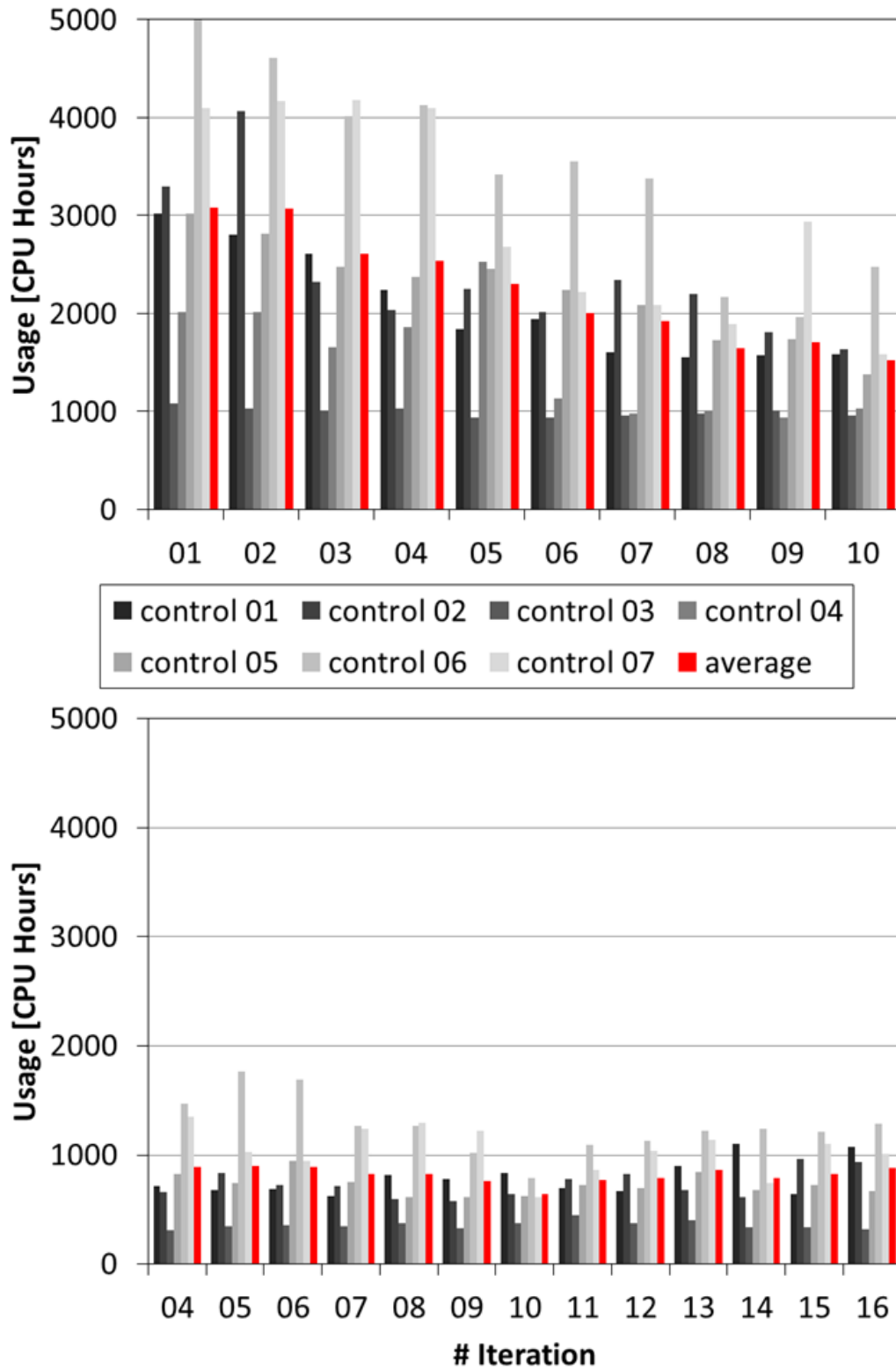


Figure 4.10: **Computational time on supercomputer.** Usage for the control group (top) and the osteoporosis group (bottom). For the control group 10 iterations were performed, for the osteoporosis group 13 iterations. Simulations for the osteoporosis group were calculated on a cluster with higher memory capacity which allowed considerable reduction of the computational time per sample and iteration.



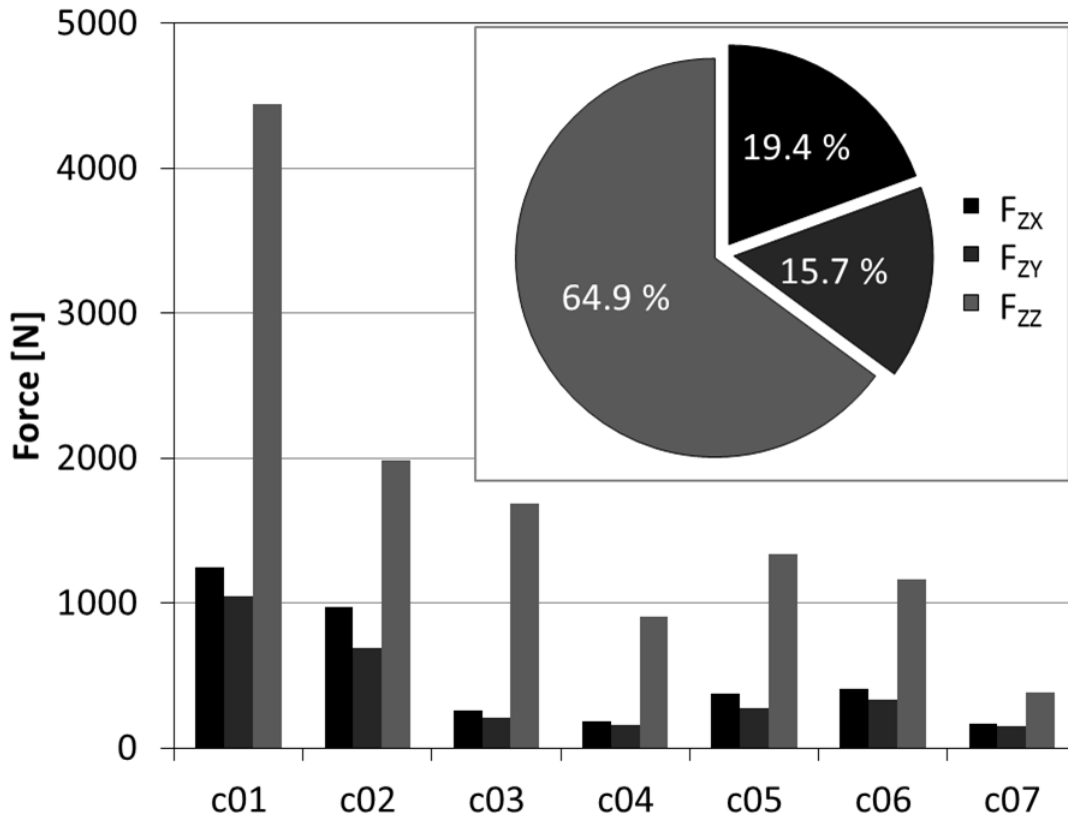


Figure 4.11: **Bone load estimation.** The pie chart shows the average distribution between the three load cases. The vertical compressive loading  $F_{ZZ}$  contributed for all samples by far the most to the total loading, followed by transverse shear  $F_{ZX}$  and sagittal shear  $F_{ZY}$ . The bar chart shows the total force for all loading cases and all samples. Typically, higher loads were calculated for samples with higher bone mass.

with an average decrease of 11.6% (biopsies 11%).

In addition to the standard comparison to morphometric indices, the mechanical behavior of the bones under load was assessed. To the authors' knowledge, such an assessment has never been performed to this extent in connection with whole human bone remodeling simulations. Compared to the drastic loss of bone (-30.7% BV/TV), stiffness was relatively well conserved (-7.87%). Today, *in vivo* assessment at the microstructural level is not possible. In a longitudinal HR-pQCT study of the forearms from postmenopausal women, an average loss in stiffness of -3% per year in the radii and -1% in the tibiae has been reported [36]. Macroscopic finite element models based on clinical computer tomography scans of L3 vertebral bodies from women at the age of 40 and 78 years calculated a decrease of the apparent stiffness by 44% [37]. Failure load for the vertical compressive force revealed an average decrease of 4.15% (Figure 4.8). In a cross-population study of the bone microstructure of HR-pQCT measured forearms, failure loads were predicted to drop by 46% in the radius and by 35% in the tibia between the ages of 20 and 90 years [38]. Even though these studies suggest that the drop in stiffness in our simulations has been underestimated, comparisons with experimental data are difficult. Experiments were performed on different bones and also on much larger timescales. Nevertheless, the trend seems to be well captured. The decrease in failure load was more pronounced for error loads to which the bone was not being adapted (sagittal plane error load -6.84%, frontal plane error load -9.08%). While the failure loads at the age of 50 were already lower for the error loads, at the simulated age of 80 they are significantly more prone to fractures (Figure 4.9). This finding is in good agreement with a study on fracture risk to different loading [20], where the pattern was found for osteoporotic bone. The change from the pre-osteoporotic, generically stable bone, to a well-adapted, but prone to infrequent load fracture structure, is hence well replicated. It also shows that despite the massive loss in bone volume, the structure is highly adapted and primarily focused on maintaining the mechanical to the primary loading condition. Our bone remodeling simulations therefore seem able to aptly represent a future state of the osteoporotic bone and thus support our hypothesis.

Boundary conditions for the remodeling simulations were estimated from the load distribution in the microstructure for the three load cases vertical compressive loading, shear in the transverse axis and shear in the sagittal axis (Figure 4.11). Accounting for more than 54.5% of the total loading for all samples, the largest share is the vertical compressive load, matching findings from experimental measurements in the lumbar spine [39, 40]. Load estimations of axial loading are in the physiological range, but for sample c01 with estimated 4441 N. Nevertheless, we assume the

values are well below individual fracture loads as experimental testing by Chevalier [41] revealed values of 5525 ( $\pm 2120$ ) N and Hulme [42] measured 2918 ( $\pm 1227$ ) N fracture loads in osteoporotic vertebral bodies. Moreover, the calculated fracture loads (Figure 4.8) are on average 219%, but at least 39% above the applied boundary condition loads.

A system upgrade of the used supercomputer during the simulation period forced us to adapt the hardware allocation parameters, but eventually helped us to reduce the CPU hours per sample by almost 70% (Figure 4.10). The solving time depends on the strain distribution in the model, with smoother transitions distributions decreasing solving time [43]. The decreasing solving time for the control group therefore already depicts that the models are being adapted to the external loads. The imbalance in bone loss and formation of the osteoporotic sample, however, does not lead to the same mechanical stability as the control samples, which could explain the little variation in the solving time for the samples in the corresponding group.

Despite some quantitative differences in the morphometric indices and mechanical strength, qualitatively the changes of the bone microstructure are captured well by our simulations. Nevertheless some limitations should be addressed. The initial adaptation steps that are performed as preprocessing to the remodeling simulations already change the structure, and show that even with the estimation of loads previous to the onset of the remodeling cannot be omitted completely. In addition, we restricted bone remodeling to the trabecular bone, without changing the structure of the cortex. Although less pronounced, cortical bone mass is also reduced in the course of postmenopausal osteoporosis [38]. This impacts on the stability of osteoporotic bone, where a larger share of the load is transferred through the cortex [15] and could explain the differences between the decrease in the stiffness of our simulations and other experiments. Finally, the model is based on a simple and deterministic model that greatly simplifies the biological processes in the bone. But nevertheless, as was hypothesized, the results revealed realistic outcomes of the osteoporotic bone loss and we believe they are sufficient for a fracture prediction of a future state.

In conclusion, we successfully simulated osteoporosis in seven high resolution whole human vertebrae, derived from  $\mu$ CT images. While images in the same range of resolution are possible on the extremities with HR-pQCT today, *in vivo* scanning of the spine is limited to a lower resolution. Nevertheless, it may be possible in the future to facilitate better patient-specific fracture risk assessment. The outcome of our simulations shows realistic osteoporotic bone loss at the microstructural level, not only by a comparison of standard morphometric indices and visual inspection,

but also by reflecting real changes in mechanical stability as found in experiments.

#### 4.1.4 Materials and Methods

##### Micro computed tomography and bone morphometric indices

Bone microstructure was derived from seven *ex vivo* high resolution ( $17.4\ \mu\text{m}$ )  $\mu\text{CT}$  scans of human L2 vertebral bodies. Scanning was performed at SA Pathology and the University of Adelaide (SkyScan 1076 in vivo micro-CT, Kontich, Belgium) with approval to use the samples for research purposes granted by the Human Research Ethics Committee at the Royal Adelaide Hospital, South Australia. The scans were downsampled with voxel averaging and interpolation to  $43.5\ \mu\text{m}$  resolution, leading to seven datasets of up to  $1300 \times 950 \times 800$  voxels. The bones were aligned along the z-axis, thresholded for binarization (189/1000 of the maximum greyscale value) and component-labelled to remove unconnected parts. Standard bone morphometric indices including BV/TV, BS/BV, Tb.Th, Tb.Sp, Tb.N, DA, SMI and TBPf were calculated for all samples and iteration steps with IPL image processing software (IPL V5.15, Scanco Medical AG, Bassersdorf, Switzerland).

##### Micro finite element analysis

The FE simulations were performed with a highly memory-efficient multigrid linear  $\mu\text{FE}$  solver (ParOSol) that included automated meshing [43]. In order to ensure physiological load transfer from the applied forces and displacements through the endplates of the vertebral body, soft tissue pads with an elastic modulus of 0.2 GPa representing intervertebral disks [20, 44] were added at the end plates. The linear elastic material properties were attributed in a grey scale space with an exponential increase of the elastic modulus with increasing density [22, 45]. The models reached sizes of up to 377 million elements.

The  $\mu\text{FE}$  and load estimation steps were performed on the Monte Rosa cluster (Cray XE6) and Piz Dora cluster (XC40) at the Swiss National Supercomputing Centre (CSCS, Lugano, Switzerland). The  $\mu\text{FE}$  analyses of the control group as well as the median osteoporosis sample were performed on Monte Rosa. An upgrade of the supercomputer during the simulation period obliged us to run the simulations for the final osteoporosis group on Piz Dora. In spite of the different hardware configuration, changes in the  $\mu\text{FE}$  analysis could not be detected during a test simulation. The increased memory capacity of Piz Dora allowed a considerable reduction of the computational time per sample and iteration (Figure 4.11).

### **Bone load estimation and mechanical analysis**

Several boundary conditions were implemented for the  $\mu$ FE analysis representing different loading cases and mechanical tests to investigate the stability towards fractures. The mechanical signal for the remodeling simulations was generated with a combination of three load cases. These forces were applied on the top nodes and include shear force in the transverse axis, shear force in the sagittal axis and vertical compressive loading. Bottom nodes were fixed in all boundary conditions. The magnitude of the loading cases was defined with a reverse engineering approach that estimates the history for an individual bone (Christen et al. 2013c; Christen et al. 2011). In brief, it takes into consideration that bone strives for uniform tissue loading due to continuous bone remodeling (Christen et al. 2014; Schulte et al. 2013a). This finding is used to optimize a linear combination of possible external loads towards most homogeneous tissue load of 0.02 MPa [32].

To assess mechanical stability, different  $\mu$ FE analysis test were performed: 1% uniform compressive displacement was used to quantify apparent stiffness. Linearly changing displacements from 0%-1% in both the sagittal and frontal plane were used as error loads [20]. Bottom nodes were fixed in all boundary conditions. Failure strength was assessed with by the Pistoia-criterion [14] as the force at which 2% of the bone elements are subjected to a displacement of 0.7% or more. Statistical significance was calculated with a pairwise-t-test and Bonferroni correction with R (R v3.1.3, The R Foundation for Statistical Computing, Vienna, Austria).

### **Bone remodeling simulations**

Bone remodeling was simulated with a framework developed and validated for mouse bone [26] and extended to use with human bone [22]. In short, theoretical background is based on Frost's mechanostat model and bone adaptation is simulated by moving the bone surface according to a mechanical signal calculated with  $\mu$ FE analysis. High signals lead to positive surface movement and hence bone thickening where low signals lead to negative movement representing bone removal. The mechanical signal is an integration of multiple weighted signals from the different loading cases within the sensing radius of osteocytes.

Model parameters for the control group (homeostatic bone adaptation) were taken from a previous study where healthy bone remodeling was simulated [22] and are shown in Table 4.1. In order to have as little changes as possible in total bone mass for the homeostatic bone turnover, the first three iteration steps were marked as initial adaptation of the simulation models and not used for the following simulations (Figure 4.12). Iteration length was set to 3 years per iteration [7]. This results in a

control group with less than 0.5% change in BV/TV within three years.

The different models for the simulation of osteoporotic bone loss are shown in Figure 4.12 and the resulting changes in bone morphometric indices in Figure 4.13. The goal was to stepwise change homeostatic model parameters to create an imbalance in the net formation and resorption towards increased resorption. No information about the age of the donors was available, so the age was set to 50 for the beginning of the simulations. Iteration length was set to 1.5 years to simulate the first 6 years (peri-menopause) and to 3 years for the remaining 8 iterations (post-menopause) [7]. The first parameter to be changed was the resorption rate. This parameter is limited to the voxel size in order to fulfill the Courant-Friedrichs-Levy condition for the used advection equation in our model. Although the resorption was stepwise increased (Model A) until the maximum, the bone reduction was less than 5% over the simulated period and thus the model was discharged. The next parameter changed was the bone resorption threshold (Model B), where an increase corresponds to reduced cell sensitivity frequently. Model C corresponds to a combined increase of resorption rate and increased bone resorption threshold. The course of Tb.Th over time revealed unnatural behavior for both Model B and Model C with a late increase of the parameter after initial decrease. Therefore two supplementary models were added with increased resorption rate and/or increased bone resorption threshold, but with reduced bone formation rates (Model D and Model E). Comparing bone morphometric indices with biopsy data [7] revealed the highest match for model D (Figure 4.13), which was subsequently used for the simulation of the osteoporosis group.

## **Acknowledgements**

The authors gratefully acknowledge Duncan Betts for his help with the bone visualization, Alexander Zwahlen for his support with the statistical analysis and Catherine Palmer for her revisions of the manuscript.

Table 4.1: Model parameters for the bone remodeling.

Parameter-set	Bone resorption rate per SED [( $\mu\text{m}/\text{iteration}$ )/MPa]	Bone formation rate per SED [( $\mu\text{m}/\text{iteration}$ )/MPa]	Resorption threshold [MPa]	Formation threshold [MPa]	Resorption saturation level [mm/iteration]	Formation saturation level [mm/iteration]
Control	2.8571	0.6667	0.0028	0.016	0.008	0.008
Model A	8.571	- <sup>a)</sup>	-	-	0.024	-
Model B	0.5714	-	0.014	-	-	-
Model C	-	-	0.0056	-	0.016	-
Model D <sub>b)</sub>	0.8163	0.0833	0.0098	-	-	-
Model E	-	0.0833	0.0056	-	0.016	-

<sup>a)</sup> Only changes to the control toup are shown. [-] denotes no change.

<sup>b)</sup> This model was used for the osteoporosis simulations.

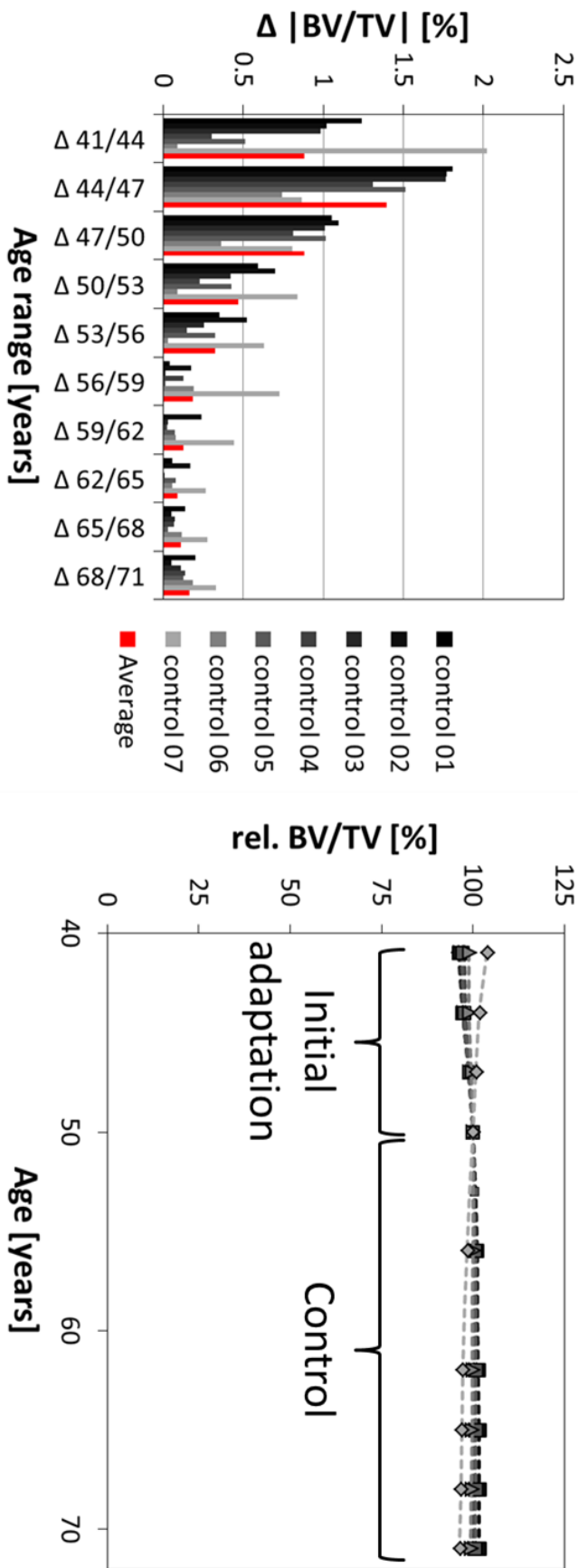


Figure 4.12: **Changes in BV/TV and definition of pre-adaptation.** The chart on the left hand side shows the difference in BV/TV between the different time steps for the control group. After an initial phase with high changes in BV/TV the bone reaches the desired homeostatic bone adaptation level with changes in BV/TV of less than 0.5% over the period of 3 years. Therefore the third iteration step was used as a starting point for all samples and further simulations and was defined as year 50.



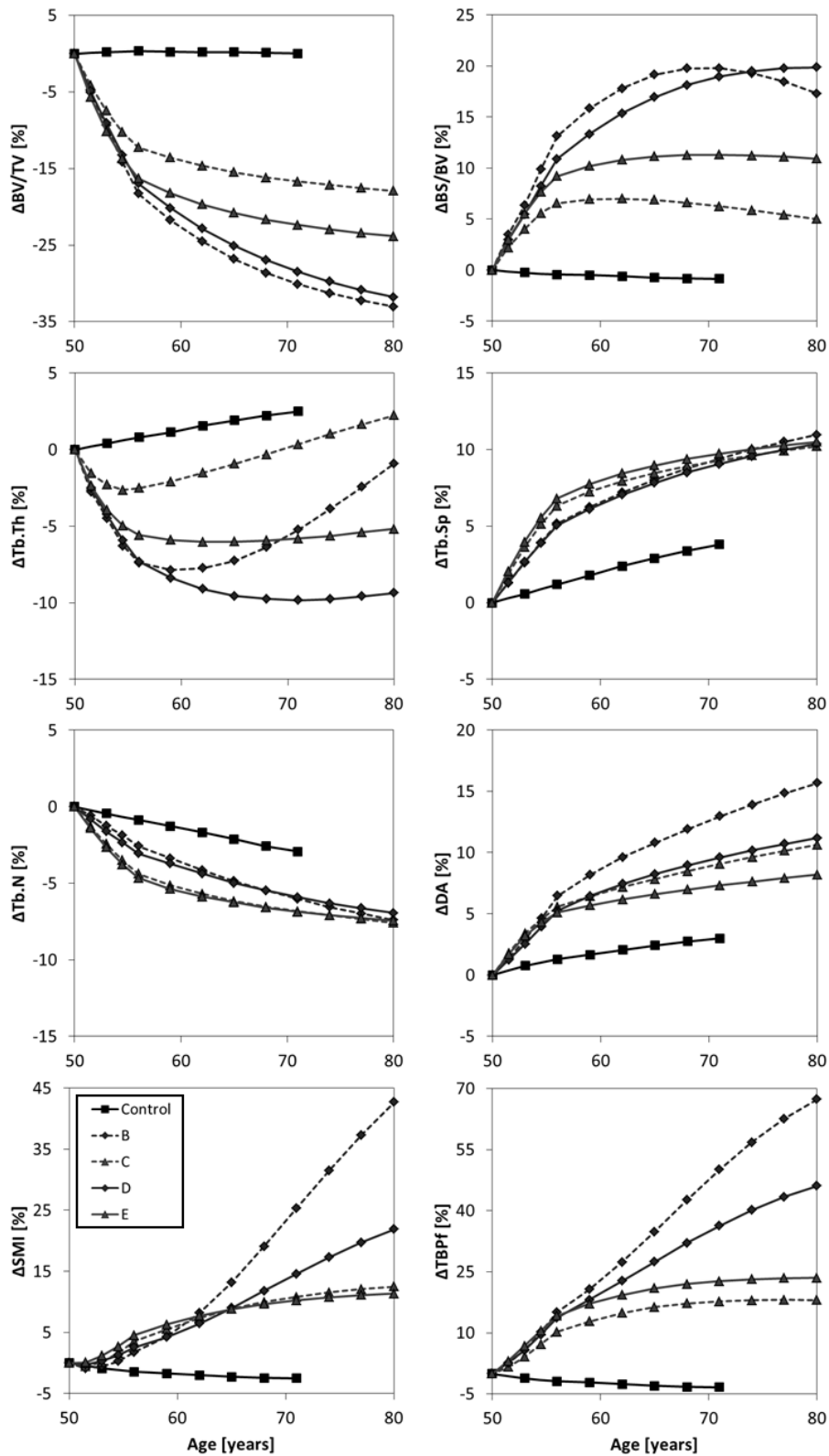


Figure 4.13: **Course of bone morphometric indices over time.** Relative values for the median sample for the models B,C,D and E. Calculated morphometric indices are (from top left to bottom right): BV/TV, BS/BV, Tb.Th, Tb.Sp, Tb.N, DA, SMI, TBPf. Because of the highest match with the biopsy data, model D was chosen for the simulation of the osteoporosis group.

## References

- [1] United-Nations. Population ageing and development. *Department of Economic and Social Affairs, Population Division, New York, NY 10017, USA, www.unpopulation.org*, 2012.
- [2] O. Johnell and J. A. Kanis. An estimate of the worldwide prevalence and disability associated with osteoporotic fractures. *Osteoporos Int*, 17(12):1726–33, 2006.
- [3] S. R. Cummings and L. J. Melton. Epidemiology and outcomes of osteoporotic fractures. *Lancet*, 359(9319):1761–7, 2002.
- [4] O. Johnell and J. Kanis. Epidemiology of osteoporotic fractures. *Osteoporos Int*, 16 Suppl 2:S3–7, 2005.
- [5] C. Holroyd, C. Cooper, E. Dennison. Epidemiology of osteoporosis. *Best Pract Res Clin Endocrinol Metab*, 22(5):671–85, 2008.
- [6] R. Burge *et al.* Incidence and economic burden of osteoporosis-related fractures in the united states, 2005-2025. *J Bone Miner Res*, 22(3):465–75, 2007.
- [7] R. Mueller. Long-term prediction of three-dimensional bone architecture in simulations of pre-, peri- and post-menopausal microstructural bone remodeling. *Osteoporos Int*, 16 Suppl 2:S25–35, 2005.
- [8] J. A. Kanis *et al.* European guidance for the diagnosis and management of osteoporosis in postmenopausal women. *Osteoporos Int*, 19(4):399–428, 2008.
- [9] J. A. Kanis *et al.* Assessment of fracture risk and its application to screening for postmenopausal osteoporosis - synopsis of a who report. *Osteoporosis International*, 4(6):368–381, 1994.
- [10] A. M. Briggs *et al.* Measurement of subregional vertebral bone mineral density in vitro using lateral projection dual-energy x-ray absorptiometry: validation with peripheral quantitative computed tomography. *Journal of Bone and Mineral Metabolism*, 30(2):222–231, 2012.
- [11] E. Perilli *et al.* Failure strength of human vertebrae: prediction using bone mineral density measured by dxa and bone volume by micro-ct. *Bone*, 50(6):1416–25, 2012.

- [12] R. Krug, A. J. Burghardt, S. Majumdar, T. M. Link. High-resolution imaging techniques for the assessment of osteoporosis. *Radiol Clin North Am*, 48(3):601–21, 2010.
- [13] D. Christen *et al.* Improved fracture risk assessment based on nonlinear micro-finite element simulations from hrpqt images at the distal radius. *J Bone Miner Res*, 28(12):2601–8, 2013.
- [14] W. Pistoia *et al.* Estimation of distal radius failure load with micro-finite element analysis models based on three-dimensional peripheral quantitative computed tomography images. *Bone*, 30(6):842–8, 2002.
- [15] E. F. Eriksen, F. Melsen, E. Sod, I. Barton, A. Chines. Effects of long-term risedronate on bone quality and bone turnover in women with postmenopausal osteoporosis. *Bone*, 31(5):620–5, 2002.
- [16] S. J. Glover, P. Garnero, K. Naylor, A. Rogers, R. Eastell. Establishing a reference range for bone turnover markers in young, healthy women. *Bone*, 42(4):623–30, 2008.
- [17] D. B. Burr. Targeted and nontargeted remodeling. *Bone*, 30(1):2–4, 2002.
- [18] J. Wolff. The classic: on the inner architecture of bones and its importance for bone growth. 1870. *Clin Orthop Relat Res*, 468(4):1056–65, 2010.
- [19] B. Van Rietbergen, R. Huiskes, F. Eckstein, P. Ruegsegger. Trabecular bone tissue strains in the healthy and osteoporotic human femur. *J Bone Miner Res*, 18(10):1781–8, 2003.
- [20] J. Homminga *et al.* The osteoporotic vertebral structure is well adapted to the loads of daily life, but not to infrequent "error" loads. *Bone*, 34(3):510–6, 2004.
- [21] T. Adachi, K. Tsubota, Y. Tomita, S. J. Hollister. Trabecular surface remodeling simulation for cancellous bone using microstructural voxel finite element models. *Journal of Biomechanical Engineering-Transactions of the Asme*, 123(5):403–409, 2001.
- [22] S. D. Badilatti *et al.* Large-scale microstructural simulation of load-adaptive bone remodeling in whole human vertebrae. *Biomech Model Mechanobiol*, in press, 2015.

- [23] P. Christen *et al.* Patient-specific bone modelling and remodelling simulation of hypoparathyroidism based on human iliac crest biopsies. *J Biomech*, 45(14):2411–6, 2012.
- [24] P. Mc Donnell, N. Harrison, M. A. Liebschner, P. E. Mc Hugh. Simulation of vertebral trabecular bone loss using voxel finite element analysis. *J Biomech*, 2009.
- [25] R. Ruimerman, P. Hilbers, B. van Rietbergen, R. Huiskes. A theoretical framework for strain-related trabecular bone maintenance and adaptation. *Journal of Biomechanics*, 38(4):931–941, 2005.
- [26] F. A. Schulte *et al.* Strain-adaptive in silico modeling of bone adaptation - a computer simulation validated by in vivo micro-computed tomography data. *Bone*, 52(1):485–92, 2013.
- [27] A. J. Fields, S. K. Eswaran, M. G. Jekir, T. M. Keaveny. Role of trabecular microarchitecture in whole-vertebral body biomechanical behavior. *J Bone Miner Res*, 24(9):1523–30, 2009.
- [28] H. M. Frost. Bone’s mechanostat: a 2003 update. *Anat Rec A Discov Mol Cell Evol Biol*, 275(2):1081–101, 2003.
- [29] F. A. Schulte *et al.* Local mechanical stimuli regulate bone formation and resorption in mice at the tissue level. *PLoS One*, 8(4):e62172, 2013.
- [30] T. Sugiyama *et al.* Bones’ adaptive response to mechanical loading is essentially linear between the low strains associated with disuse and the high strains associated with the lamellar/woven bone transition. *J Bone Miner Res*, 27(8):1784–93, 2012.
- [31] P. Christen *et al.* Bone remodelling in humans is load-driven but not lazy. *Nat Commun*, 5:4855, 2014.
- [32] P. Christen *et al.* Subject-specific bone loading estimation in the human distal radius. *J Biomech*, 46(4):759–66, 2013.
- [33] P. Christen, B. van Rietbergen, F. M. Lambers, R. Mueller, K. Ito. Bone morphology allows estimation of loading history in a murine model of bone adaptation. *Biomech Model Mechanobiol*, 2011.
- [34] R. Mueller and W. Hayes. Biomechanical competence of microstructural bone in the progress of adaptive bone remodeling. *Proc. SPIE*, 3149(69):69–81, 1997.

- [35] M. Ding and I. Hvid. Quantification of age-related changes in the structure model type and trabecular thickness of human tibial cancellous bone. *Bone*, 26(3):291–5, 2000.
- [36] A. J. Burghardt *et al.* A longitudinal hr-pqct study of alendronate treatment in postmenopausal women with low bone density: Relations among density, cortical and trabecular microarchitecture, biomechanics, and bone turnover. *J Bone Miner Res*, 25(12):2558–71, 2010.
- [37] B. A. Christiansen, D. L. Kopperdahl, D. P. Kiel, T. M. Keaveny, M. L. Bouxsein. Mechanical contributions of the cortical and trabecular compartments contribute to differences in age-related changes in vertebral body strength in men and women assessed by qct-based finite element analysis. *J Bone Miner Res*, 26(5):974–83, 2011.
- [38] H. M. Macdonald, K. K. Nishiyama, J. Kang, D. A. Hanley, S. K. Boyd. Age-related patterns of trabecular and cortical bone loss differ between sexes and skeletal sites: a population-based hr-pqct study. *J Bone Miner Res*, 26(1):50–62, 2011.
- [39] N. Arjmand, A. Shirazi-Adl, B. Bazrgari. Wrapping of trunk thoracic extensor muscles influences muscle forces and spinal loads in lifting tasks. *Clin Biomech (Bristol, Avon)*, 21(7):668–75, 2006.
- [40] J. Calisse, A. Rohlmann, G. Bergmann. Estimation of trunk muscle forces using the finite element method and in vivo loads measured by telemeterized internal spinal fixation devices. *J Biomech*, 32(7):727–31, 1999.
- [41] Y. Chevalier, D. Pahr, P. K. Zysset. The role of cortical shell and trabecular fabric in finite element analysis of the human vertebral body. *J Biomech Eng*, 131(11):111003, 2009.
- [42] P. A. Hulme, S. K. Boyd, S. J. Ferguson. Regional variation in vertebral bone morphology and its contribution to vertebral fracture strength. *Bone*, 41(6):946–57, 2007.
- [43] C. Flaig and P. Arbenz. A scalable memory efficient multigrid solver for micro-finite element analyses based on ct images. *Parallel Computing*, 37(12):846–854, 2011.

- [44] R. K. Wilcox *et al.* A dynamic investigation of the burst fracture process using a combined experimental and finite element approach. *Eur Spine J*, 13(6):481–8, 2004.
- [45] E. F. Morgan, H. H. Bayraktar, T. M. Keaveny. Trabecular bone modulus-density relationships depend on anatomic site. *J Biomech*, 36(7):897–904, 2003.

## 4.2 Simulations of microstructural bone adaptation in augmented whole human vertebrae

Sandro D. Badilatti<sup>1</sup>, Patrik Christen<sup>1</sup>, Stephen J. Ferguson<sup>1</sup> and Ralph Müller<sup>1</sup>

<sup>1</sup>Institute for Biomechanics, ETH Zurich, 8093 Zurich, Switzerland

### **in preparation as:**

Computational modelling of long-term effects of preventive vertebroplasty on microstructural bone adaptation

### **Abstract:**

Cement augmentation in vertebrae (vertebroplasty) is usually used to restore mechanical strength after fractures, but could also be used preventive. So far, the mechanical competence has been determined immediate post-treatment, without considering long-term effects of bone adaptation. In this work, we investigated such long-term effects of vertebroplasty on the stiffness of the augmented bone by means of computational simulation of bone adaptation. Using micro-finite element analysis, we determined sites of increased mechanical stress (stress-raisers) and stress-shielding and based on the simulations, regions with increased or less bone loss due to augmentation. Cement volumes connecting the endplates led to increased stress-shielding and bone loss. The increased stiffness due to the augmentation cement, however, remained constant over the simulation time of 30 years. If the intervention was performed at an earlier time point, it did lead to more bone loss, but again, it did not affect long-term stability. In particular around the augmentation cement, bone structures were preserved, suggesting a long-term integration of the cement in the augmented bone. We conclude that, from a biomechanical perspective, the impact of vertebroplasty on the bone at the microstructural level is less detrimental than previously thought.

### **Keywords:**

Bone Adaptation, Fracture Prevention, Micro Finite Element Analysis, Computational Simulation

### **4.2.1 Introduction**

Cement augmentation of the vertebral body, referred to as vertebroplasty, has become an established approach to treat fractured osteoporotic vertebrae. It is generally accepted to stabilize the fractured spine and reduce pain postoperative [1,2], but complications due to cement leakage have been reported [3] and fractures of the adjacent vertebrae as a result of increased stresses are possible [4,5]. To avoid fractures in adjacent bones, preventive vertebroplasty has been proposed [6]. Due to the increasingly better understanding of the individual patient's health, however, preventive vertebroplasty could also be used to avoid primary vertebral fractures if a patient has been diagnosed with high risk of fracture [5].

The success of restoring mechanical integrity due to bone augmentation interventions has been estimated by finite element (FE) analysis that allows calculating stresses and strains within the bone tissue. It suggests that a cement volume connecting the endplates is the most effective approach to provide mechanical stability [7,8]. However, it is known that bone tissue adapts to changes in mechanical loading, particularly to stress shielding, as seen in failure of total hip replacements, for example [9]. The mechanism behind this mechanoregulated bone adaption is the continuous resorption and formation of bone at locations of low and high tissue loading, respectively [10,11]. Computational simulations of mechanoregulated bone adaptation address the tissue response to mechanical loading and are capable to predict the future bone microstructure of whole bones [12,13]. They thus have the potential to predict the long-term stability of a bone after adaptation to a changed mechanical environment as seen after bone augmentation.

Detailed assessment of the long-term success of bone augmentation at the microstructural level is difficult and only single human cases are reported, but limited to two years of augmentation and single histological slices [14,15]. Computer simulations of bone adaptation would not only allow to analyze much longer time spans of augmentation and whole bone microstructures, but also one-to-one comparison of the same specimen with and without treatment as well as of different treatments against each other. We therefore believe that such simulations have the potential to give a better understanding of the long-term effects of vertebroplasty, particularly important when addressing the impact of preventive bone augmentation.

Here we use computational simulations of bone adaptation as introduced earlier [12] to test the following hypotheses: I. A cement volume bridging the endplates leads to higher stress shielding and should lead to more bone loss, thus eventually leading to weaker mechanical integrity in the long-term. II. Because of the longer exposure to stress-shielding an early preventive augmentation will lead to mechanically weaker



bone in the long-term compared to a preventive augmentation performed at a later time point because of the longer exposure to stress-shielding.

## 4.2.2 Materials and Methods

### Study setup

In an earlier study [12], we simulated osteoporotic bone loss from 50 to 80 years of age in whole human vertebral bodies based on high-resolution micro-computed tomography ( $\mu$ CT) images. In the present study, we used three samples with low bone mass at age 50 as a starting point for four different treatment scenarios (Figure 4.14) from the previous study. Starting at two time points, we conducted virtual cement augmentation with both, connecting and not connecting the endplates. The early treatments start 1.5 years after the onset of osteoporotic bone loss in our model, when we assume menopause was diagnosed. The late treatments start at the age of 62 years, when the bone volume fraction (BV/TV) of the samples fell under 10% assuming diagnosed osteoporosis. Bone adaptation was simulated with an algorithm described in detail elsewhere [12, 16, 17]. In short, bone adaptation of trabecular bone is simulated by increasing bone mass where a strain energy density (SED) threshold for formation is exceeded, while bone is removed where the SED falls below a lower threshold for resorption. Because it is unclear whether bone adaptation is possible within the augmentation region, no changes in this region was assumed. It was thus excluded from the analysis, with the exception of the calculation of total bone stiffness where it seemed to be appropriate to keep the bone within the cement intact.

### Samples

Simulations were based on three *ex vivo* high-resolution ( $17.4\ \mu\text{m}$ )  $\mu$ CT scans (SkyScan 1076 in vivo micro-CT, Kontich, Belgium) of human L2 vertebral bodies from a previous study [12]. They were downsampled with voxel averaging and interpolation to  $43.5\ \mu\text{m}$  voxel resolution still accounting for the detailed trabecular bone microstructure with great fidelity but allowing computations within reasonable time. Approval to use the samples for research purposes was granted by the Human Research Ethics Committee at the Royal Adelaide Hospital, South Australia.

### Virtual augmentation

For the virtual augmentation, an augmentation center at the anterior third of the medial line was assumed [18]. A filling volume of 15% of the total vertebral body

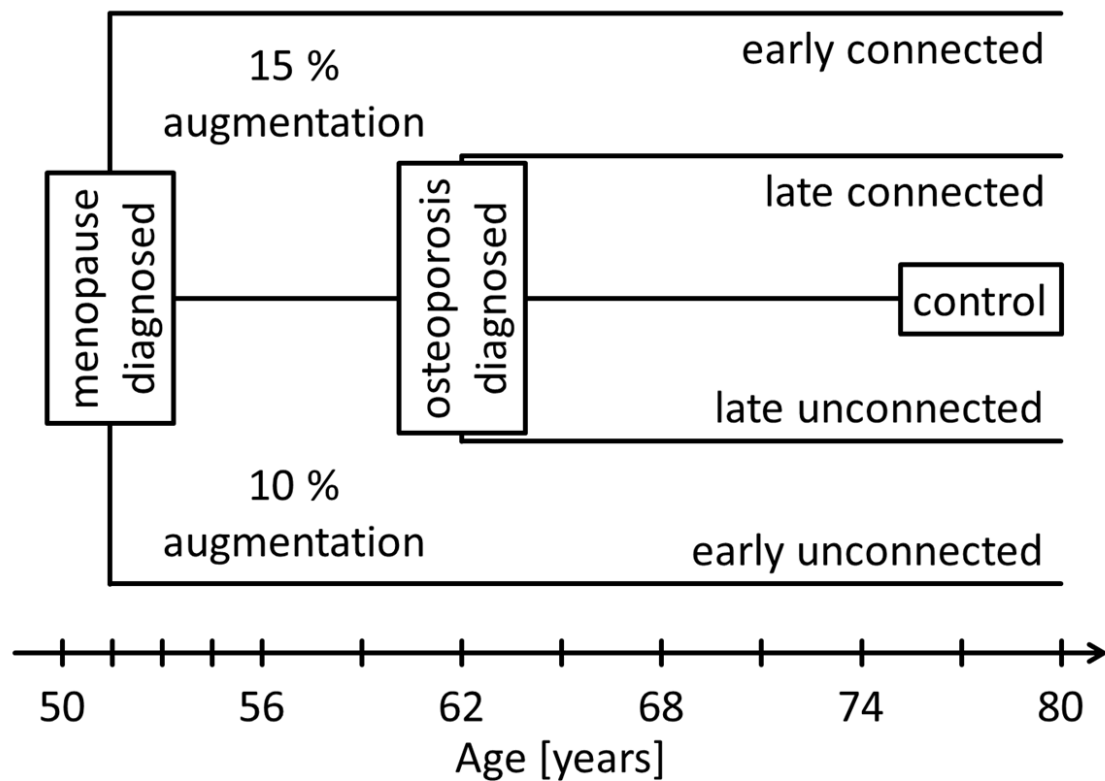


Figure 4.14: Study setup for the different treatment groups. Cement augmentation connecting endplates and not connecting endplates start at two different time points each. In the first case, preventive vertebroplasty is performed 1.5 years after the onset of bone loss when menopause is diagnosed. In the second case, preventive vertebroplasty is performed at the age of 62 years, when osteoporosis is diagnosed for our models.

was used for the endplate to endplate connecting cement volume, 10% for the non-connecting, respectively [7,8]. The shape of the volume was defined spheroid (Figure 4.15), with the semi major being 110% of the vertebral body height for the connecting and 90% of the height for the unconnected case, but bounded by the bone boundary (no leakage). The cement replaced bone marrow while the trabecular structure remained intact.

## MicroFE analysis

FE models were created by translating each voxel of the  $\mu$ CT images into an element of the FE models. This approach is thus referred to as  $\mu$ FE analysis. It was performed both for the bone adaptation simulations and bone stiffness calculations with a highly memory-efficient  $\mu$ FE solver [19]. A greyscale nonlinear material map with Young's moduli ranging from 0.2 GPa for the intervertebral disks up to 12 GPa for fully mineralized trabecular bone [20] was used. For the poly-methyl-methacrylate (PMMA) bone cement, the Young's modulus was set to 2.7 GPa [21]. Stiffness was calculated assuming intervertebral disks on top and bottom [7] by 1% displacement of the top nodes. Using a previously developed approach that allows deriving a bone's loading history from its microstructure (Christen et al. 2012), physiological boundary conditions were estimated as a combination of the most prevalent compressive axial loading (67%) and lower shear forces in the transverse (18%) and sagittal (15%) axis prior to the simulations [22,23]. The boundary conditions were left unchanged during the course of the subsequent simulations.

## Data analysis

Standard bone morphometric indices including bone volume fraction (BV/TV), trabecular thickness (Tb.Th), trabecular spacing (Tb.Sp), trabecular number (Tb.N), degree of anisotropy (DA), structure model index (SMI) and trabecular bone pattern factor (Tb.Pf) were calculated with IPL image processing software (IPL V5.15, Scanco Medical AG, Bassersdorf, Switzerland). Statistical significance was calculated with pairwise t-test and Bonferroni correction using R (R v3.1.3, The R Foundation for Statistical Computing, Vienna, Austria). Near cement volume of interests (VOIs) were defined as the projection of the cement volume in the main (axial) direction, distant cement VOIs as the complement within the trabecular region.

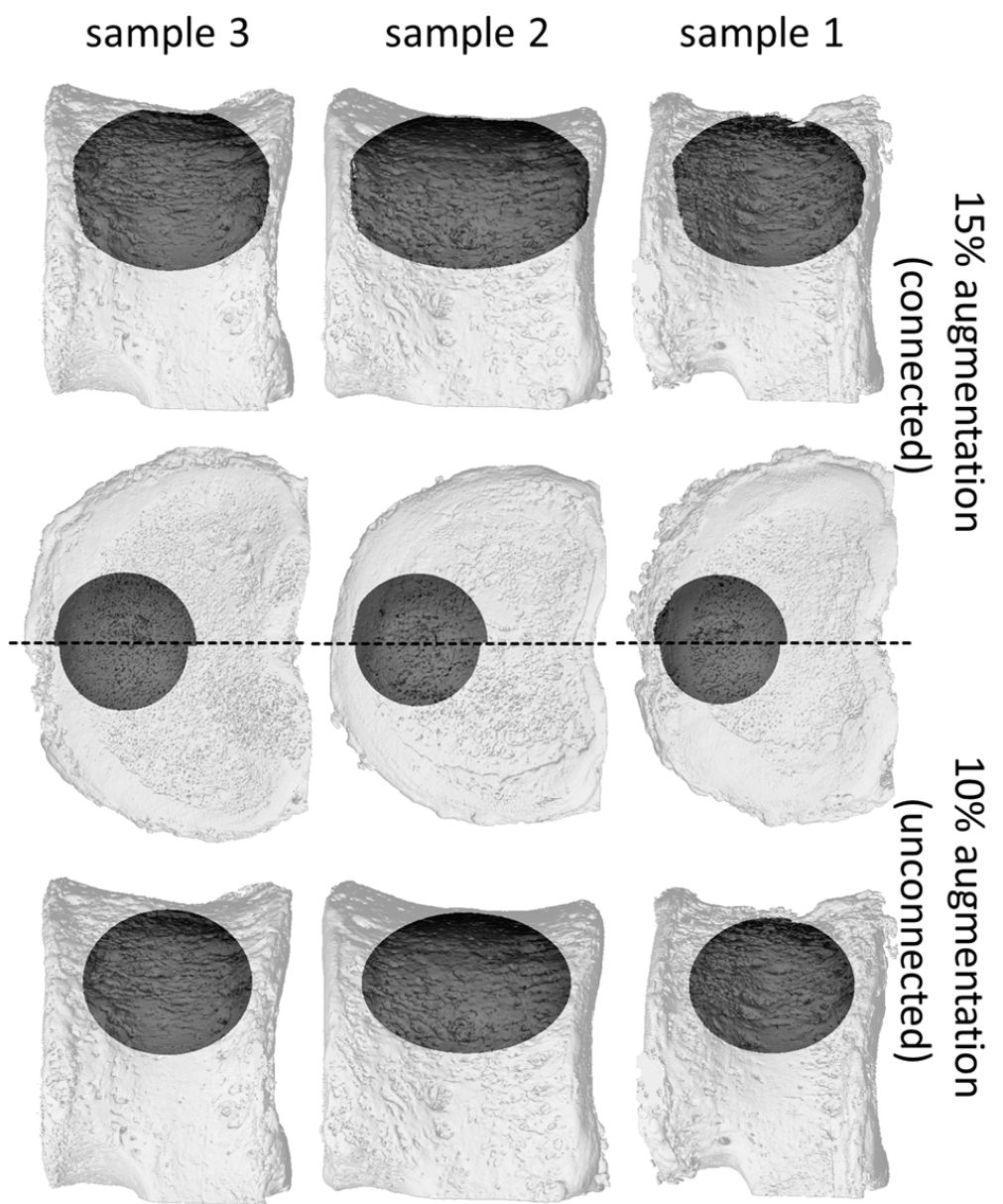


Figure 4.15: Bone augmentation volumes for the three simulated samples. Augmentation volumes with 15% of the total vertebral body volume connecting the endplates are shown on the left, the unconnected cement volumes (10%) on the right.

### 4.2.3 Results

Higher loss of BV/TV was observed for all augmented cases compared to the control with the early connected case showing the largest (-11%) and the late unconnected case the smallest (-3.4%) difference at the age of 80 years (Figure 4.16). For both, early (-5.4%) and late augmentation (-3.9%), the connected case led to more bone loss than the unconnected case. Similarly, for both connected (-3.6%) and unconnected (-2.2%) cases, early augmentation led to more bone loss than the late augmentation.

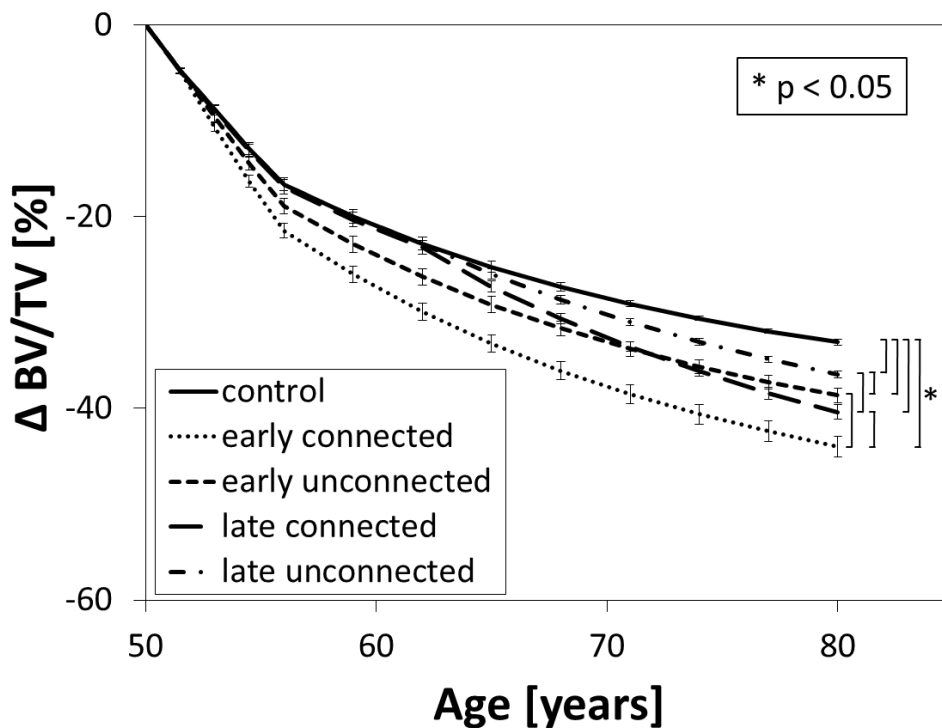


Figure 4.16: Course of the bone volume fraction for the different augmentation cases and the control over the simulated period. In the peri-menopause from the age of 50 to 56 years, the duration of a remodeling cycle is reduced.

Cement augmentation led to an increase in stiffness for all cases (Figure 4.17). Over time, the stiffness was reduced for the control group (-11%) as well as for all augmentation cases. At 80 years, all augmentation cases were significantly stiffer than the control, and the connecting cement volume models significantly stiffer than the non-connecting augmentation models. Early and late augmentation cases, however, showed no differences. Relative to the control, the average proportional increase in stiffness remained almost constant during the simulated period (+50%)

early connected, +51% late connected, +24% early unconnected, +24% late unconnected).

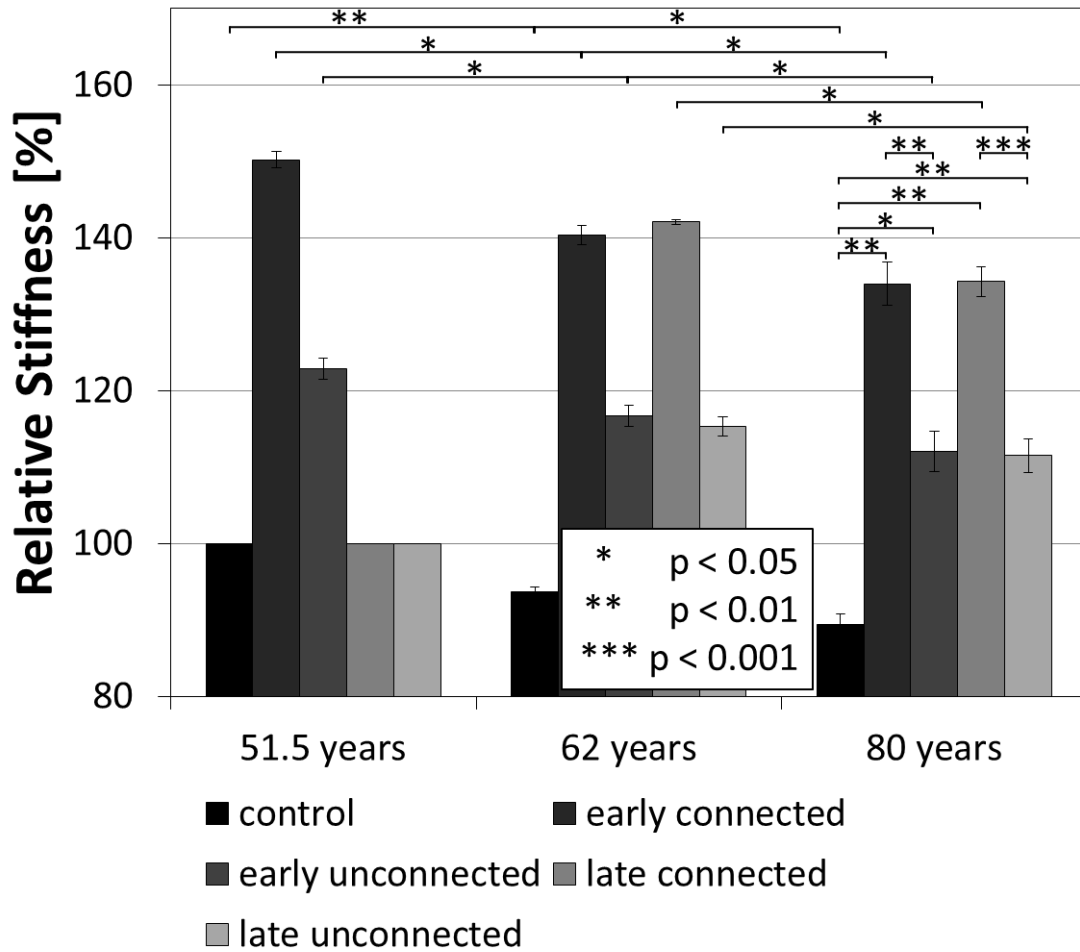


Figure 4.17: Stiffness relative to control for the time-point of the early augmentation (51.5 years), the late augmentation (62 years) and at the end point (80 years).

Analysis of the sites of bone adaptation showed relatively uniform bone resorption in the whole trabecular bone region, but sites of bone formation are concentrated around the augmentation volumes, in particular in the axial direction (Figure 4.18). Corresponding sites with locations of increased stress due to cement augmentation are observed in the  $\mu$ FE SED distribution maps (Figure 4.19). These stress-raisers can be found around the augmentation volume, whereas stress-shielding is found more frequently in distal regions and in cortical bone.

The shift in SED distribution is also visualized in stacked histograms, where the sites of bone resorption, formation and quiescent are distinguished (Figure 4.20). For the near-cement VOIs, the total amount of voxels with a SED high enough to

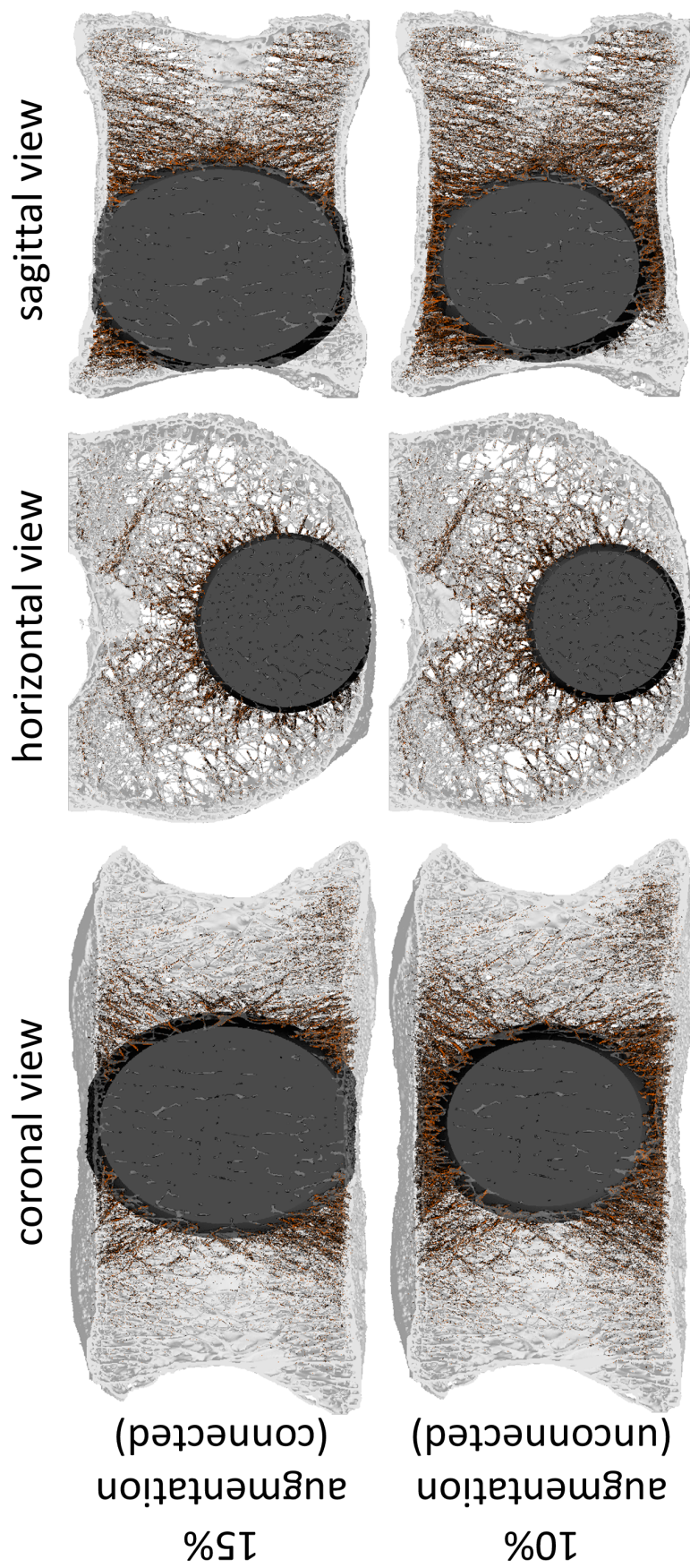


Figure 4.18: Visualization of formation sites (dark orange) for three perpendicular anatomical slices of one sample over the duration of the simulation. Increased formation can be detected around the augmentation volume (dark grey). Bone resorption is not shown.



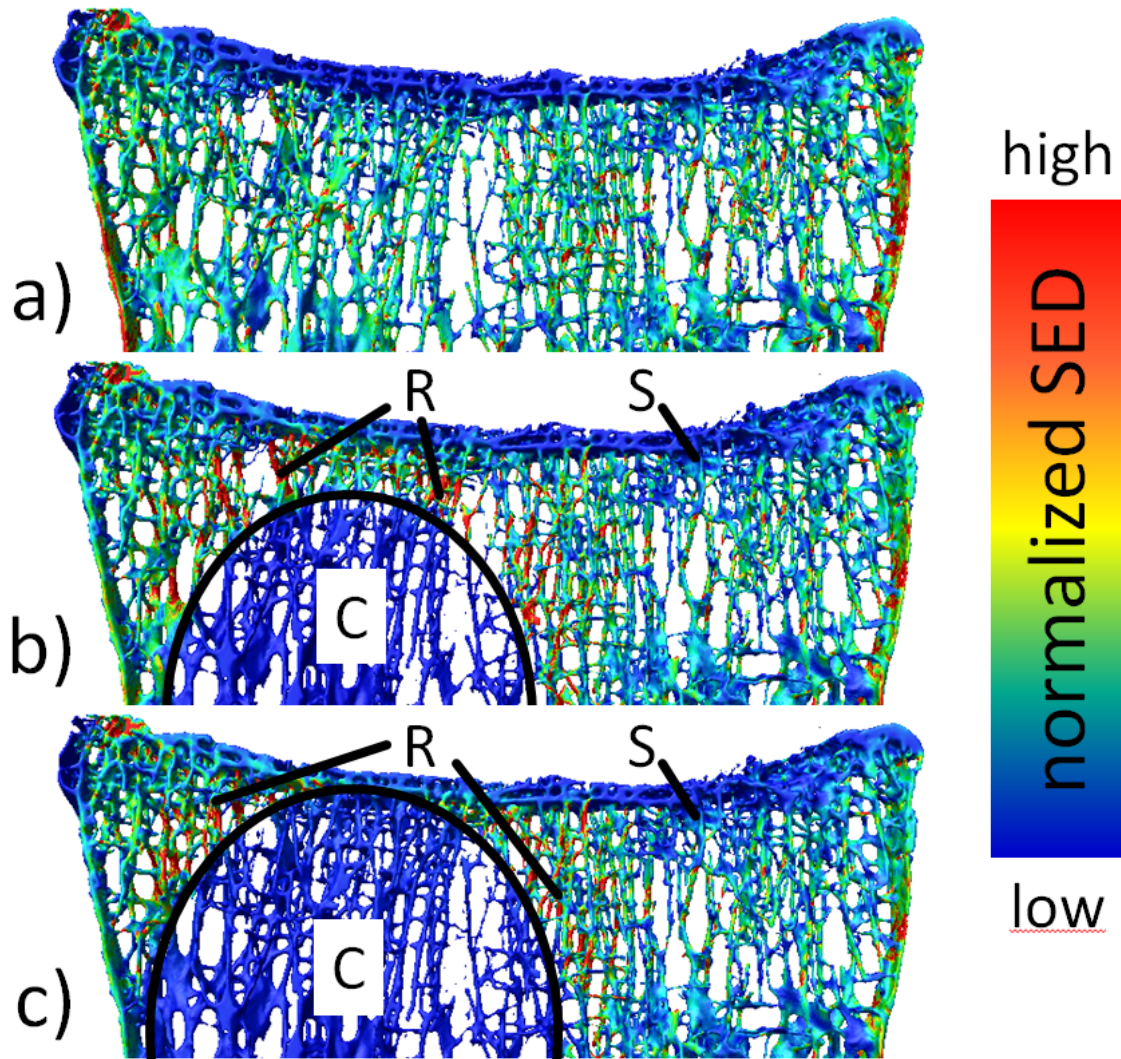


Figure 4.19: SED distribution for the control (a), not connecting augmentation (b) and connecting augmentation case (c) of one sample at the age of 51.5 years. The line denotes the border of the augmentation cement. Stress-raisers (R) and stress-shielding (S) can be shown in both augmentation cases. Bone within the augmentation region is only weakly loaded (C).



lead to bone formation is increased compared to the control, in particular for the unconnected augmentation. At the same time, the resorption area is increased for the near-connected VOI, but decreased for the near-unconnected VOI. In the distant VOIs, the resorption volume is increased while the quiescent and formation volumes decrease. More bone was resorbed in all augmented VOIs compared to control, except for the near-unconnected VOI (Table 4.2 and Table 4.3). In the distant-cement VOIs, more bone was lost in the connected than in the unconnected case for both, early and late augmentation. While Tb.Th was increased near-cement, it decreased distant-cement. Tb.Sp was increased particularly in near-cement. Tb.N remained similar near-cement, but decreased in the distant-cement VOIs of augmented bones. The structural indices (SMI, TBPf and DA) show the same trend for the augmented and control bones, but larger changes when the bone is augmented.

#### 4.2.4 Discussion

In this study, we investigated changes between osteoporotic bone and different preventive augmentation scenarios in the course of osteoporotic bone degradation. The goal of preventive cement augmentation is to avoid fractures due to structural weakening and maintain mechanical stability, which was assessed in stiffness calculations by means of  $\mu$ FE analysis. Augmentation increased stiffness by 51% if the endplate were connecting due to the injected bone cement and by 24% if they did not connect. We hypothesized that cement bridging the endplates would lead to more bone loss due to stress-shielding and thus decreased mechanical integrity in the long-term. Compared to the control, a decreased bone volume mass of 11% was found for early augmentation, but the stiffness decreased only proportional and remained about 50% above the native bone. Furthermore, we hypothesized that early augmentation would lead to weaker bone in the long-term compared to late augmentation. As assumed, more bone mass was removed in the early intervention, but again this had no effect on the stiffness of the augmented bone. Contrary to our hypotheses, the reduced bone mass appears to have minor effect on the total stability of the augmented bone. The reason for these small effects is most likely the uneven distribution of stress shielding. While regions distant to the augmentation volume indeed show reduced SED values, we could show that regions near the augmented cement even show stress-raisers, particularly in the case of the non-connecting augmentation volumes. Our hypotheses were mostly based on knowledge about failure of total hip replacements [9]. While the relatively stiff stem increases loads in the proximal and distal regions, due to bending, large regions around the middle part of the implant are stress-shielded, where most of the stem anchorage is happening.

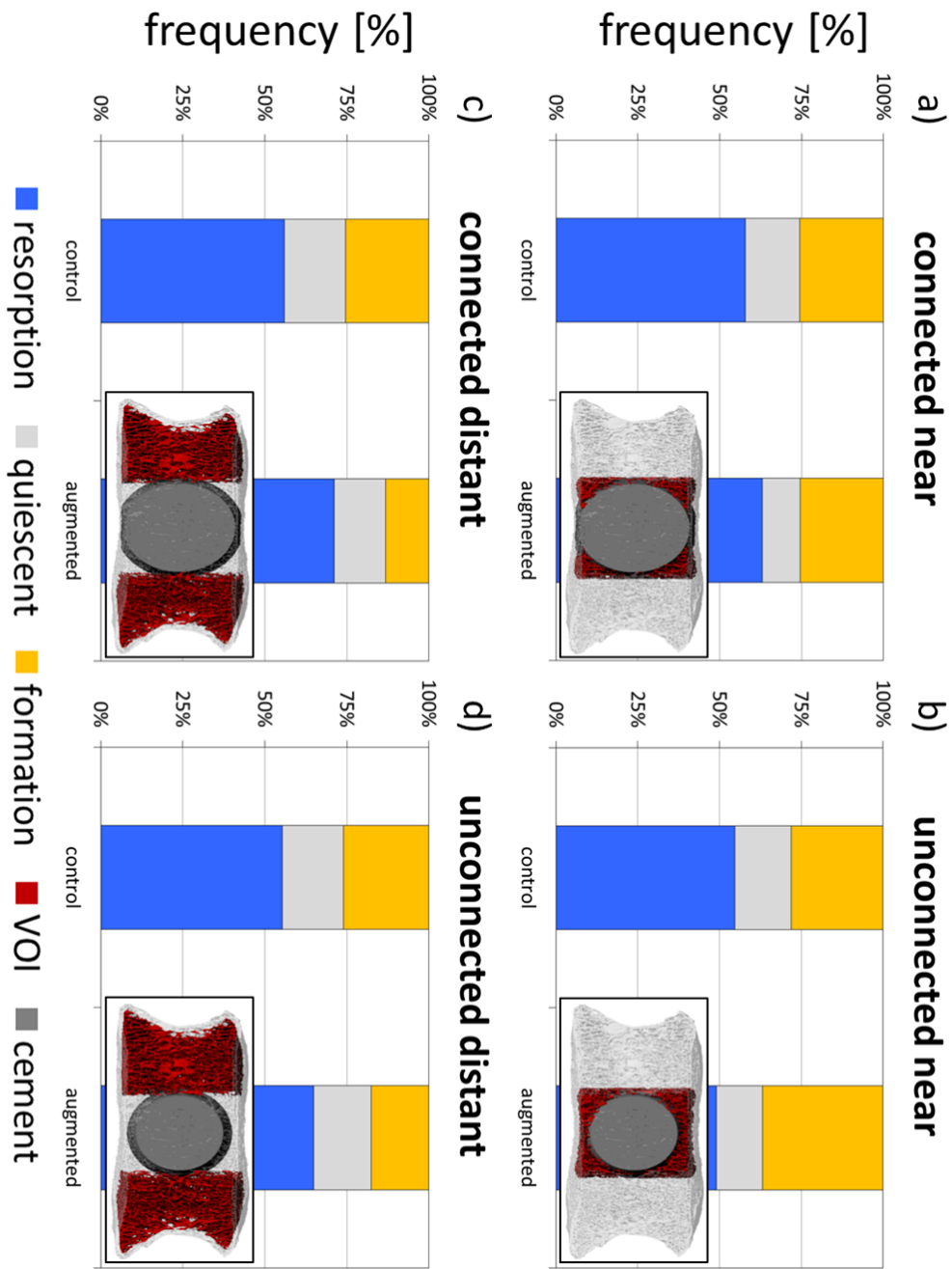


Figure 4.20: Stacked histograms for the sites of bone resorption, bone formation and quiescent bone for one sample at the age of 51.5 years. a) and b) show the distributions for the near-cement VOI, c) and d) show the distributions for the distant-cement VOI. The VOI are visualized in the corresponding charts.

Table 4.2: Morphometric indices for the near cement VOIs

Volume	Age [years]	Case	BV/TV [%]±SD	Tb.Th [mm]±SD	Tb.Sp [mm]±SD	Tb.N [1/mm]±SD	SMI [1/mm]±SD	TBPf [1/mm]±SD	DA [1/mm]±SD
connected	52.5	control	12.531±1.152	0.221±0.028	0.922±0.088	1.030±0.085	2.003±0.118	4.605±0.459	1.438±0.096
	62	control	10.753±0.839	0.206±0.023	0.962±0.092	0.997±0.083	2.002±0.119	5.037±0.450	1.502±0.114
		early	10.596±0.724	0.206±0.023	0.967±0.092	0.996±0.084	2.009±0.154	5.085±0.513	1.528±0.112
	80	control	9.704±0.692	0.196±0.018	0.984±0.093	0.975±0.082	2.137±0.146	5.698±0.344	1.545±0.120
		late	9.490±0.566	0.197±0.018	0.989±0.092	0.971±0.080	2.165±0.136	5.827±0.356	1.583±0.124
	early	early	9.552±0.503	0.203±0.020	0.989±0.093	0.968±0.079	2.298±0.136	6.104±0.402	1.596±0.121
unconnected	52.5	control	11.341±0.805	0.220±0.025	0.949±0.095	0.999±0.088	2.090±0.120	5.110±0.231	1.441±0.095
	62	control	9.638±0.678	0.189±0.017	0.990±0.098	0.968±0.087	2.075±0.093	5.572±0.209	1.513±0.115
		early	10.414±0.620	0.204±0.025	0.985±0.097	0.968±0.087	2.059±0.107	5.237±0.276	1.517±0.108
	80	control	8.686±0.730	0.185±0.015	1.013±0.100	0.947±0.085	2.204±0.103	6.254±0.083	1.599±0.118
		late	9.486±0.693	0.198±0.021	1.008±0.100	0.946±0.085	2.155±0.102	5.747±0.173	1.570±0.114
	early	early	10.025±0.600	0.206±0.023	1.004±0.099	0.947±0.085	2.179±0.092	5.594±0.241	1.568±0.109

Table 4.3: Morphometric indices for the distant cement VOIs

Volume	Age	Case	BV/TV	Tb.Th	Tb.Sp	Tb.N	SMI	TbPf	DA
	[years]		[%]	[mm]	[mm]	[1/mm]	[-]	[1/mm]	[-]
connected	52.5	control	12.002±0.229	0.196±0.023	1.003±0.095	0.954±0.095	1.763±0.096	4.560±0.615	1.461±0.042
		control	9.610±0.264	0.179±0.020	1.050±0.091	0.923±0.087	1.875±0.139	5.549±0.798	1.539±0.049
	62	early	8.698±0.268	0.171±0.020	1.059±0.093	0.921±0.086	1.911±0.147	6.043±0.839	1.562±0.055
		control	8.239±0.149	0.174±0.016	1.077±0.089	0.901±0.081	2.287±0.116	7.194±0.691	1.597±0.051
	80	late	7.343±0.155	0.167±0.016	1.087±0.091	0.898±0.080	2.436±0.110	8.194±0.675	1.629±0.060
		early	6.836±0.161	0.163±0.015	1.093±0.091	0.896±0.080	2.553±0.109	8.899±0.630	1.644±0.066
unconnected	52.5	control	11.944±0.116	0.196±0.022	1.005±0.096	0.951±0.095	1.771±0.091	4.576±0.579	1.463±0.043
		control	9.617±0.165	0.180±0.019	1.052±0.092	0.921±0.088	1.878±0.136	5.533±0.759	1.541±0.050
	62	early	9.068±0.189	0.175±0.019	1.058±0.093	0.920±0.087	1.900±0.141	5.821±0.787	1.554±0.055
		control	8.291±0.067	0.175±0.015	1.079±0.090	0.899±0.082	2.273±0.118	7.100±0.655	1.597±0.053
	80	late	7.749±0.083	0.171±0.015	1.085±0.091	0.897±0.081	2.363±0.115	7.679±0.657	1.616±0.059
		early	7.397±0.104	0.168±0.015	1.089±0.091	0.896±0.081	2.435±0.116	8.106±0.630	1.626±0.063

The situation in the vertebra is very different and our simulations revealed that this is not the case around the augmentation cement. Stress-raisers in the region around the augmentation prevent excessive bone loss and maintain structural stability at the bone-cement interface. In terms of stiffness increase, the beneficial augmentation seems to outweigh the increased bone loss of the distant-cement trabecular bone.

Evidence supporting our  $\mu$ FE calculated stiffness results can be found in the literature, where previous studies show similar increase in stiffness for cement volumes connecting and non-connecting the endplates: In a two-dimensional  $\mu$ FE model including two vertebrae and the intervertebral disk, an increase of the apparent stiffness modulus of about 10% to 30% was reported [8]. In a continuum FE model, stiffening by approximately 1 to 2 times was reported for non-connecting cement volumes, but a 1 to 8 times increase was reported for connecting cement volumes [7]. In experimental tests of augmented vertebrae, stiffening of 174% for a 27% to 46% volume injection was reported [24].

Case reports of augmented human bone after fracture indicate osteoid and viable bone around augmentation cement, suggesting bone adaptation [14,15]. In addition, no direct apposition to the PMMA was found [15]. Vertebroplasty models in sheep revealed similar results, where new bone formation was found in the vicinity of PMMA, without apposition to the cement [25,26]. Our simulations predicted such formation and are thus in agreement with the previous case reports and sheep study.

Some limitations to our simulations should be addressed nevertheless: First, our model does not allow bone adaptation in the cortex. Although a considerable fraction of the loads is transferred through the trabecular structures in the vertebra, weakening of the cortical bone due to stress-shielding (Figure 4.19) might impact the mechanical stability of the augmented structure. Then, the augmentation volumes we used have been artificially generated and represent rather ideal shapes [27] and the effects of our moderate augmentation volumes of 10% and 15%, respectively, might correspond to higher volumes in real augmentation. Finally, our bone adaptation simulations are deterministic and purely mechanically driven. Necrotic tissue and inflammatory reactions in the course of augmentation that might influence or even inhibit the adaptive behavior of the bone are neglected.

We showed that preventive bone augmentation leads to greater bone loss in the trabecular region, however, this bone loss did not affect the mechanical stability. Therefore, we conclude that, from a biomechanical perspective, the impact of vertebroplasty on the bone at the microstructural level is less detrimental than previously thought. However, preventive augmentation may still expose patients to risks linked to the intervention such as cement leakage, adjacent bone fractures or infections.

## Acknowledgements

The authors gratefully acknowledge funding from the European Union Osteoporotic Virtual Physiological Human Project (VPHOP FP7-ICT2008-223865) and the Swiss National Supercomputing Center in Lugano, Switzerland, for computational time (CSCS ID 5372).

## References

- [1] L. Alvarez *et al.* Percutaneous vertebroplasty: functional improvement in patients with osteoporotic compression fractures. *Spine (Phila Pa 1976)*, 31(10):1113–8, 2006.
- [2] G. C. Anselmetti *et al.* Pain relief following percutaneous vertebroplasty: results of a series of 283 consecutive patients treated in a single institution. *Cardiovasc Intervent Radiol*, 30(3):441–7, 2007.
- [3] P. A. Hulme, J. Krebs, S. J. Ferguson, U. Berlemann. Vertebroplasty and kyphoplasty: a systematic review of 69 clinical studies. *Spine (Phila Pa 1976)*, 31(17):1983–2001, 2006.
- [4] G. Baroud, J. Nemes, P. Heini, T. Steffen. Load shift of the intervertebral disc after a vertebroplasty: a finite-element study. *Eur Spine J*, 12(4):421–6, 2003.
- [5] P. A. Hulme, S. K. Boyd, P. F. Heini, S. J. Ferguson. Differences in endplate deformation of the adjacent and augmented vertebra following cement augmentation. *Eur Spine J*, 18(5):614–23, 2009.
- [6] C. H. Yen, M. M. Teng, W. H. Yuan, Y. C. Sun, C. Y. Chang. Preventive vertebroplasty for adjacent vertebral bodies: a good solution to reduce adjacent vertebral fracture after percutaneous vertebroplasty. *AJNR Am J Neuroradiol*, 33(5):826–32, 2012.
- [7] Y. Chevalier *et al.* Cement distribution, volume, and compliance in vertebroplasty: some answers from an anatomy-based nonlinear finite element study. *Spine (Phila Pa 1976)*, 33(16):1722–30, 2008.
- [8] T. S. Keller, V. Kosmopoulos, I. H. Lieberman. Vertebroplasty and kyphoplasty affect vertebral motion segment stiffness and stress distributions: a microstructural finite-element study. *Spine (Phila Pa 1976)*, 30(11):1258–65, 2005.

- [9] I. D. Learmonth, C. Young, C. Rorabeck. The operation of the century: total hip replacement. *Lancet*, 370(9597):1508–19, 2007.
- [10] P. Christen *et al.* Bone remodelling in humans is load-driven but not lazy. *Nat Commun*, 5:4855, 2014.
- [11] F. A. Schulte *et al.* Local mechanical stimuli regulate bone formation and resorption in mice at the tissue level. *PLoS One*, 8(4):e62172, 2013.
- [12] S. D. Badilatti *et al.* Large-scale microstructural simulation of load-adaptive bone remodeling in whole human vertebrae. *Biomech Model Mechanobiol*, in press, 2015.
- [13] F. A. Gerhard, D. J. Webster, G. H. van Lenthe, R. Mueller. In silico biology of bone modelling and remodelling: adaptation. *Philosophical Transactions of the Royal Society a-Mathematical Physical and Engineering Sciences*, 367(1895):2011–2030, 2009.
- [14] C. W. Kim, J. Minocha, C. E. Wahl, S. R. Garfin. Response of fractured osteoporotic bone to polymethylacrylate after vertebroplasty: case report. *Spine J*, 4(6):709–12, 2004.
- [15] D. Togawa, T. W. Bauer, I. H. Lieberman, S. Takikawa. Histologic evaluation of human vertebral bodies after vertebral augmentation with polymethyl methacrylate. *Spine (Phila Pa 1976)*, 28(14):1521–7, 2003.
- [16] A. Levchuk *et al.* The clinical biomechanics award 2012 - presented by the european society of biomechanics: large scale simulations of trabecular bone adaptation to loading and treatment. *Clin Biomech (Bristol, Avon)*, 29(4):355–62, 2014.
- [17] F. A. Schulte *et al.* Strain-adaptive in silico modeling of bone adaptation - a computer simulation validated by in vivo micro-computed tomography data. *Bone*, 52(1):485–92, 2013.
- [18] K. Kobayashi *et al.* Unilateral transpedicular percutaneous vertebroplasty using puncture simulation. *Radiat Med*, 24(3):187–94, 2006.
- [19] C. Flaig and P. Arbenz. A scalable memory efficient multigrid solver for micro-finite element analyses based on ct images. *Parallel Computing*, 37(12):846–854, 2011.

- [20] E. F. Morgan, H. H. Bayraktar, T. M. Keaveny. Trabecular bone modulus-density relationships depend on anatomic site. *J Biomech*, 36(7):897–904, 2003.
- [21] B. Helgason, P. Stirnimann, R. Widmer, A. Boger, S. J. Ferguson. Influence of cement stiffness and bone morphology on the compressive properties of bone-cement composites in simulated vertebroplasty. *J Biomed Mater Res B Appl Biomater*, 2012.
- [22] P. Christen *et al.* Subject-specific bone loading estimation in the human distal radius. *J Biomech*, 46(4):759–66, 2013.
- [23] P. Christen, K. Ito, A. A. Santos, R. Mueller, R. Bert van. Validation of a bone loading estimation algorithm for patient-specific bone remodelling simulations. *J Biomech*, 46(5):941–8, 2013.
- [24] P. F. Heini *et al.* Augmentation of mechanical properties in osteoporotic vertebral bones—a biomechanical investigation of vertebroplasty efficacy with different bone cements. *Eur Spine J*, 10(2):164–71, 2001.
- [25] N. Kobayashi *et al.* Histological and radiographic evaluation of polymethylmethacrylate with two different concentrations of barium sulfate in a sheep vertebroplasty model. *J Biomed Mater Res A*, 75(1):123–7, 2005.
- [26] J. Krebs *et al.* Effect of vertebral cement augmentation with polymethylmethacrylate on intervertebral disc and bone tissue. *J Biomed Mater Res B Appl Biomater*, 2011.
- [27] R. P. Widmer Soyka, A. Lopez, C. Persson, L. Cristofolini, S. J. Ferguson. Numerical description and experimental validation of a rheology model for non-newtonian fluid flow in cancellous bone. *Journal of the Mechanical Behavior of Biomedical Materials*, 27(0):43–53, 2013.



# Chapter 5

## Synthesis

In daily life, we experience bones as something static. Bone, however, is made of a highly dynamic tissue that is constantly renewed. In this process of bone remodeling, interactions of different cell types perpetually remodel the structure, most evidently seen in trabecular bone [1,2]. In healthy bone, this process helps to renew the bone matrix and maintain the stiffness and to adapt the bone structure to the changing mechanical needs [3]. When the fragile balance between bone forming and bone resorbing cells is perturbed, such as during osteoporosis, drastic loss of bone mass is the consequence. This loss makes bones more fragile to fractures and the important load bearing capacity is reduced. Osteoporosis mostly affects postmenopausal women, where a substantial reduction of bone tissue occurs in just a few years [4]. With a constantly increasing share of the world population being aged people [5], the number of patients suffering osteoporotic bone fractures is going to increase, unless we find better ways of prevention.

A key for effective prevention of osteoporotic bone fractures is the quality of the fracture risk assessment [6, 7]. Dual-energy X-ray absorptiometry is the standard approach today [8], but latest developments in high-resolution peripheral quantitative computer tomography combined with  $\mu$ FE further improve the accuracy of the assessment [9]. However, all these techniques are limited by the fact that they merely look at the risk of fracture at the day of the measurements, but have limited predictive power for the future stability of the bones.

It is known, though, that bone remodeling is not a purely stochastic process, but driven by mechanosensitive cells [10, 11]. This behavior has been described in mathematical models [12] and successfully reproduced in computer simulations [13–17]. What these previous bone remodeling simulations are missing, however, is how microstructural changes adapt the bone on the organ-scale and the resulting impact on the mechanical stability of the whole bone. Until recently, not only was it impossible to get high-resolution  $\mu$ CT datasets of whole human bones, but also

was the post-processing constricted due to the limited computational power. Today, technical progress made both available and accessible.

The primary aim of this thesis was to set up a framework capable of performing large-scale simulations of load-adaptive bone remodeling in whole human vertebrae and to investigate its potential. Using high-resolution  $\mu$ CT datasets of human vertebrae, we aimed to realistically predict the long-term outcome of mechanoregulated remodeling in disease and treatments. We aimed to simulate osteoporotic bone loss, since it is the most prevalent disease in bone. Because of the high impact on the mechanical load transfer, preventive vertebroplasty was selected as a possible treatment. More specifically, we defined the following three key aims that are important to give better insight into microstructural bone remodeling in whole bones:

- Aim 1:** Development of large-scale simulations of load-adaptive bone remodeling in whole human vertebrae and investigation of its functioning from the microstructure to trabecular bone and the organ as a whole.
- Aim 2:** Simulations of osteoporotic bone loss in native whole human vertebrae and demonstrating the potential benefits over conventional bone fracture assessment in the long-term.
- Aim 3:** Simulations of microstructural bone adaptation in augmented whole human vertebrae and investigation of the impact of preventive vertebroplasty on the mechanical stability and the microstructure in the long-term.

## 5.1 Large-scale simulations of load-adaptive bone remodeling

The major achievements in the first aim were the establishment of a routine allowing smooth solving of the large-scale  $\mu$ FE calculations as well as the inclusion of patient specific bone loading conditions into the framework. Previous simulations of microstructural bone remodeling were limited to subvolumes or small animal bones [13–17]. This restriction has manifold simplifications on the  $\mu$ FE analysis: First, small volumes solve faster and because of the reduced complexity converge more easily towards a stable solution. Our work included  $\mu$ FE models with up to 365 million elements. The models had to converge for three loading conditions for up to 15 iterations, where the internal bone structure was changed and where particularly trabecular thinning resulted in decreased convergence stability. This hurdle was overcome by the application of soft pads mimicking the intervertebral disks better

distributing the applied force on the bones and by changing from binary  $\mu$ FE to gray-scale  $\mu$ FE models. This approach can be found in several low-resolution  $\mu$ FE models [18, 19], but is novel for high-resolution  $\mu$ FE as the standard there are still linear elastic models using a single material only [20]. Second, the previously used small volumes did usually not account for *in vivo* boundary conditions to calculate the mechanical loading. In order to get realistic physiological bone remodeling in whole bones however, physiological loading of the bone is required. If unphysiological loading is applied, the calculated internal local loadings will be wrong and lead to large and unnatural changes of the internal structures. This was achieved with the implementation of a bone load estimation algorithm [21–23] into the remodeling framework that defined case-specific boundary conditions for every single bone prior to the simulation start. The importance of using complex physiologic boundary conditions has been recognized in other work too [24–26], but is not applied to models at high resolutions such as used in the present work.

The large datasets required technical efforts also on the bone remodeling algorithm. By upgrading to a system with large memory access, the process was optimized with combined in-house developed software and commercially available tools. On the same system, post-processing and evaluation of the results of such large datasets could be performed. Together with the  $\mu$ FE setup and the bone load estimation, this allowed bone remodeling simulations on models sizes never reached before. Large-scale simulations of load-adaptive bone remodeling in whole bones are not found elsewhere in the scientific literature. Because of the difficulty to handle large datasets, a new approach is to go towards multiscale solutions where changes of a morphometric entity is derived by analytical solution of a simplified problem on the cellular or microscale level and translating the information to higher continuum levels [27, 28]. While the effects of drug treatments or cell activity can be analysed with the approach, translating the results to accurate fracture prediction may still be challenging and not as accurate as with large-scale simulations.

While the bone load estimation approach was validated earlier [21–23], we presented calculations on whole human vertebrae. The predicted magnitudes were in the expected physiological range thus verifying the proper functioning of the algorithm. Remodeling simulations of the whole bones revealed realistic outcomes for the simulations of 10 years of healthy bone adaptation. Because *in vivo* high-resolution imaging of whole human vertebrae is not possible today, direct validation of the results was not possible, but the model was extensively evaluated in a series of simulations of subvolumes. In a well-controlled environment the local load adaptation was tested on synthetic single trabeculae. The effects of varying the boundary con-

ditions were investigated on a trabecular subvolume showing the necessity of using multiple load cases for as a mechanical input for remodeling simulations. In addition, forced re-adaptation to a changed mechanical environment was demonstrated on the trabecular subvolume as well.

A last finding from the first aim comes from the investigation of the resolution dependency of the  $\mu$ FE analysis. We showed that reducing the resolution of a trabecular bone volume shifts the calculated SED distributions towards higher values. Resolutions between 17.4  $\mu\text{m}$  and 43.5  $\mu\text{m}$  showed only minor changes. It can therefore be assumed that the resolution of new high-resolution peripheral quantitative computer tomography may be sufficient to perform accurate bone remodeling simulations.

## **5.2 Simulations of osteoporotic bone loss in native vertebrae**

The major achievement of the second aim is to provide a complete tool for realistically predicting the future fracture risk of whole human bones in the course of osteoporosis. While current fracture risk assessments estimate the fracture risk at the time-point of the scanning, this is the first time the microstructure of whole bones is simulated in the course of ageing and the mechanical competence assessed for all time stamps. The tool is composed of three main components: the case-specific calculation of the boundary conditions, the realistic simulation of the future microstructure and an elaborated evaluation of the stiffness and fracture loads at each time-point from the onset of menopause at the age of 50 to the age of 80.

Starting from a single bone where remodeling parameters were chosen such that changes in morphometric parameters matched previous experimental work [4], simulations of 30 years of osteoporotic bone loss were conducted on a group of seven high-resolution scans of whole human vertebrae. The simulations revealed that in spite of the deterministic nature of the algorithm and the simplified modeling of the biological process, by matching the morphometry only, the load-adaptive bone remodeling predicted the future mechanical competence of the bone in a realistic fashion. It was confirmed that such large-scale simulations of load-adaptive bone remodeling have the potential to enhance long-term fracture risk assessment in individual patients.

Moreover, a brief parameter study for the used bone remodeling parameters in the mechanostat approach was reported. Compared to the homeostatic bone remodeling of the control group, the most prevalent change was an increase of the bone

resorption threshold corresponding to reduced sensitivity of the mechanosensitive cells.

### 5.3 Simulations of microstructural bone adaptation in augmented vertebrae

The major achievement of the third aim is to provide insight into the long-term effects of bone augmentation. Previous computational studies were limited to the immediate post-augmentation state [29, 30], experimental work limited to a maximum of two years [31, 32]. Evaluation of the changes in load transfer are in agreement with previous reports, and despite some simplifications in the modeling of the bone biology, the results are comparable to findings from histology. As the main finding, this work showed that bone augmentation may be less detrimental to the trabecular structure in the vicinity of the cement and that the mechanical stability of the augmented bone is maintained in the long-term. Additionally, this is the first analysis of preventive bone augmentation that has been reported in the scientific literature. Our results suggest that, from a biomechanical perspective and in order to prevent fractures, this intervention is beneficial in individual vertebrae. Whether this intervention changes the mechanics in neighboring vertebrae such that bone is adapting to this needs to be investigated.

Furthermore, this work included three-dimensional  $\mu$ FE analysis of augmented vertebrae. The resulting stiffness calculations were closer to experimental findings compared to continuum-FE models, supporting evidence for the increased quality of the use of microstructural analysis. In addition, not only could we detect stress-raised and stress-shielded areas, but visualize the changed strains on the trabecular level.

### 5.4 Limitations and future research

Several limitations of this work should be mentioned. The implemented computational model simplifies biological events to the net change in bone mass and distribution. It is purely mechanically driven and hence deterministic. Bone biology is more complex with multiple cell-types involved, signaling pathways leading to gene expression and eventually leading to bone formation or resorption. Possible stochastic effects such as untargeted remodeling were excluded. Nevertheless, the results revealed realistic outcomes and seem to be sufficient for long-term assessment of mechanical stability and fracture prediction. In the future, high-resolution imaging

techniques with less radiation dose may allow a desirable validation of our model *in vivo*. Also, this work opens up the field for research in the direction of determining which aspect of osteoporosis should be targeted, in order to most efficiently prevent bone loss. For example increasing the loading, increasing the cell sensitivity, increase bone formation, reduce bone resorption, or combinations of the previously mentioned.

The model includes a lazy-zone, a region where no bone adaptation is occurring. Recent studies have put a question mark to the existence of such a zone [10,11,33,34]. Simulations of bone remodeling in mouse bone also showed good results compared to experiments with a mechanostat lacking a lazy-zone [35]. For the osteoporosis simulations, the parameter set leading to the best match to experimental work leads to a narrow lazy-zone including only about 20% of the total voxels. Though, because formation and resorption near the lazy-zone are in a sub-voxel region, much more voxels are regarded quiescent in the morphometric analysis of the binarized files. Possibly, the narrow lazy-zone is just a matter of image resolution.

The presented model does not consider damage accumulation in the bone as a consequence of the loading. Handling damage accumulation is difficult, as microcracks are, if at all, difficult to spot on  $\mu$ CT data. It has been shown, however, that bone loading can induce microdamage, which may lead to bone failure [24,25]. In addition, damage accumulation appears to be higher if complex loading are applied [24,25]. In the presented work, the bone was considered as intact, that is without microcracks at the beginning of the simulations. In the course of the bone remodeling simulations, sites with high local strains led to local formation of bone and possible damage was excluded. Because physiological loading conditions were used, no major formation of microcracks is expected. Other presented models include microdamage in bone remodeling simulations by removing bone packages when a local fracture strain is exceeded [16] and such an approach could be implemented in the presented framework.

In the presented model, bone remodeling is limited to the trabecular region, without changing the structure of the cortex. Although less pronounced, cortical bone is also remodeled during postmenopausal osteoporosis [36] and impacts the stability of the bone. Including bone remodeling of the cortex in the future would thus improve the quality of the calculations of failure strength, in particular when looking at other bones with a higher relative volume fraction of cortical versus trabecular bone.

Finally, three limitations regarding the augmented models should be mentioned: We used artificially generated augmentation volumes representing rather ideal shapes. The mechanical influence of these shapes thus may correspond to higher

augmentation volumes in reality. Validated simulations of realistic virtual bone augmentation exist [37–40], and could be used in combination with our bone adaptation approach. Moreover, we excluded the possible occurrence of necrotic tissue and inflammatory reactions around the augmentation cement, possibly inhibiting the adaptive capacity of the trabecular bone. As mentioned earlier, the formation of microcracks was not considered in the remodeling simulations and in the augmented bone strength assessment. In the strength assessment of the osteoporotic bone the pistoia criterion that includes crack formation was used to determine fracture strength [41]. In the bone cement composite of the augmented bones, it was not possible to use the same approach. Also, the assumption that the applied physiological loads would not lead to major formation of microcracks may be wrong, as the loads around the augmentation cement are altered and could be increased beyond crack formation. If this was the case, the augmentation volume could lose some connections to the trabecular bone which would induce new cracks in other trabecula and ultimately lead to a failure of the implant. In the scientific literature, no such failure is reported however. This supports the assumption that the altered mechanical loading due to bone cement augmentation does not induce excessive formation of microcracks.

Despite these limitations, our simulations revealed realistic biomechanical outcomes for the assessment of future fracture prediction opening up the field for investigation of other affected sites in the body or the combination with fracture healing. Also, such approaches could eventually be used in clinical settings, provided the computational costs can be reduced or the technical capabilities improved. Instead of restarting the  $\mu$ FE de novo for every iteration, a bone adapted map of the previously calculated SED could be used as an input and massively speed-up the calculation process.

Although our deterministic model seems adequate for the assessment of future fracture risk, enhancements such as the inclusion of untargeted remodeling or the formation of micro-cracks could help to further improve the quality of the simulated microstructure, in particular the overestimated trabecular number.

Last but not least, our simulations of preventive bone augmentation revealed promising results supporting the approach from a biomechanical point of view. If our results can be confirmed by experimental work and the advantages outbalance the risks of the intervention this could clear the way for preventive vertebroplasty.

## 5.5 Conclusion

Bone remodeling simulations have been available for many years. The models were limited in size and their application thus limited to the investigation of the mechanisms of bone adaptation. We have achieved the aim of this thesis to simulate large-scale load-adaptive bone remodeling in whole human vertebrae. In two applications, we show the potential of such simulations in disease and treatment. Bone remodeling simulations can give better insight into microstructural changes and thus have the potential to improve future fracture risk prediction. Also, these simulations can be useful to investigate novel treatments in bones and their impact in the long-term.

## References

- [1] E. F. Eriksen, F. Melsen, E. Sod, I. Barton, A. Chines. Effects of long-term risedronate on bone quality and bone turnover in women with postmenopausal osteoporosis. *Bone*, 31(5):620–5, 2002.
- [2] S. J. Glover, P. Garnero, K. Naylor, A. Rogers, R. Eastell. Establishing a reference range for bone turnover markers in young, healthy women. *Bone*, 42(4):623–30, 2008.
- [3] D. B. Burr. Targeted and nontargeted remodeling. *Bone*, 30(1):2–4, 2002.
- [4] R. Mueller. Long-term prediction of three-dimensional bone architecture in simulations of pre-, peri- and post-menopausal microstructural bone remodeling. *Osteoporos Int*, 16 Suppl 2:S25–35, 2005.
- [5] United-Nations. Population ageing and development. *Department of Economic and Social Affairs, Population Division, New York, NY 10017, USA, www.unpopulation.org*, 2012.
- [6] D. Christen, D. J. Webster, R. Mueller. Multiscale modelling and nonlinear finite element analysis as clinical tools for the assessment of fracture risk. *Philos Transact A Math Phys Eng Sci*, 368(1920):2653–68, 2010.
- [7] M. Viceconti, E. Schileo, F. Taddei, S. Martelli, D. Testi. Personalised multi-scale models for risk fracture prediction. *Osteoporos Int*, (21):1067–1071, 2010.



- [8] J. A. Kanis *et al.* Assessment of fracture risk and its application to screening for postmenopausal osteoporosis - synopsis of a who report. *Osteoporosis International*, 4(6):368–381, 1994.
- [9] D. Christen *et al.* Improved fracture risk assessment based on nonlinear micro-finite element simulations from hrpqct images at the distal radius. *J Bone Miner Res*, 28(12):2601–8, 2013.
- [10] P. Christen *et al.* Bone remodelling in humans is load-driven but not lazy. *Nat Commun*, 5:4855, 2014.
- [11] F. A. Schulte *et al.* Local mechanical stimuli regulate bone formation and resorption in mice at the tissue level. *PLoS One*, 8(4):e62172, 2013.
- [12] H. M. Frost. Bone’s mechanostat: a 2003 update. *Anat Rec A Discov Mol Cell Evol Biol*, 275(2):1081–101, 2003.
- [13] R. Ruimerman, P. Hilbers, B. van Rietbergen, R. Huiskes. A theoretical framework for strain-related trabecular bone maintenance and adaptation. *Journal of Biomechanics*, 38(4):931–941, 2005.
- [14] P. Christen *et al.* Patient-specific bone modelling and remodelling simulation of hypoparathyroidism based on human iliac crest biopsies. *J Biomech*, 45(14):2411–6, 2012.
- [15] T. Adachi, K. Tsubota, Y. Tomita, S. J. Hollister. Trabecular surface re-modeling simulation for cancellous bone using microstructural voxel finite element models. *Journal of Biomechanical Engineering-Transactions of the Asme*, 123(5):403–409, 2001.
- [16] P. Mc Donnell, N. Harrison, M. A. Liebschner, P. E. Mc Hugh. Simulation of vertebral trabecular bone loss using voxel finite element analysis. *J Biomech*, 2009.
- [17] F. A. Schulte *et al.* Strain-adaptive in silico modeling of bone adaptation - a computer simulation validated by in vivo micro-computed tomography data. *Bone*, 52(1):485–92, 2013.
- [18] Y. Chevalier *et al.* Biomechanical effects of teriparatide in women with osteoporosis treated previously with alendronate and risedronate: results from quantitative computed tomography-based finite element analysis of the vertebral body. *Bone*, 46(1):41–8, 2010.

- [19] B. A. Christiansen, D. L. Kopperdahl, D. P. Kiel, T. M. Keaveny, M. L. Bouxsein. Mechanical contributions of the cortical and trabecular compartments contribute to differences in age-related changes in vertebral body strength in men and women assessed by qct-based finite element analysis. *J Bone Miner Res*, 26(5):974–83, 2011.
- [20] K. K. Nishiyama, H. M. Macdonald, D. A. Hanley, S. K. Boyd. Women with previous fragility fractures can be classified based on bone microarchitecture and finite element analysis measured with hr-pqct. *Osteoporos Int*, 24(5):1733–40, 2013.
- [21] P. Christen, B. van Rietbergen, F. M. Lambers, R. Mueller, K. Ito. Bone morphology allows estimation of loading history in a murine model of bone adaptation. *Biomech Model Mechanobiol*, 2011.
- [22] P. Christen *et al.* Subject-specific bone loading estimation in the human distal radius. *J Biomech*, 46(4):759–66, 2013.
- [23] P. Christen, K. Ito, A. A. Santos, R. Mueller, R. Bert van. Validation of a bone loading estimation algorithm for patient-specific bone remodelling simulations. *J Biomech*, 46(5):941–8, 2013.
- [24] Y. Chevalier *et al.* A patient-specific finite element methodology to predict damage accumulation in vertebral bodies under axial compression, sagittal flexion and combined loads. *Comput Methods Biomech Biomed Engin*, 11(5):477–87, 2008.
- [25] U. Wolfram, H. J. Wilke, P. K. Zysset. Damage accumulation in vertebral trabecular bone depends on loading mode and direction. *J Biomech*, 44(6):1164–9, 2011.
- [26] K. Tsubota *et al.* Computer simulation of trabecular remodeling in human proximal femur using large-scale voxel fe models: Approach to understanding wolff’s law. *J Biomech*, 42(8):1088–94, 2009.
- [27] M. Colloca, R. Blanchard, C. Hellmich, K. Ito, B. van Rietbergen. A multi-scale analytical approach for bone remodeling simulations: linking scales from collagen to trabeculae. *Bone*, 64:303–13, 2014.
- [28] S. Scheiner, P. Pivonka, C. Hellmich. Coupling systems biology with multiscale mechanics, for computer simulations of bone remodeling. *Computer Methods in Applied Mechanics and Engineering*, 254:181–196, 2013.

- [29] Y. Chevalier, D. Pahr, P. K. Zysset. The role of cortical shell and trabecular fabric in finite element analysis of the human vertebral body. *J Biomech Eng*, 131(11):111003, 2009.
- [30] T. S. Keller, V. Kosmopoulos, I. H. Lieberman. Vertebroplasty and kyphoplasty affect vertebral motion segment stiffness and stress distributions: a microstructural finite-element study. *Spine (Phila Pa 1976)*, 30(11):1258–65, 2005.
- [31] C. W. Kim, J. Minocha, C. E. Wahl, S. R. Garfin. Response of fractured osteoporotic bone to polymethylacrylate after vertebroplasty: case report. *Spine J*, 4(6):709–12, 2004.
- [32] D. Togawa, T. W. Bauer, I. H. Lieberman, S. Takikawa. Histologic evaluation of human vertebral bodies after vertebral augmentation with polymethyl methacrylate. *Spine (Phila Pa 1976)*, 28(14):1521–7, 2003.
- [33] J. W. Dunlop, M. A. Hartmann, Y. J. Brechet, P. Fratzl, R. Weinkamer. New suggestions for the mechanical control of bone remodeling. *Calcif Tissue Int*, 85(1):45–54, 2009.
- [34] T. Sugiyama *et al.* Bones’ adaptive response to mechanical loading is essentially linear between the low strains associated with disuse and the high strains associated with the lamellar/woven bone transition. *J Bone Miner Res*, 27(8):1784–93, 2012.
- [35] A. Levchuk. In silico investigation of bone adaptation in health and disease. *in preparation, ETH Bibliothek, Doctoral Thesis, ETH Zurich*, 2015.
- [36] H. M. Macdonald, K. K. Nishiyama, J. Kang, D. A. Hanley, S. K. Boyd. Age-related patterns of trabecular and cortical bone loss differ between sexes and skeletal sites: a population-based hr-pqct study. *J Bone Miner Res*, 26(1):50–62, 2011.
- [37] R. P. Widmer and S. J. Ferguson. A mixed boundary representation to simulate the displacement of a biofluid by a biomaterial in porous media. *J Biomech Eng*, 133(5):051007, 2011.
- [38] R. P. Widmer and S. J. Ferguson. On the interrelationship of permeability and structural parameters of vertebral trabecular bone: a parametric computational study. *Comput Methods Biomech Biomed Engin*, 2012.

- [39] R. P. Widmer and S. J. Ferguson. A comparison and verification of computational methods to determine the permeability of vertebral trabecular bone. *Proc Inst Mech Eng H*, 227(6):617–28, 2013.
- [40] R. P. Widmer Soyka, A. Lopez, C. Persson, L. Cristofolini, S. J. Ferguson. Numerical description and experimental validation of a rheology model for non-newtonian fluid flow in cancellous bone. *Journal of the Mechanical Behavior of Biomedical Materials*, 27(0):43–53, 2013.
- [41] W. Pistoia *et al.* Estimation of distal radius failure load with micro-finite element analysis models based on three-dimensional peripheral quantitative computed tomography images. *Bone*, 30(6):842–8, 2002.

# Curriculum Vitae

Sandro Domenico Badilatti

Born on the 14<sup>th</sup> of March 1983 in Samedan, Switzerland

## *Education*

---

2015	Doctoral thesis under the supervision of Prof. Dr. Ralph Müller
2009 – 2015	Doctoral candidate at the Institute for Biomechanics, ETH Zurich
2007 – 2009	M.Sc. Biomedical Engineering, ETH Zurich
2003 – 2007	B.Sc. Physics, ETH Zurich
2003	Matura type B (humanistic Matura), Lyceum Alpinum Zuoz, Switzerland

## *Publications*

---

S. D. Badilatti, P. Christen, A. Levchuk, J. H. Marangalou, B. van Rietbergen, I. Parkinson and R. Müller. Large-scale microstructural simulation of load-adaptive bone remodeling in whole human vertebrae. *Biomech Model Mechanobiol*, published online, 2015.

S. D. Badilatti, G. A. Kuhn, S. J. Ferguson and R. Müller. Computational modelling of bone augmentation in the spine. *J Orthop Translat*, published online, 2015.

S. D. Badilatti, P. Christen, I. Parkinson and R. Müller. Load-adaptive remodeling simulations reveal osteoporotic microstructural and mechanical changes in human vertebrae. in preparation, 2015.

S. D. Badilatti, P. Christen, S. J. Ferguson and R. Müller. Computational modelling of long-term effects of preventive vertebroplasty on microstructural bone adaptation. in preparation, 2015.

A. Levchuk, A. Zwahlen, C. Weigt, F. M. Lambers, S. D. Badilatti, F. A. Schulte, G. Kuhn and R. Müller. The Clinical Biomechanics Award 2012 - Presented by

the European Society of Biomechanics: Large scale simulations of trabecular bone adaptation to loading and treatment. *Clin. Biomech.*, **29**,355-362, 2014.

### *Conference Proceedings and Abstracts*

---

S. D. Badilatti, P. Christen, S.J. Ferguson and R. Müller. Simulation of Long-term Adaptation to Cement Augmentation in Whole Human Vertebrae. *2015 Annual Meeting, Swiss Society for Biomedical Engineering, Neuchatel, Switzerland*, August 26.-27., 2015.

S. D. Badilatti, L. Sommerhalder and R. Müller. Modeling of biodegradation in the augmented spine. *2014 Annual Meeting, Swiss Society for Biomedical Engineering, Zürich, Switzerland*, **47**, August 27.-28., 2014.

S. D. Badilatti, P. Christen, A. Levchuk, I. Parkinson and R. Müller. Towards simulation of whole bone microstructure adaptation. *7th World Congress of Biomechanics, Boston, USA*, July 6.-11., 2014.

A. Levchuk, R. Sommer, S. D. Badilatti, F.M. Lambers, C. Weigt, G. Kuhn and R. Müller. Long-term *in silico* simulations predict longitudinal *in vivo* bone remodeling in a mouse model of postmenopausal osteoporosis. *7th World Congress of Biomechanics, Boston, USA*, July 6.-11., 2014.

A. Levchuk, R. Sommer, S. D. Badilatti, F. A. Schulte, D. Ruffoni, C. Weigt, G. Kuhn and R. Müller. *In silico* simulations of bone remodeling with improved parameter estimation from local strains and dynamic morphometry *in vivo*. *ASBMR 2013 Annual Meeting, Baltimore, USA, J. Bone Miner. Res.*, **28(S1)**, 2013.

S. D. Badilatti, A. Levchuk, D. J. Webster and R. Müller. Long-term *in silico* bone adaptation in high-resolution human bones. *5th International Conference on Computational Bioengineering, Leuven, Belgium*, September 11.-13., 2013.

F. A. Schulte, S. D. Badilatti, I. Parkinson, J. Goldhahn and R. Müller. Bone morphometry from human peripheral quantitative computer tomography scans is preserved by virtual high-resolution image reconstruction. *40th European Symposium on Calcified Tissues, European Calcified Tissue Society (ECTS), Lisbon, Portugal*, May 18.-21., 2013.

S. D. Badilatti, R. P. Widmer, A. Levchuk, D. J. Webster, S. J. Ferguson and R. Müller. Bone adaptation modeling for treatment planning in virtually augmented high-resolution human bones. *11th International Symposium of Computer Methods in Biomechanics and Biomedical Engineering, Salt Lake City, USA*, April 3.-6., 2013.

S. D. Badilatti, A. Zwahlen, A. Levchuk, F. A. Schulte and R. Müller. *In silico* bone remodeling of a whole human vertebra before and after bone augmentation. *18th Congress of the European Society of Biomechanics (ESB)*, Lisbon, Portugal, **1512**, July 1.-4., 2012.

R. Müller, A. Levchuk, S. D. Badilatti, A. Zwahlen, F. A. Schulte, F. M. Lambers, C. Weigt, D. J. Webster and G. Kuhn. Computational prediction of load induced bone remodeling in response to aging, disease and treatment *in vivo*. *10th International Symposium on Computer Methods in Biomechanics and Biomedical Engineering*, Berlin, Germany, April 11.-14., 2012.

S. D. Badilatti, F. A. Schulte, F. M. Lambers, G. A. Kuhn and R. Müller. *In silico* modeling of the growth of a new bone trabecula. *17th Congress of the European Society of Biomechanics (ESB)*, Edinburgh, UK, **736**, July 5.-8., 2010.